MARCH 2019

Ph. D. in Food Engineering

EDA ADAL

UNIVERSITY OF GAZİANTEP

GRADUATE SCHOOL OF

NATURAL & APPLIED SCIENCES

ENCAPSULATION OF OILS FROM SOUR CHERRY KERNEL AND BERRY SEEDS BY PROTEIN-PROTEIN COMPLEXES

Ph. D. THESIS

IN

FOOD ENGINEERING

BY

EDA ADAL

MARCH 2019

Encapsulation of oils from sour cherry kernel and berry seeds by protein-protein complexes

Ph. D. Thesis

in

Food Engineering

University of Gaziantep

Supervisor

Prof. Dr. Esra İBANOĞLU

by

Eda ADAL

March 2019

©2019 [Eda ADAL]

REPUBLIC OF TURKEY

UNIVERSITY OF GAZİANTEP
GRADUATE SCHOOL OF NATURAL & APPLIED SCIENCES
DEPARTMENT OF FOOD ENGINEERING

Name of the thesis: Encapsulation of oils from sour cherry kernel and berry seeds by protein-polysaccharide complexes

Name of the student: Eda ADAL

Exam date: 22.02.2019

Approval of the Graduate School of Natural and Applied Sciences

Prof. Dr. A. Necmeddin YAZICI
Director

I certify that this thesis satisfies all the requirements as a thesis for the degree of Doctor of Philosophy.

Prof. Dr. Medeni MASKAN
Head of Department

This is to certify that we have read this thesis and that in our consensus opinion it is fully adequate, in scope and quality, as a thesis for the degree of Doctor of Philosophy.

Prof. Dr. Esra İBANOĞLU
Supervisor

Examining Committee Members:	Signature
----------	……..
----------	……..
----------	……..
----------	……..
----------	……..

I hereby declare that all information in this document has been obtained and presented in accordance with academic rules and ethical conduct. I also declare that, as required by these rules and conduct, I have fully cited and referenced all material and results that are not original to this work.

Eda ADAL

ABSTRACT

ENCAPSULATION OF OILS FROM SOUR CHERRY KERNEL AND BERRY SEEDS BY PROTEIN-PROTEIN COMPLEXES

ADAL, Eda
Ph. D. in Food Engineering
Supervisor: Prof. Dr. Esra İBANOĞLU

March 2019
148 pages

In this study, the encapsulation of raspberry seed oil (RSO) and sour cherry seed oil (CHSO) which have high amount of Omega 3 and 6 fatty acids by heteroprotein complexes and coacervates was investigated. In the first part of thesis, formation of complexes and coacervates was examined between two oppositely charged globular proteins, lactoferrin (LF) and pea protein isolate (PPI) with a specific PPI/ LF molar ratio at room temperature. Structural aspects of the electrostatic complexes probed at different length scales were investigated as a function of pH by means of dynamic light scattering, small angle X-ray scattering (SAXS), turbidity measurements, transmission electron microscopy (TEM) and atomic force microscopy (AFM). In an optimum narrow range of pH 5.0-5.8, a viscous liquid phase of complex coacervate was obtained whereas soluble complexes were formed between pH 6.2-7.5.

In the second part, emulsions were prepared with different methods at optimum complex (pH 7) and coacervate (pH 5.4) conditions. The most appropriate method was determined as formation of complexes and coacervates at the last stages of encapsulation based on droplet size, droplet charge, emulsion stability and microstructure analysis. The effect of oil concentrations on (2-10 wt%) droplet size and rheology of emulsions was evaluated in the third part of thesis. Emulsions were later freeze dried to evaluate loading capacity, encapsulation efficiency, loading efficiency, moisture content and encapsules morphology. The results revealed that increasing oil concentration cause significantly effect on encapsulation efficiency and particle morphology ($p<0.05$). Encapsules produced at optimized conditions (6 wt% oil, 2 wt% protein) with RSO and CHSO were evaluated for their physicochemical properties and oxidative stability. They were stable at 45°C during storage. Pure oil showed higher lipid oxidation which indicates protective effect of encapsulation on oxidative stability. Based on the results, it was found that heteroprotein complexes and coacervates can be used to encapsulate omega rich oil.

Key Words: Lactoferrin, Pea protein isolate, Raspberry seed oil, Sour cherry kernel oil, Complex coacervation, Encapsulation

ÖZET

VİŞNE VE AHUDUDU-BÖĞÜRTLEN TÜRÜ MEYVE ÇEKİRDEĞİ YAĞLARININ PROTEİN-PROTEİN KOMPLEKSLERİ İLE KAPSÜLLENMESİ

ADAL, Eda

Doktora Tezi, Gıda Mühendisliği
Tez Yöneticisi: Prof. Dr. Esra İBANOĞLU
Mart 2019
148 sayfa

Bu çalışmada, yüksek Omega 3 ve 6 yağ asitleri içeren ahududu çekirdeği ve vişne çekirdeği yağlarının zıt yüklü protein kompleksleri ve koaservatları ile enkapsüllenmesi incelenmiştir. Tezin ilk bölümünde, belirli oranlarda iki zıt yüklü protein laktoferrin (LF) ve bezelye proteini izolatı (BPİ) arasında gerçekleşen elektrostatik etkileşim çalışılmıştır. Elektrostatik komplekslerin yapısal yönleri dinamik ışık saçılımı, küçük açı X-Ray saçılma (SAXS) , bulanıklık, geçirimli elektron mikroskopu (TEM) ve atomik kuvvet mikroskopu (AFM) ile incelenmiştir. Vizkoz yapıdaki kompleks koaservat dar bir pH aralığında (pH 5.0 and 5.8) elde edilirken çözünür kompleksler pH 6.2-7.5 aralığında oluşturulmuştur.

İkinci kısımda, emülsiyonlar optimum kompleks (pH 7) ve koaservat (pH 5.4) koşullarında farklı yöntemlerle hazırlandı. En uygun yöntem, damlacık büyüklüğü, damlacık yükü, emulsiyon stabilitesine bakılarak kompleks ve koaservatların enkapsülasyon işleminin son aşamasında oluşturulması olarak belirlendi. Tezin üçüncü bölümünde, farklı yağ konsantrasyonunun (ağırlıkca %2-10) emülsiyonların damlacık büyüklüğü ve reolojisi üzerindeki etkisi incelenmiştir Emülsiyonlar daha sonra yükleme kapasitesini, enkapsülasyon verimini, yükleme verimini, nem içeriğini ve enkapsül morfolojisini değerlendirmek üzere dondurularak kurutuldu. Yağ konsantrastonun artışı enkapsülasyon verimi ve enkapsül morfolojisi üzerinde olumsuz etki göstermiştir ($p<0.05$). Optimum koşullarda (ağırlıkça %6 yağ ve %2 protein) ahududu çekirdeği ve vişne çekirdeği yağı enkapsülleri üretilmiş ve oksidatif kararlılığı incelenmiştir. Enkapsüle edilmiş yağların 45°C'de daha kararlı olduğu gözlemlenmiştir. Sonuç olarak, enkapsülasyon bu tür hassas yağların oksidasyona karşı korunmasına yardımcı olmuştur. Bu çalışma ile birlikte, zıt yüklü proteinlerle oluşturulan kompleksler ve koaservatlar omega bakımından zengin yağların enkapsüllenmesinde kullanılabileceği tespit edilmiştir.

Anahtar Kelimeler: Laktoferrin, Bezelye proteini izolatı, Ahududu çekirdeği yağı, Vişne çekirdeği yağı, Kompleks koaservasyon, Enkapsülasyon

To My Mom

ACKNOWLEDGEMENTS

I would like to express my deepest gratitude to my supervisor Prof. Dr. Esra İBANOĞLU for her guidance, advice, criticism, encouragements and insight throughout this study.

I would like to thank Prof. Dr. Şenol İBANOĞLU for his interest and help.

I would also to thank my advisor Dr. Anwesha SARKAR in School of Food Science and Nutrition at University of Leeds in United Kingdom for providing excellent advice and constructive criticism to enable me to progress through my study. I would like to acknowledge the Food Hydrocolloids staff at University of Leeds for their kindly help and technical support

I would also like to thank Dr. Kirsi JOUPPILA in Department of Food and Environmental Science at University of Helsinki to encourage me about studying encapsulation.

I also express my gratitude to TUBITAK for the scholarship from 2214-A International Research Fellowship Programme (for PhD students) (Doktora Sırası Araştırma Bursu).

I am grateful for assistance and friendship from my friends Tuğba AKTAR, Ayşe Nur YÜKSEL, Seydi KAÇMAZ, Erkan AĞYÜZ, Burak ŞAHİN.

I would like to than Ekrem ERİKÇİ and Neşe KÜRCE for their administrative support.

Last but not least, very special thanks to my mother (Gülseren ADAL), father (Ahmet ADAL), brother (Mehmet ADAL), sister (Havva BAĞCI), sister's husband (Murat BAĞCI) and nieces (Bade and Eylül BAĞCI) for their moral and support and being my side through this tough journey.

TABLE OF CONTENTS

Page

ABSTRACT ..... **v**

ÖZET ..... **vi**

ACKNOWLEDGEMENTS ..... **viii**

TABLE OF CONTENTS ..... **ix**

LIST OF TABLES ..... **xii**

LIST OF FIGURES ..... **xvi**

CHAPTER 1 ..... **1**

INTRODUCTION **1**

CHAPTER 2 ..... **5**

LITERATURE SURVEY **5**

2. 1 Encapsulation 5

2. 1. 1 Encapsulation Methods 7

2. 1. 2 Materials used for Encapsulation 15

2. 1. 3 Encapsulation of oils 16

2. 1. 4 Characterisation of encapsulated oils 19

2. 1. 5 Application of encapsulated oils in the food industry 21

2. 2 Encapsulation of oils by complex coacervation 22

2. 2. 1 Coacervation 22

2. 2. 1. 1 Simple coacervation 22

2. 2. 1. 2 Complex coacervation 23

2. 2. 2 Factors affecting complex coacervation 23

2. 2. 3 Heteroprotein complex coacervation 24

2. 2. 4 Encapsulation studies of oils by complex coacervation in the literature 26

2. 3 Lactoferrin 28

2. 4 Pea protein isolate 29

2. 5 Rasberry seed and sour cherry kernel oils 30

2. 5. 1 Omega-3 rich oils 30

2. 5. 2 Sour Cherry seed oil 32

2. 5. 3 Raspberry seed oil 33

CHAPTER 3 ..... **35**
MATERIALS AND METHODS **35**
3. 1 Materials 35
3. 2 Characterization of Raspberry Seed and Sour Cherry Kernel Oils 35
3. 2. 1 Fatty Acid Composition 35
3. 2. 2 Refractive Index and Density 36
3. 2. 3 Peroxide Value 36
3. 2. 4 Colour Measurement 37
3. 2. 5 Induction Time (IT) Measurement 37
3. 3 LF-PPI Complex and Coacervate Preparation 37
3. 4 Protein content, solubility curve and composition 39
3. 5 Emulsions preparation for method Optimization 40
3. 6 Emulsion preparations for Oil/Wall material concentration optimization 42
3. 7. Freeze drying of encapsules 42
3. 8 Formation of encapsulated Raspberry Seed and Sour cherry Kernel Oils 43
3. 9 Storage conditions for oxidative stability 43
3. 10 Size and ζ-potential Measurements 43
3. 11 Turbidity measurements 44
3. 12 Small-angle X-ray scattering 44
3. 13 Transmission electron microscopy 45
3. 14 Atomic force microscopy measurements 45
3. 15 Droplet size analysis 46
3. 16 Microstructure analysis 46
3. 17 Emulsion stability 47
3. 18 Optical microscopy 47
3. 19 Rheological measurement 47
3. 20 Moisture content determination of powders 48
3. 21 Encapsulation yield calculation 48
3. 22 Loading capacity , Loading efficiency and Encapsulation efficiency 48
3. 23 Morphological analysis by Scanning Electron Microscopy 49
3. 24 Peroxide value determination 49
3. 25 Fourier transforms infrared radiation analysis 49
3. 26 Statistical Analysis 50

CHAPTER 4 ..... **51**
RESULTS AND DISCUSSIONS **51**
4. 1 Characterizations of oils 51
4. 2 Formation of heteroprotein complexes and coacervates 56
4. 2. 1 Protein content, solubility curve and composition 56
4. 2. 2 Effects of biopolymer mixing ratio on LF-PPI complex formation 57
4. 2. 3 Effects of pH on coacervate formation 60
4. 2. 4 Identification of boundary conditions for coacervate formation 64
4. 2. 5 Small Angle X-ray Scattering (SAXS) 66
4. 2. 6 Electron micrographs of the coacervates 70
4. 3 Emulsion studies Part I: Method optimization 74
4. 3. 1 Droplet Size of Emulsions 74
4. 3. 2 Droplet charge of emulsions 75
4. 3. 3 Emulsion Stability 76
4. 3. 4 Microstructure results 78
4. 4 Emulsion studies Part II: Oil/Wall material concentration optimization 78
4. 4. 1 Droplet size of emulsions 80
4. 4. 2 Rheological measurement 82
4. 5 Freeze drying of emulsions 88
4. 5. 1 Moisture Content of Encapsules 88
4. 5. 2 Encapsulation Yield 88
4. 5. 3 Loading Capacity, Loading Efficiency, Encapsulation Efficiency 90
4. 5. 4 Scanning Electron Microscopy (SEM) 93
4. 6 Formation and characterization of Encapsulated RSO and CHSO oils at optimum conditions 98
4. 6. 1 Moisture Content of Powders 98
4. 6. 2 Color Properties of Powder 99
4. 6. 3 Fourier transforms infrared radiation (FTIR) Analysis 101
4. 6. 4 Oxidative Stability of RSO and CHSO oils 107
CONCLUSION **109**
REFERENCES **111**
APPENDIX **129**
CURRICULUM VITAE **145**

LIST OF TABLES

Page

Table 2. 1 The encapsulation methods commonly applied for food applications and the corresponding examples 8

Table 2. 2 The main materials applied for encapsulating bioactive extracts and compounds. 16

Table 2. 3 Natural sources of ω-3 fatty acids 32

Table 4. 1 Fatty acid composition of studied cold pressed oils (%) 52

Table 4. 2 Quality parameters of studied seed oils 52

Table 4. 3 Color value of studied oils 53

Table 4. 4 Assigment of absorption bands in the IR spectra of the oils 54

Table 4. 5 Radius of gyration of PPI, LF and their complex at pH 7.0 68

Table 4. 6 Radius of gyration of LF-PPI coacervates (at pH 5.4 and 5.8) and soluble complexes (at pH 6.2 and 7.0) 69

Table 4. 7 Sauter mean diameter (d_{32}) and volume mean diameter (d_{43}) of emulsions 75

Table 4. 8 Droplet charge (ζ-potential) of emulsions 76

Table 4. 9 Rheological parameters of emulsions prepared with 2 wt% LF-PPI complexes and 2-10 wt% RSO at pH 5.4 and pH 7 85

Table 4. 10 Moisture content of Encapsulated RSO and CHSO produced at optimum conditions (2 wt% LF-PPI complex and 6 wt% RSO or CHSO) 99

Table 4. 11 Color values of encapsulated RSO and CHSO produced at optimum conditions (2 wt% LF-PPI complex and 6 wt% RSO or CHSO) 100

Table A. 1 Sauter mean diameter (d_{32}) and volume mean diameter (d_{43}) of emulsions prepared with different RSO concentration at pH 5.4 129

Table A. 2 Sauter mean diameter (d_{32}) and volume mean diameter (d_{43}) of emulsions prepared with different RSO concentration at pH 7 129

Table A. 3 MC, EY, LC, LE and EE (%) of encapsules prepared with different RSO concentration at pH 7 130
Table A. 4 MC, EY, LC, LE and EE (%) of encapsules prepared with different RSO concentration at pH 5.4 131
Table A. 5 ANOVA result of Influence of changing RSO concentration on Volume mean diameter (d_{43}) value of emulsions prepared with 2 wt% LF-PPI complexes at pH 7 135
Table A. 6 Multiple range test result for Volume mean diameter (d_{43}) value of emulsions prepared with 2 wt% LF-PPI complexes and RSO (different concentration) at pH 7..... 135
Table A. 7 ANOVA result of Influence of changing RSO concentration on Sauter mean diameter (d_{32}) value of emulsions prepared with 2 wt% LF-PPI complexes at pH 7 135
Table A. 8 Multiple range test result for Sauter mean diameter (d_{32}) value of emulsions prepared with 2 wt% LF-PPI complexes and RSO (different concentration) at pH 7..... 136
Table A. 9 ANOVA result of Influence of changing RSO concentration on Volume mean diameter (d_{43}) value of emulsions prepared with 2 wt% LF-PPI complexes at pH 5.4 136
Table A. 10 Multiple range test result for Volume mean diameter (d43) value of emulsions prepared with 2 wt% LF-PPI complexes and RSO (different concentration) at pH 5.4..... 136
Table A. 11 ANOVA result of Influence of changing RSO concentration on Sauter mean diameter (d_{32}) value of emulsions prepared with 2 wt% LF-PPI complexes at pH 5.4..... 137
Table A. 12 Multiple range test result for Sauter mean diameter (d_{32}) value of emulsions prepared with 2 wt% LF-PPI complexes and RSO (different concentration) at pH 5.4..... 137
Table A. 13 ANOVA result of Influence of changing RSO concentration on Encapsulation Yield value of emulsions prepared with 2 wt% LF-PPI complexes at pH 5.4..... 137
Table A. 14 Multiple range test result for Encapsulation Yield value of emulsions prepared with 2 wt% LF-PPI complexes and RSO (different concentration) at pH 5.4..... 138

Table A. 15 ANOVA result of Influence of changing RSO concentration on Moisture Content value of emulsions prepared with 2 wt% LF-PPI complexes at pH 5.4 138
Table A. 16 Multiple range test result for Moisture Content value of emulsions prepared with 2 wt% LF-PPI complexes and RSO (different concentration) at pH 5.4 138
Table A. 17 ANOVA result of Influence of changing RSO concentration on Encapsulation Efficiency value of emulsions prepared with 2 wt% LF-PPI complexes at pH 5.4 139
Table A. 18 Multiple range test result for Encapsulation Efficiency value of emulsions prepared with 2 wt% LF-PPI complexes and RSO (different concentration) at pH 5.4 139
Table A. 19 ANOVA result of Influence of changing RSO concentration on Loading Efficency value of emulsions prepared with 2 wt% LF-PPI complexes at pH 5.4 139
Table A. 20 Multiple range test result for Loading Efficiency value of emulsions prepared with 2 wt% LF-PPI complexes and RSO (different concentration) at pH 5.4 140
Table A. 21 ANOVA result of Influence of changing RSO concentration on Loading Capacity value of emulsions prepared with 2 wt% LF-PPI complexes at pH 5.4 140
Table A. 22 Multiple range test result for Loading Capacity value of emulsions prepared with 2 wt% LF-PPI complexes and RSO (different concentration) at pH 5.4 140
Table A. 23 ANOVA result of Influence of changing RSO concentration on Encapsulation Yield value of emulsions prepared with 2 wt% LF-PPI complexes at pH 7 141
Table A. 24 Multiple range test result for Encapsulation Yield value of emulsions prepared with 2 wt% LF-PPI complexes and RSO (different concentration) at pH 7 141
Table A. 25 ANOVA result of Influence of changing RSO concentration on Moisture Content value of emulsions prepared with 2 wt% LF-PPI complexes at pH 7 141

Table A. 26 Multiple range test result for Moisture Content value of emulsions prepared with 2 wt% LF-PPI complexes and RSO (different concentration) at pH 7 142
Table A. 27 ANOVA result of Influence of changing RSO concentration on Encapsulation Efficiency value of emulsions prepared with 2 wt% LF-PPI complexes at pH 7 142
Table A. 28 Multiple range test result for Encapsulation Efficiency value of emulsions prepared with 2 wt% LF-PPI complexes and RSO (different concentration) at pH 7 142
Table A 29 ANOVA result of Influence of changing RSO concentration on Loading Efficiency value of emulsions prepared with 2 wt% LF-PPI complexes at pH 7 143
Table A. 30 Multiple range test result for Loading Efficiency value of emulsions prepared with 2 wt% LF-PPI complexes and RSO (different concentration) at pH 7 143
Table A. 31 ANOVA result of Influence of changing RSO concentration on Loading Capacity value of emulsions prepared with 2 wt% LF-PPI complexes at pH 7 143
Table A. 32 Multiple range test result for Loading Capacity value of emulsions prepared with 2 wt% LF-PPI complexes and RSO (different concentration) at pH 7 144

LIST OF FIGURES

Page

Figure 2. 1 Schematic diagram of two representative types of encapsules, A: mononuclear capsule, B: aggregate. 5

Figure 2. 2 A schematic process showing the spray-drying encapsulation process.....10

Figure 2. 3 A schematic process showing a fluidized-bed encapsulation process.....13

Figure 2. 4 a) Dispersion of core material in a shell polymer solution;
b) Separation of coacervate from the solution;
c) Coacervate micro-droplets coat the core material;
d) The coacervates coalesce to form a continuous shell around the core particles.....24

Figure 2. 5 Schematic representation of between oppositely charged proteins.....25

Figure 2. 6 Phase separation of chia seed oil.....27

Figure 2. 7 A) Structure of Lactoferrin **B)** Powder form of Lactoferrin.....29

Figure 2. 8 Image of yellow pea A) Seed form B) Powder form 31

Figure 3. 1 Schematic illustrations of steps of production of heteroprotein complex coacervate showing the visual aspect of the viscous phase (macroscale).....39

Figure 4. 1 FTIR spectra of RSO 55

Figure 4. 2 FTIR spectra of CHSO 55

Figure 4. 3 SDS-PAGE of LF (0.047 mM) and PPI (0.007 mM) stock solutions. M is the molecular weight marker (10–250 kDa). 56

Figure 4. 4 Solubility curve of PPI stock solution after centrifugation and filtration (1.2 g/L). 57

Figure 4. 5 Visual images (A) and dependence of hydrodynamic radius, R_h (bold line), turbidity (dotted line) (B) on PPI/ LF ratio on mixing LF (0.047 mM) with different concentrations of PPI at pH 7....59

Figure 4. 6 Mean ζ-potential values as a function of PPI/ LF ratio on mixing LF (0.047 mM) with different concentrations of PPI at pH 7. Error bars represent standard deviations.....60
Figure 4. 7 Evolution of hydrodynamic radius, R_h of 0.047 mM LF solution (■), 0.007 mM PPI solution (●) and mixture of 0.047 mM LF and 0.007 mM PPI solutions (▲) as a function of pH.....62
Figure 4. 8 Turbidity of 0.047 mM LF solution (■), 0.007 mM PPI solution (●) and mixture of 0.047 mM LF and 0.007 mM PPI solutions (▲) as a function of pH.....63
Figure 4. 9 Mean ζ-potential values of 0.047 mM LF solution (■), 0.007 mM PPI solution (●) and mixture of 0.047 mM LF and 0.007 mM PPI solutions (▲) as a function of pH.....65
Figure 4. 10 A) SAXS curves of 0.007 mM PPI, 0.047 mM LF and their complex formed at pH=7. The solid lines represent the fitted curves obtained by Indirect Fourier Transfor B) The corresponding Pair-Distance Distribution Functions (PDDFs) are displayed as a function of the radial distance (r).....67
Figure 4. 11 A) Small angle scattering curves of the LF-PPI coacervates and/or soluble complexes at various pH values. B) The corresponding Pair-Distance Distribution Functions (PDDFs).....69
Figure 4. 12 TEM micrographs of LF-PPI mixtures (PPI/LF molar ratio = 0.15) at pH 5.4 (A) and pH 7.0, (B). Scale bars 500 nm.....70
Figure 4. 13 Tapping mode AFM images with size analysis histograms of individual proteins, either as isolated particles or when they can be clearly discriminated within complexes.....72
Figure 4. 14 AFM topography image of pH 5.4 coacervate at 2048 pixel resolution, ...73
Figure 4. 15 Visual appearance of emulsions after 1 day.....77
Figure 4. 16 Visual appearance of emulsions after 7 days.....77
Figure 4. 17 Micrustructure of emulsions.....79

Figure 4. 18 Optical microscopic images of emulsions prepared with 10 wt% RSO and A: 1 wt% LF-PPI complex B: 2 wt% LF-PPI complex C: 3 wt% LF-PPI complex at pH 7 (scale: 50 µm) 80
Figure 4. 19 Influence of changing RSO concentration and pH on Sauter mean diameter (d_{32}) value of emulsions prepared with LF-PPI complexes (2 wt%) and RSO (2-10 wt%) 81
Figure 4. 20 Influence of changing RSO concentration and pH on Volume mean diameter (d_{43}) value of emulsions prepared with LF-PPI complexes (2 wt%) and RSO (2-10 wt%).....82
Figure 4. 21 Influence of changing RSO concentration (2-10 wt%) on Flow behaviour of emulsions prepared with 2 wt% LF-PPI complexes at pH 5.4 84
Figure 4. 22 Influence of changing RSO concentration (2-10 wt%) on Flow behaviour of emulsions prepared with 2 wt% LF-PPI complexes at pH 7 84
Figure 4. 23 Influence of changing RSO concentration on Viscoelastic moduli (G´-open symbols, G´´-filled symbols) of emulsions prepared with 2 wt% LF-PPI complexes at pH 5.4; A) 2 wt% RSO oil, B) 4 wt% RSO oil, C) 6 wt% RSO oil, D) 8 wt% RSO oil, E) 10 wt% RSO oil.....86
Figure 4. 24 Influence of changing RSO concentration on Viscoelastic moduli (G´-open symbols, G´´-filled symbols) of emulsions prepared with 2 wt% LF-PPI complexes at pH 7; A) 2 wt% RSO oil, B) 4 wt% RSO oil, C) 6 wt% RSO oil, D) 8 wt% RSO oil, E) 10 wt% RSO oil.....87
Figure 4. 25 Influence of changing RSO concentration (2-10 wt%) on Moisture Content (MC) (%) of encapsules prepared with 2 wt% LF-PPI complexes at pH 5.4 and 7.....88
Figure 4. 26 Influence of changing RSO concentration (2-10 wt%) on Encapsulation Yield (EY) (%) of encapsules prepared with 2 wt% LF-PPI complexes at pH 5.4 and 7.....89

Figure 4. 27 Influence of changing RSO concentration (2-10 wt%) on Loading Capacity (LC) (%) of encapsules prepared with 2 wt% LF-PPI complexes at pH 5.4 and 7.....91
Figure 4. 28 Influence of changing RSO concentration (2-10 wt%) on Loading Efficiency (LE) (%) of encapsules prepared with 2 wt% LF-PPI complexes at pH 5.4 and 7.....92
Figure 4. 29 Influence of changing RSO concentration (2-10 wt%) on Encapsulation Efficiency (EE) (%) of encapsules prepared with 2 wt% LF-PPI complexes at pH 5.4 and 7.....92
Figure 4. 30 Influence of changing RSO concentration on Microstructure of encapsules prepared with 2 wt% LF-PPI complexes at pH 7 A) 2 wt% RSO oil, B) 4 wt% RSO oil, C) 6 wt% RSO oil, D) 8 wt% RSO oil, E) 10 wt% RSO oil (A-E for 250x images, 25 µm scale) 94
Figure 4. 31 Influence of changing RSO concentration on Microstructure of encapsules prepared with 2 wt% LF-PPI complexes at pH 7 A) 2 wt% RSO oil, B) 4 wt% RSO oil, C) 6 wt% RSO oil, D) 8 wt% RSO oil, E) 10 wt% RSO oil (A-E for 800x images, 25 µm scale) 95
Figure 4. 32 Influence of changing RSO concentration on Microstructure of encapsules prepared with 2 wt% LF-PPI complexes at pH 5.4 A) 2 wt% RSO oil, B) 4 wt% RSO oil, C) 6 wt% RSO oil, D) 8 wt% RSO oil, E) 10 wt% RSO oil (A-E for 250x images, 25 µm scale) 96
Figure 4. 33 Influence of changing RSO concentration on Microstructure of encapsules prepared with 2 wt% LF-PPI complexes at pH 5.4 A) 2 wt% RSO oil, B) 4 wt% RSO oil, C) 6 wt% RSO oil, D) 8 wt% RSO oil, E) 10 wt% RSO oil (A-E for 1200x images, 10 µm scale) 97
Figure 4. 34 Image of freeze-dried encapsules; A) LF-PPI (2 wt%) coated RSO (6 wt%) at pH 5.4, B) LF-PPI (2 wt%) coated RSO (6 wt%) at pH 7, C) LF (2 wt%) coated RSO (6 wt%) at pH 7, D) PPI (2 wt%) coated RSO (6 wt%) at pH 7.....100

Figure 4. 35 Image of freeze-dried encapsules; A) LF-PPI (2 wt%) coated CHSO (6 wt%) at pH 5.4, B) LF-PPI (2 wt%) coated CHSO (6 wt%) at pH 7, C) LF (2 wt%) coated CHSO (6 wt%) at pH 7, D) PPI (2 wt%) coated CHSO (6 wt%) at pH 7 101
Figure 4. 36 FTIR spectra of A: LF-PPI coated CHSO encapsules at pH 5.4, B: LF-PPI coated CHSO encapsules at pH 7, C: CHSO, D: LF (freeze dried), E: PPI (freeze dried) 103
Figure 4. 37 FTIR spectra of a: CHSO, b: LF-PPI coated CHSO encapsules at pH 7, c: LF-PPI coated CHSO encapsules at pH 5.4, d: PPI (freeze dried), e: LF (freeze dried) at Amide I bands (NH_2 bending) 104
Figure 4. 38 FTIR spectra of a: CHSO, b: LF-PPI coated CHSO encapsules at pH 7, c: LF-PPI coated CHSO encapsules at pH 5.4, d: LF (freeze dried), e: PPI (freeze dried) at CH_2 streching region (2800-2900 cm^{-1}) 104
Figure 4. 39 FTIR spectra of A: LF-PPI coated RSO encapsules at pH 5.4, B: LF-PPI coated RSO encapsules at pH 7, C: RSO, D: LF (freeze dried), E: PPI (freeze dried) 105
Figure 4. 40 FTIR spectra of a: CHSO, b: LF-PPI coated CHSO encapsules at pH 7, c: LF-PPI coated CHSO encapsules at pH 5.4, d: PPI (freeze dried), e: LF (freeze dried) at Amide I bands (NH_2 bending) 106
Figure 4. 41 FTIR spectra of a: CHSO, b: LF-PPI coated CHSO encapsules at pH 7, c: LF-PPI coated CHSO encapsules at pH 5.4, d: LF (freeze dried), e: PPI (freeze dried) at CH_2 streching region (2800-2900 cm^{-1}) 106
Figure 4. 42 PV of bulk and encapsulated RSO and CHSO oils at pH 7 during storage 107
Figure 4. 43 PV of bulk and encapsulated RSO and CHSO oil at pH 5.4 during storage 108
Figure A. 1 Droplet size volume distribution of LF-PPI coated emulsion with 2 wt% oil at pH 5.4 132
Figure A. 2 Droplet size volume distribution of LF-PPI coated emulsion with 10 wt% oil at pH 5. 132

Figure A. 3 Image of Ultrasound application 133
Figure A. 4 Image of high speed homogenizer application 133
Figure A. 5 Image of Freeze drying of samples 134
Figure A. 6 Emulsion Sample A) Before Freeze Drying B) After Freeze Drying .. 134

CHAPTER 1
INTRODUCTION

In the world, especially in recent years, sensitivity and consciousness about healthy eating have increased significantly. The demographic change sand socio-economic change of the populations in the world and in Turkey show the need for healthy, easy to prepare food. In line with all these changes, scientific research has shifted to the search and development of foods that are defined as " functional foods " that contain natural bioactive components as well as traditional foods that are constantly consumed. Consumption of such foods is effective in preventing the illness caused by the disease, as well as increasing the health costs of the elderly population, by preventing the disease and decreasing the risk of disease. Specific minerals, vitamins, fatty acids or dietary fiber containing foods, phytochemical or antioxidant-added foods and probiotics containing foods are some examples of functional foods.

The berry and cherry seed oils we will use in the present study are produced from the waste and include essential fatty acids (Omega-3 and Omega-6) that cannot be synthesized by the body and needed to be taken from food or supplements. These fatty acids (Omega-3 and Omega-6) provide potential health benefits in the risk reduction of heart disease, cancer hypertension, and autoimmune disorders. According to recent studies, reducing the dietary ratio of Omega-6 to Omega-3 fatty acids might play role in decreasing the risk of heart disease and cancer. The current dietary ratio of Omega-6 to Omega-3 fatty acids is about 10:1, and the recommended ratio is estimated to be 4:1 or lower (Simopoulos, 2008). The oil from berry seed and sour cherry kernel oil has 2:1and 4:1 Omega-6 to Omega-3, respectively (Parry et al., 2005; Yılmaz and Gökmen, 2013).

Today, oils containing Omega 3 and 6 fatty acids are directly involved in food. But these oils, which are sensitive to light, heat and moisture, can easily undergo oxidation during the storage and processing of food products.

Encapsulation is one of the most common methods used to partially prevent this problem of oils, to give a new form (powder) and to increase its functionality for use in food products (Kaushik et al., 2015). Encapsulation is a method of protecting the bioactive substances by forming a barrier between the encapsulated substance and the environment. According to the literature review, spray drying (Frascareli et al., 2012), freeze drying (Heinzelmann et al., 2000), extrusion (de Vos et al., 2010), fluidized bed (Kuang et al., 2010), co-crystallization (Gouin, 2004) and coacervation (Piacentini et al., 2013) are the most common methods used to encapsulate food ingredients. In these methods, coacervation is a physical method used recently in the encapsulation of bioactive substances such as omega fatty acids sensitive to environmental factors.

Interaction of oppositely charged biopolymers in aqueous media, mostly driven by electrostatic forces can lead to a spontaneous liquid-liquid phase separation into biopolymer-rich phase (coacervate phase) and solvent-rich phase (Salvatore et al., 2011). During initial stages, the biopolymer molecules tend to form intrapolymeric soluble complexes. Further electrostatic interaction leads to the formation of a dense and viscous liquid phase (coacervate) from a homogeneous macromolecular solution of poor solvency as a result of thermodynamic incompatibility. The significance of complex coacervation ranges from its natural occurrence in biological systems, such as providing the outer physical protection of mussels and sand castle worms (Hwang et al., 2018), to biomedical applications, such as scaffold based tissue engineering (Toh et al., 2005), drug delivery (Jin and Kim, 2008) and various food applications, such as biodegradable films, fat replacer and meat analogues (Wu et al., 2014). Type and size of biopolymers, mixing ratio, total biopolymer concentration, chain conformation and flexibility, distribution of reactive groups and the charge density, solvent conditions (pH, ionic strength and temperature), stirring and pressure are important physicochemical parameters influencing the associative interaction between the two biopolymers (Schmitt et al., 1998).

Although complex coacervation has been studied in a wide range of polyelectrolyte systems, protein-protein complex coacervation is a relatively new undertaking. Understanding the mechanism of the heteroprotein complex coacervation will open enormous opportunities for immediate use in food and non-food applications (pharmaceuticals, cosmetics, biomedicals), where biocompatibility is a key issue. Heteroprotein complex coacervation between cationic lactoferrin (LF) and anionic β-

lactoglobulin ((Chapeau et al., 2016; Du et al., 2015; Flanagan et al., 2015; Kizilay et al., 2014; Peixoto et al., 2016; Tavares et al., 2015; Yan et al., 2013) as well as casein (Anema and de Kruif, 2011, 2016) has captured much research attention in recent years. Yan and co-workers (Yan et al., 2013) observed that LF and BLG coacervates were formed at very low salt concentration and narrow pH range around 5.7−6.2, which has been recently confirmed by Peixoto and coworkers (Peixoto et al., 2016) using fluorescence intensity measurements and nuclear magnetic resonance. On the other hand, Anema and de Kruif (2014) observed that the coacervation of lactotransferrin and β-lactoglobulin over a relatively wide pH range of pH 5-7.3 and higher ionic strength. Studies by Nigen *et al.* showed presence of both coacervation and complexation with presence of unique micro-spherical particles between lysozyme and calcium-depleted α-lactalbumin (apo α-LA) (Nigen et al., 2007a), which was largely temperature dependent (Nigen et al., 2007b).

In this study, we utilized two globular proteins: lactoferrin (LF) and a mixed plant protein, pea protein isolate (PPI). Lactoferrin (LF) is a metal-binding glycoprotein with a molar mass of 80 kDa and a high isoelectric point (pI) of ~8.5 providing it a novel feature of maintaining positive charge over a wide range of pH (Yan, Y. F. et al., 2013). Pea (*Pisum sativum L.)* is an important vegetable source of protein and has attracted significant research attention because of its biological value, functional properties in food applications, and relatively low cost. Pea protein is dominated by two major globulin (legumin and vicilin) and one minor (convicilin) proteins. Pea protein is limited in sulphur-containing amino acids, so it might be a strategy to complement the protein with dairy protein, the latter being rich in all essential amino acids. To our knowledge, there are no reported studies on heteroprotein coacervation between LF and plant protein. Nonetheless, LF/ PPI coacervate-based biomaterials can not only lead to a novel class of food matter, but can potentially be employed in a wide range of applications. However, to design such a functional coacervate, efforts must be undertaken to identify the precise range of working conditions for formation of complexes, coacervate and their structural aspects at different length scales.

The goal of all our research plans was to investigate the availability of complex coacervation between proteins (lactoferrin, pea protein isolate) to be used by using two functional proteins, to increase the encapsulation efficiency, to investigate the usability

of bioactive oils in powder form to be obtained in food products. For this purposes, the thesis consists of following parts;

- In the first part, conditions for creation of LF/ PPI heteroprotein coacervate and complexes were identified, which were characterized by electrophoretic mobility, dynamic light scattering (DLS), turbidimetry and TEM (transmission electron microscopy). In addition, SAXS (small-angle X-ray scattering) and AFM (atomic force microscopy) were employed to gain structural insights of the LF-PPI complexes and coacervate at specified conditions.
- In the second part, emulsion studies were carried out by using the optimum coacervation conditions obtained from the first part. In these studies, the most suitable emulsion formation model for encapsulation were selected by looking at the emulsion droplet size, zeta potential, creaming index. Ultrasonication, which has received great interest in the formation of emulsions in recent years, was used to achieve finer droplet size and more stable emulsions.
- In the third part, the encapsulation process was started using the emulsion formation model determined in the second part. Oil/ coating material ratio was optimized according to the best encapsulation efficiency and morphology of the samples.
- In the fourth section, powder capsules were produced with raspberry and sourcherry seed oils and stored for a certain period at specific temperatures to investigate characterizations and oxidation stability of encapsules.

CHAPTER 2
LITERATURE SURVEY

2. 1 Encapsulation

Encapsulation refers to a technique of an active agent (one substance) within another substance usually known as wall material (Nedovic et al., 2011). The encapsulated content other than the active agents is known as the core, fill, internal, or payload phase. On the other hand the encapsulating substance is often referred to as the membrane, carrier material, matrix, coating, external phase or shell (Fang and Bhandari, 2010). In general, capsules can be classified according to their size: macrocapsules (>5,000µm), microcapsules (0.2 to 5,000µm) and nanocapsules (<0.2µm). In terms of their shape and structure, capsules can be divided into two groups: mononuclear capsule (A) and aggregate (B) (Figure 2.1).

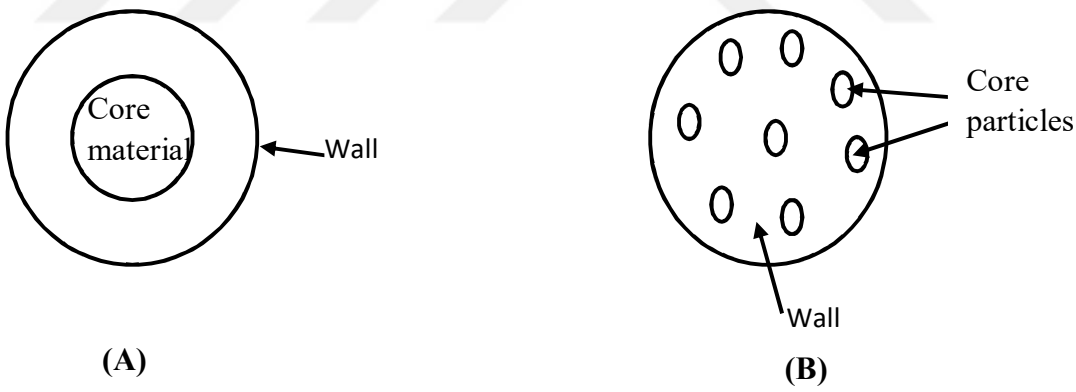

Figure 2. 1 Schematic diagram of two representative types of encapsules, A: mononuclear capsule, B: aggregate.

Typically, encapsulation has been applied in the food industry for a number of reasons. The process is considered vital because it improves how bioactive molecules and living cells are delivered into foods (de Vos et al., 2010). Typically, encapsulation entails a technology where bioactive compounds are entirely covered, protected, and enveloped

by a physical barrier; bioactive components do not have a provision to protrude (McClements et al., 2009). Additionally, encapsulation has turned out to be an essential process of packaging gaseous, liquids, or solid substances in form of tiny capsules. The capsules discharge their contents in a regulated manner under particular conditions over a prolonged period (de Vos et al., 2010). Originally presented in the field of biotechnology, encapsulation was supposed to improve the efficiency of production processes since the matrix enveloping the cells enables efficient and rapid separation of metabolites and producer cells. Though the process was founded more than six decades ago, it has attracted significant interest in the pharmaceutical and food industry. Recently, the food industry has experienced a surge in demand for functional compounds albeit these compound are normally vulnerable to gastro-intestinal and environmental conditions thus encapsulation has provided a protective mechanism to preserve their functionality. Precisely, functional compounds including bioactive compounds are beneficial because they preserve and control the texture, flavour, and colour of products.

Another goal achieved by encapsulation is the preservation of stability of bioactive materials. This is important during processing and hoarding because it averts unwanted interference with the food matrix. Naturally, bioactive food compounds quickly undergo rapid inactivation, and such compounds stand to benefit from encapsulation because it decelerates the rate of degradation or prevents it in totality until the product is conveyed to the desired location (Lesmes and McClements, 2009). The technology creates a barrier between the environment and bioactive materials that are sensitive implying masking of organoleptic characteristics including masking of bad smelling and taste, increased bioavailability, differentiation of taste and aroma, stabilisation of food ingredients. Consequently, the bioactive component remains fully functional, and homogenous dispersion of the active agent and adequate concentration are guaranteed (Onwulata, 2012).

According to (Dias et al., 2015), encapsulation provides a crucial means to safeguard natural compounds and extracts from interference from abiotic, biotic, and biological effects. It is considered a dependable methodology in the field of health and nutrition where bioavailability, efficacy, and stability of extracts and compounds are required. From the practical perspective, the technique protects the core content of the material hence increasing the shelf life of the product. There is minimal transfer between the

nearby medium and the core besides protection of the molecules from reacting with other food components because this may reduce the product's bioavailability (Fang and Bhandari, 2010). Besides bioavailability, this technique increases the dispersibility, flow, and solubility of the bioactives (Kuang et al., 2010). Based on the encapsulated bioactive and the method applied, the response of the generated delivery system appears to vary since individual compounds have particular characteristics. Taken from that, the design of a suitable micro-encapsulation process ought to take into account such attributes. For example, phenolic compounds (which contain strong antioxidant molecules) pose a major problem in respect to their bioavailability considering that they are converted to sulphated, methylated, and glucuronated metabolites after ingestion. Another group of compounds that have organoleptic-related problems are essential oils with most of them presenting high volatility, poor water solubility, and unpleasant odour and taste. However, such limitations have been overcome through encapsulation which minimises the sensory effect and improves the effectiveness of their biological functions (de Vos et al., 2010).

2. 1. 1 Encapsulation Methods

There exists an array of encapsulation techniques that have resulted in diverse microstructures or nanostructures hence a variety of delivery and physicochemical properties. The selection of the method or microencapsulation process depends on the properties of the core and the coating materials, the release mechanism desired, process type, capsule morphology and particle size (Augustin and Hemar, 2009). Both physical and chemical processes are available to encapsulate a range of bioactive ingredients. Each of the techniques are reviewed below (Table 2.1).

Spray Drying and Spray Chilling

Spray drying is the most commonly used method in the food industry. Bioactive ingredients encapsulated by this method include fats and oils, flavours, essential oils and other oil-soluble bioactives. In spray drying, the core elements are dispersed in an emulsion or a solution laced with polymers and sprayed into a hot chamber as illustrated in the diagram below. The shell material attaches itself on the core particles as it solidifies accompanied by the evaporation of the solvent. Following this, the microcapsules formed are of matrix or polynuclear type (Figure 2.2).

Table 2. 1 The encapsulation methods commonly applied for food applications and the corresponding examples (Tavares et al., 2014)

Technique	Concept	Examples of applications
Spray drying	Drying of the encapsulated material dispersed in the shell material. Encapsulation by starch, polysaccharides, maltodextrins and/or proteins. This technique produces particles between 10 and 100 µm	Encapsulation of flavor compounds, polyphenols and vitamins
Spray cooling/ chilling	Incorporation of the core material in the warm and liquefied shell material (often vegetable oils). Relatively low-cost encapsulation technique. Through product atomization, and consequently cooling, micro-capsules are formed	Encapsulation of flavor compounds, minerals, vitamins and probiotics
Freeze drying	Co-lyophilization of the core and the shell materials after a homogenization process. Normally this technique produces non-uniform particles	Encapsulation of flavor compounds, fatty acids and probiotics
Extrusion	Formation of core material droplets that became microparticles after immersion in a hardening bath with the shell material. Normally the shell material is a glassy carbohydrate matrix. The core material may be released in a high temperature medium. The encapsulation efficiency is small, moreover the produced particles show high stability and an extended shelf-life	Encapsulation of flavor compounds, vitamins and food ingredients (lactic acid)
Spinning disk	Passage through a spinning disk of a suspension of the core material in the shell material. During processing, the shell material forms a thin film around the core material particles. Production of particles from 20 mm to few millimeters of diameter	Encapsulation of cells (yeast)
Supercritical fluid extraction	This technique is similar to spray drying, except that the shell material and the core material are solubilized/dispersed in a supercritical fluid	Encapsulation of heat-sensible cores as vitamins and polyphenols

Table 2. 1 cont'd. The encapsulation methods commonly applied for food applications and the corresponding examples (Tavares et al., 2014)

Technique	Concept	Examples of applications
Cocrystallization	Spontaneous crystallization of a supersaturated solution of sucrose simultaneously with the addition of the core material, forming a crystalline irregular network, allowing the encapsulation into the pores of the network	Encapsulation of acids, flavor compounds, antioxidants and minerals
Fluidized bed	This technique is applied for solid particle encapsulation (100 mm to few mm). The shell material is atomized onto core material fluidized by an upward stream of air	Encapsulation of acidulates, vitamins and cells
Coacervation	Phase separation of one or many polyelectrolytes from a solution and deposition of the colloidal particles around the active ingredient suspended or emulsified in the same reaction media. When hydrocolloids are used, they can be cross-linked using appropriate chemical or enzymatic agent	Encapsulation of fatty acids and flavonoids
Liposomes	Spherical particles consisting of a membranous system formed by one or more concentric bi-layers of lipids (often phospholipids). They can be used in the entrapment, delivery and released of water-soluble, lipid-soluble and amphiphilic materials	Encapsulation of vitamins, enzymes and peptides
Inclusion	This technique refers to the supra-molecular association through non-covalent interactions of a ligand ("encapsulated" compound) into a cavity formed by a "shell" material (e.g., cyclodextrins)	Encapsulation of vitamins, flavor compounds and essential oils

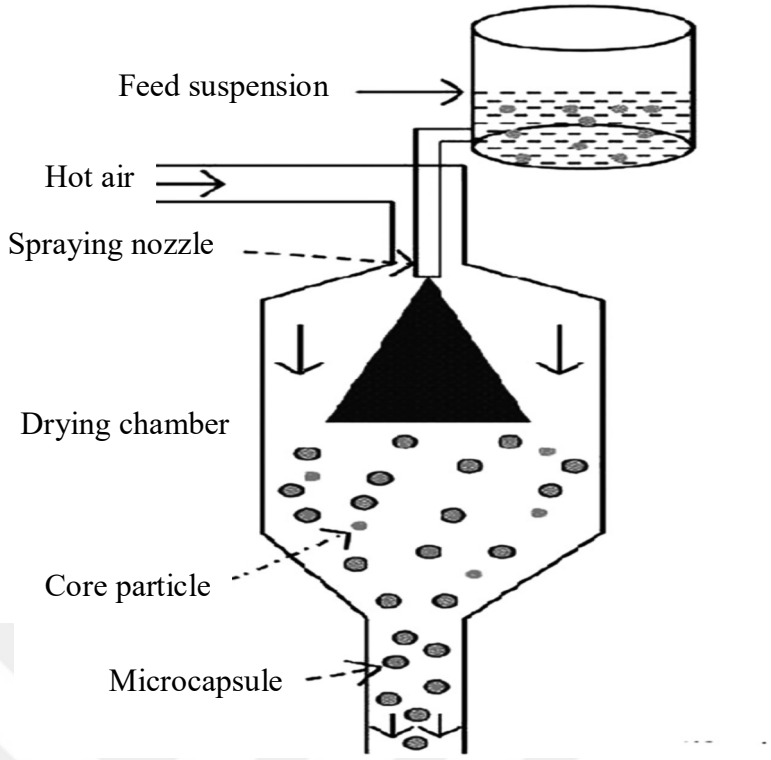

Figure 2. 2 A schematic process showing the spray-drying encapsulation process (Chawda et al., 2017)

It is considered a straightforward and flexible process allowing uninterrupted production thus a cost effective process compared to other several encapsulation processes. Concisely, the technique works perfectly with carbohydrates as shell materials though this may hinder encapsulation of some bioactive materials. High quality microcapsules measuring less than 40µm have been produced using this process. Although spray-dryers are widespread in the food industry, there are several disadvantages of this technique such complexity of the equipment, non-uniform conditions in the drying chamber and it is not always easy to control particle size (Dordevic et al., 2015).

In the spray chilling technique, the core is dispersed into liquefied coating agent that is warm and sprayed via a heated nozzle into an environment that is controlled. Micro-capsules are developed after solidification of the encapsulant (Tavares et al., 2014). Similar equipments applied in the spray drying are also used in spray chilling save for the process air that is not heated.

Freeze Drying

Freeze drying is also referred to as cryodessication or lyophilisation, and in this particular drying procedure, the temperature of the solvent (or suspension) medium is lowered up to the freezing point prior to sublimation from the solid to gaseous phase (Oetjen and Haseley, 2004). This technique can be broken into three phases, that is, the freezing, primary, and secondary drying stages. Prior to frying, the content is suspended or dissolved in a solution (normally water) and temperatures lowered to between -40°C and -20°C; at this point the water is completely crystallized together with some soluble lipids and solid components. Within the confines of the solids and crystallized ice is the unfrozen water which has amorphous concentrated solids and its state is mechanically solid. The primary drying phase involves the main drying and sublimation process whereas the secondary drying stage entails desorption drying. Food ingredients and nutraceuticals can be encapsulated by this method through dissolution, dispersion, and emulsification of the core materials within the shell matrix system followed by co-lyophilizing. Unfortunately, Fang and Bhandari (2010) allege that this may lead to a non-shrunken and porous product with an uncertain structure. Since the dehydration process for freeze-drying is conducted at very low temperatures, the method is considered suitable for drying of compounds such as peptides, enzymes, and probiotics which are sensitive to heat. Besides that, the moisture levels of the final product can be regulated. Also, the dried products are characterised by excellent stability and high quality looking at features such as colour and the texture. These products can be reconstituted in water easily because of their porous structure (increases their specific surface area) and their large coarse size (Oetjen and Haseley, 2004). The freezing drying process can complement other encapsulation techniques to transform the encapsulated core content into a powder form.

Considerably, rapid technological evolution in the food industry and biotechnology sector has been realised and processes such as spray-freeze drying (SFD) have come in handy to improve the traditional freeze-drying technique. SFP encompasses atomization of liquid ingredients to form droplets followed by freezing and eventually subliming using ice at a very low pressure and temperature (Costantino et al., 2000). SFD has some properties that distinguish it from the traditional freeze-drying process: (i) improvement of the heat and mass transfer between the frozen material and the circulating drying ingredient (ii) achievement of high quality and homogenous

properties and improved retention capability of volatile aromatic compounds (iii) Rather than a dry cake, the dry product is in form of a free-flowing fine powder with superior instant solubility and wetting properties (Mumenthaler and Leuenberger, 1991).

Fludized bed

In this technology the core particles are sprayed using the liquid coating in addition to rapid evaporation which helps in the creation of an outer layer. The coating process can be performed using a top, bottom, and tangential spray mechanism. The first method entails a downward spray containing the coating material applied on the fluid bed where the porous or solid ingredients get encapsulated as they travel to the coating area (Figure 2.3). To increase the efficiency of encapsulation and prevent formation of clusters, the flow of particles and the coating materials is opposed. Higher yields in terms of encapsulated particles are achieved by using the top spray method compared to the other two. The second (bottom spray) method is comprised of a coating chamber fitted with a nozzle designed in cylindrical shape (for spraying the coating material) and a perforated plate on the bottom side. As the particles travel upwards via the plate into the nozzle region, they get encapsulated. Attachment to the core particle occurs when the solvent evaporates or the encapsulated particle cools. Once the desired weight and thickness has been attained, the coating process is halted. The tangential spray mechanisms is made up of a spinning disc located at the bottom of the coating chamber. The disc diameter and the chamber are similar though there is a gap created between the edge of the chamber and the disc, and this is realised by elevating the disc. The tangential nozzle from which the coating elements are released is positioned above the disc. The particles travels via the gap to enter the spraying one and get encapsulated. Since the distance travelled by the particles is small, a higher yield of encapsulation is achieved (Jyothi et al., 2010).

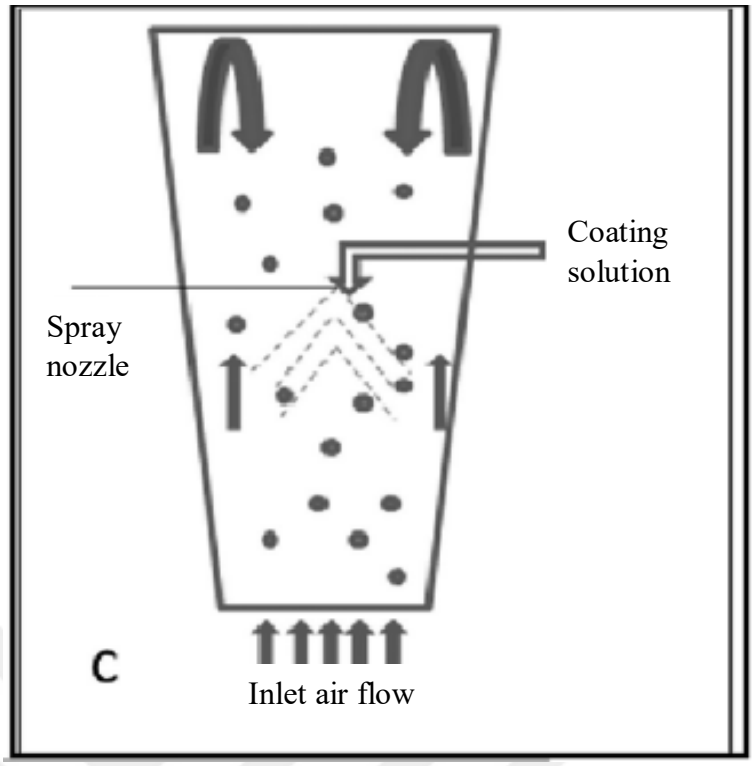

Figure 2. 3 A schematic process showing a fluidized-bed encapsulation process (Kaushik et al., 2015).

Extrusion

They are not frequent methods and can be classified as either electrostatic extrusion or co-extrusion. In the first category, a polymer melt in combination with a solubilised bioactive material is passed through a nozzle or concentric nozzles giving rise to particles with high encapsulation efficiency and density. Extrusion-based processes are primarily applied in the encapsulation unstable flavours and volatiles (Gouin, 2004). Co-extrusion has been incorporated in the production of spherical microbeads using a hydrophobic core though the same method can be applied to encapsulate hydrophilic compounds in alginate beads as demonstrated by Piazza and Roversi (2011).

Coacervation

It is the second-most commonly used technique that encompasses partial desolvation of a uniform polymer solution into two phases, that is, the coacervation medium (poor polymer phase) and the rich polymer phase known as coacervate. Presently, coacervation comprises two processes; the simple and complex coacervation process. Other than the technique providing high encapsulation efficiency, it triggers controlled

release that depends on the biological or mechanical mechanisms and temperature providing the required versatility to boost the development of an array of food products (Gouin, 2004). Complex coacervation is based on the complexity of two polymers that are oppositely charge, and which form a strong polymeric matrix or shell. In respect to simple coacervation, the temperature or pH is altered to assist in the precipitation of the initially soluble polymer (de Kruif et al., 2004; Schmitt and Turgeon, 2011). Some of the wall materials included in simple coacervation are pectins laced with the poly-glycerol poly-ricinoleate (PGPR) and milk proteins.

Emulsion based processes

This particular category allow the encapsulation of both oil and water soluble food ingredients. Techniques under this category have successfully encapsulated bioactive compounds including vitamins, fatty acids, anthocyanins, bioactive extracts, phenolic compounds, and oils. Sometime, the emulsion-based process is conducted in the presence of another procedure, mostly a spray-drying based method. The combination produces a dry precipitate that can be introduced to food products. Particularly, most encapsulation procedures commence with the first step being the preparation of an emulsion (Desai and Jin Park, 2005; Dias et al., 2015).

Ultrasound-based processes

These processes including ultrasound and sonication are regarded reliable because they are mostly used with double functions, that is, extraction of bioactives and formation of microcapsules. Ultrasonic technology has a wide scope of industrial application including cleaning equipment, extraction of substances from organic matrices, inhibition of microorganism activity, and extraction linked to enzymatic activity. Application of this technology in emulsification processes have shown positive results with higher kinetic stability to phase separation. Moreover, the ultrasonic process has a distinct micro-shear mechanism which is closely linked to emulsifiers that have high rates of adsorption in the oil/water interface (Leong et al., 2017).

The ultrasound technology is categorised into two, low and high intensity categories. The low intensity technology is basically used in investing the physico-chemical properties of food materials. Contextually, the frequency levels are typically more than

1 MHz and low power intensities which are less than 1 W/cm^2. With these conditions in place, there are no alterations realised in terms of chemical and physical properties of food products; the ultrasonic waves do not have destructive powers. Conversely, high-intensity ultrasonic processes utilise acoustic frequencies ranging from 20 to 100 KHz and high power intensities of up to 1000 W/cm^2 (McClements, 1997). From the perspective of food preservation and processing, the high-intensity process is employed since it enhances changes in the physical and chemical properties of ingredients. Therefore, the process is ideal for extraction of bioactive materials, modification of crystals, surface cleaning, cell disruption, enzyme inhibition, and emulsification. Using stable emulsions, the high intensity ultrasonic technology has proved necessary when handling nutraceutical compounds that are oil soluble. This implies that the ultrasound technology for encapsulating nutraceuticals is proving to be an alternative for preservation and protection of target compounds, especially those that are unstable and susceptible when exposed to oxygen and light (Le and Le, 2015).

2. 1. 2 Materials used for Encapsulation

Several materials may be used encapsulate or coat gases, liquids, or solids having different properties. Further, the coating material and its physical make-up strongly determine how products are developed. In view of strict regulations set for the food additives, the compounds widely used for drug encapsulation cannot be applied in the food industry (de Vos et al., 2010). Materials harnessed for design of a protective coat for encapsulates ought to exhibit the following properties; biodegradable, they must be food-grade, not toxic to organisms, and have the capacity to produce a barrier at the interface of internal content and external medium. Other than being natural, the encapsulation material, mostly biomolecules, should be able to provide maximum protection against environmental invasions, have proper rheological properties at high concentrations, be inert to the active material, and be able to confine the active material within the capsule structure during storage or processing. Encapsulation is classified in four main categories, that is, water soluble polymers, water soluble non-polymers, non-water soluble polymers, and non-water soluble non-polymers (Kuang et al., 2010). The encapsulation materials under these categories are further highlighted in the Table 2.2. The first and the most commonly used group of materials consists of carbohydrate polymers (cellulose, starch and their derivatives). Plant extracts and exudates include galactomannans, gum, soybean polysaccharides, and pectins.

Alginate and carrageenan fall under marine extracts. Chitosan, gellan, xanthan, and dextran belong to microbial and animal derived polysaccharides. This is in addition to lipids, proteins, paraffin, and some inorganic substances (Zuidam and Shimoni, 2010). What remains as an imminent factor in picking the most ideal materials is the cost factor. Also, the conversion process of the physico-chemical properties of the encapsulating material determines how successful the food product developed is going to be like.

Table 2. 2 The main materials applied for encapsulating bioactive extracts and compounds.

Material Class	Types of Materials
Proteins	Albumin, caseinate, gelatin, gluten, peptides, soy protein, whey proteins, zein, other vegetable proteins
Sugars and sugar products	Fructose, galactose, glucose, maltose, sucrose, oligosaccharide, corn syrup solids, dried glucose syrup
Starch and starch products	Maltodextrin, dextrins, starches, modified starches
Gums	Agar, alginates, carrageenan, gum acacia, gum Arabic, pectins
Cellulose material	Acetylcellulose, carboxymethyl cellulose, cellulose acetate butylate phthalate, cellulose acetate phthalate, ethyl cellulose, methyl cellulose, nitrocellulose
Lipids	Acetoglycerides, beeswax, diglycerides, natural fats and oils, fractionated fats, hardened fats, lecithin, liposomes, mono-glycerides, paraffin, tristearic acid, waxes
Other carbohydrates	Chitosan, cyclodextrins

2. 1. 3 Encapsulation of Oils

Clinical and epidemiological studies have shown that fats and oils embedded with polyunsaturated fatty acids (PUFAs) including omega-6 and omega-3 nutrients usually supply essential health benefits besides provision of energy and transportation of lipid soluble nutrients (Orsavova et al., 2015). Considering that the human body is not able to synthesise PUFAs in the required quantities, they are referred to as essential fatty

acids (EFAs) hence they need to be introduced to the body by way of diet or dietary supplements. Plant-based PUFAs such as linoleic acid (LA) and a-linolenic acid (ALA) are short chain fatty acids (SCFAs). PUFAs have a chemical structure with two or more double bonds majorly comprising of bis-allylic methylene groups (-CH=H-CH_2-CH=CH-); all the double bonds forming the structure have a *cis*-configuration. Unfortunately, such a structural formation contributes to their inherently instability and exposes them to polymerisation, isomerisation, and oxidation in the event they come across environmental stressors like light, heat, metallic ions, and oxygen (Rustan and Drevon, 2001). It is important to note that oxidation of lipids results to unwanted and detrimental volatile compounds causing rancidity in food substance. What more, an appropriate protective delivery system is requisite to minimise degradation of PUFAs-rich oils when they are being processed, stored, or transported in addition to their being assimilated in processed foods. Encapsulation is a key technique that has been capitalised on in the food industry though incorporation of synthetic or natural anti-oxidants in fats and oils to abate oxidation may be applied as well (Gouin, 2004).

During the encapsulation process, the core material, normally the PUFAs-rich oils, are entrapped inside a shell or a thin layer coating substance. Contextually, polysaccharides and proteins (applied individually or in a complex form) may be used as coating materials (Timilsena et al., 2017) to prevent the internal phase interacting with the external environment. At the same time organoleptic properties of the core material are maintained to ensure its palatability and sensory characteristics are either improved or at least not undermined. In recent times, encapsulation has been designed to achieve controlled release formulations to attain sustained and targeted delivery of lipids (Wilson and Horan, 2007). Spray drying is the oldest technique that was applied in 1927 to encapsulate flavour oil, and it is still being used in the industry to protect several unstable food ingredients (Arslan et al., 2015). Concisely, complex coacervation is considered as a low-cost, reproducible, simplest, most effective, and scalable process of encapsulating hydrophobic substances (Barrow and Shahidi, 2007). It yields low surface oil and has considerable high encapsulation efficiency thus providing substantial oxidative stability of the core material (Gouin, 2004; Wang et al., 2015). Besides that, complex coacervation can be conducted at mild processing settings without the inclusion of toxic solvents. Oppositely charge polymers which form complex coacervates are more desirable than individual polysaccharide or protein

since they are perceived to be more surface active; they enhance encapsulation efficiency thus the core substance is guaranteed of higher oxidative stability.

The freeze drying process has also been investigated producing almost similar results as those of the spray drying procedure. The procedure is initiated by freezing the emulsion between -90°C and -40°C before drying through sublimation. This should happen at low pressure levels. This particular technology has one key advantage in that it removes oxygen at low temperatures and for this reason, oxidation of the product is minimised. Based on that, it is deemed a suitable microencapsulation technology of highly sensitive products such as PUFAs and probiotics. Despite that, a study by Heinzelmann et al. (2000) demonstrates that freeze drying of encapsulated fish oil produces powders with structures that have high porosity which implies a shortened shelf life. Apart from that, the technology is 30 to 50 times costlier than the spray drying process (Carneiro et al., 2013).

Some emerging technologies have been explored to determine their impact in encapsulation of omega-3 oils. The first two are spray-based methods, that is, electrospraying for ultrathin coating and spray granulation, and fluidized-bed film coating. The third is an ultrasonic-based procedure namely encapsulation using ultrasonic atomiser. In the first method, the docosahaxaneoic acid (DHA) was encapsulated using ultra-thin layers of zein promaline. Nanometer-sized coated particles were produced through electrospraying coupled with an increased induction period for the encapsulated oil. An improved oxidative stability was realised because of the presence of zein prolamine. Further, the ultra-thin film had negligible effect on the texture properties of the product. Accordingly, the technology has a bright future in the food industry. A combination of fluid bed coating and spray granulation were tested by Anwar et al. (2010) to improve the stability of fish oil. Two successive steps were involved in coming up with the fish oil microcapsules. First, maltodextrin and soybean polysaccharides were used to emulsify the fish oil and spray dried to make granules. Once the granules were produced, they were coated with hydroxypropyl betacyclodextrin. Experimental results showed that the coating was not effective and could not abate oxidation of the lipids, therefore, its inapplicability in stabilisation of omega-3. The third process uses a typical pressure spray nozzle that cannot control the size of droplets hence they release droplets that are wide-sized. Smaller droplets are produced by using ultrasonic atomisers which employ ultrasound energy. A successful

procedure was carried out by Klaypradit and Huang (2008) who got small-sized particles and ideal emulsion stability. The wall material matrix was combination of maltodextrin and chitosan. Regrettably, the payload and encapsulation efficiency for the atomisation technology is low even though the process has some potential to microencapsulate omega-3 oils.

2. 1. 4 Characterisation of Encapsulated Oils

Processing variables and material properties influence the final outcome of the microcapsules. It is necessary to explore the characteristics of microcapsules to ascertain their bioavailability and efficacy for a targeted application. Encapsulated oils can be characterised using chemical, physical, and physico-chemical properties. The characteristics generally consists of the encapsulation efficiency (EE), microcapsules shape and particle size, payload and surface oil, sensory performance, and oxidation stability (Zhang et al., 2009). Some of these characteristics are briefly reviewed below.

Encapsulation Efficiency

Encapsulation efficiency is determined by dividing the mass of the core material encapsulated in the wall material by the core material utilised in the formulation. The mass of the free oil (non-encapsulated or surface oil) ought to be low for higher efficiency values of encapsulation to be attained. On the other hand, the mass of the completely encapsulated oil needs to have high values. It is important to assess the surface oil because it can oxidise really fast and this means that high surface oil is correlated to poor stability and flavour of microcapsules. Measurement of the surface oil can be performed by employing a typical procedure of fat determination by way of fat extraction with the help of a Soxhlet equipment and an organic solvent such as methanol, ethyl acetate or hexane. The extracted fat is measured using either quantitative spectroscopic methods (IR spectroscopy) or gravimetrically. Ideally, the quantity of surface oil ought not to be more than 0.1% for safe custody of microcapsules albeit most emulsion products have values higher than that (Kaushik et al., 2015). Mathematically, the encapsulation technology (EE) is expressed as follows,

$$EE = \frac{W_t - W_s}{W_t} * 100\% \quad (1)$$

The encapsulation yield (EY) is determined as follows,

$$EY = \frac{W_t}{W_i} \quad \text{.....} \quad (2)$$

Where,

W_t = mass of total oil in g

W_s = mass of the surface oil of the microcapsules

W_i = mass of the oil introduced to the capsule in g

Payload

It refers to the percentage of the active or oil component per unit weight of the powder, usually one gram. A higher load of the encapsulation process means an economically feasible process because the quantity of the powder needed per serving of the food is low. It is determined by evaluating the ratio of the mass of the encapsulated omega-3 (or oil) to the total mass of the powder. It is possible to measure the mass of the encapsulated omega-3 or oil gravimetrically through quantitative extraction of oil from a certain amount of microcapsules. Nonetheless, the process is destructive in nature besides being expensive and time consuming for quality control purpose. Recently, a Fourier transformed infrared (FTIR) has been deployed to measure payload (Vongsvivut et al., 2012).

Particle Size

In food applications, the microcapsules should not be more than 100µm to prevent the mouth feel impact of the preservative product. Despite that, the particle size distribution ought to be considerably narrow so as to maintain the consistency of the product. Particle size imaging using a microscope and laser scattering techniques are some of the methods used to measure the size of microcapsules. Detail morphology of the microcapsules can be studied using the confocal laser scanning microscope (CLSM) or electron microscopy, tools which have high resolution imaging. But to get a better understanding on the distribution and properties of the hydrophobic core and shell, CSLM is usually integrated with staining techniques (Kaushik et al., 2015).

Stability

The main objective of encapsulating omega-3 rich oils is to ensure the fatty acids are less vulnerable to oxidation, and this is achieved by developing a barrier with the help of a shell or wall material. Various wall materials have differing oxidative stability though this primarily depends on their ability to impede the transfer of oxygen. This property can be studied by keeping microcapsules under a set humidity and temperature level for a certain period and then evaluating the pattern of formation of oxidative products. Examples of the oxidative products formed from omega-3 fatty acids include peroxides, aldehydes, conjugated dienes, propanal, and aldehydes (Frankel et al., 2002). Quantification of the extent of oxidation is done by gauging the oxygen headspace concentration though fast analysis using oxypress or rancimat is still applicable (Kulås and Ackman, 2001). Sensory evaluation is a qualitative assessment procedure that can be used to determine the level of oxidation of the encapsulated ω-3 products. In fact, with the assistance of a trained sensory panel, the initial oxidative damage of the encapsulated ω-3 products can be qualitatively detected very fast (Kaushik et al., 2015).

2. 1. 5 Application of Encapsulated Oils in the Food Industry

Evidently, encapsulated oils have proved useful in the food industry because of preservation abilities provided to foods in times of storage or delivery. Many studies have turned their attention to new packaging technologies where active packaging has received significant consideration because of its role in improving the shelf life of food products, minimising, and eliminating the presence of microorganisms in food (da Silva et al., 2014). Essential oils are preferred as anti-microbial products in that they have a natural effect and have been deemed as safe food additives (Generally Recognised as Safe, GRAS). Essential oils have been adopted as antimicrobial food packaging additives to prevent food substances from internal and external conditions so that the shelf-life of such foods get prolonged.

Foods fortified by ω-3 fatty acids are getting consumer interest significantly day by day. Such kind of foods are now readily available around the world, such as dairy products (cheese, yogurt, and milk), bread, spaghetti, pasta, juice, meat, and baby food products. However, the challenge in producing fortified foods has been remarkable.

The major challenge in producing these foods is related to the stability of oil in the product (Bakry et al., 2016).

2. 2 Encapsulation of Oils by Complex Coacervation

2. 2. 1 Coacervation

This is a term applied in colloidal chemistry denoting the process of associative phase separation brought about by changes in ionic strength, solubility, temperature and the pH levels of the dissolving medium (Dickinson, 2008). The term originates from the Latin term *'acervus'* denoting a 'heap'. Coacervation is considered as the first procedure to be applied in the industrial production of microcapsules. Precisely, coagulation encompasses splitting of two liquid phases in a colloidal solution. One of the two phases is rich in polymer (the coacervate phase) and the poor polymer phase is known as the equilibrium solution. When the coacervation involves a single polymer, it is referred to as simple coacervation while the one involving two or more polymers that are oppositely charged is known as complex coacervation technology (Schmitt et al., 1998; Turgeon et al., 2003).

2. 2. 1. 1 Simple Coacervation

The mechanism of forming microcapsules in this method is similar to that of complex procedures save for the mode of phase separation. In regards to simple coacervation, a desolvation material is added to aid in phase separation. On the contrary, the complex process involves complexation of two polymers with opposite charges. A simple coacervation experiment conducted by (Wu and Xiao, 2005) consisted of fish oil that was emulsified into hydroxypropyl methylcellulose (HPMC) solution by homogenising at the room temperature (25°C) and a working pressure of 40MPa; the mixture was passed twice in a high-pressure homogeniser. Coacervation took place when maltodextrin was inputted and solubilised into the above emulsion while being agitated continuously. Eventually, a microencapsulated fish oil powder was attained through spray drying with the inlet and outlet temperature being 200°C and 100°C, respectively.

2. 2. 1. 2 Complex coacervation

The complex coacervation process is divided in three steps: (i) production of three immiscible phases; (ii) deposition of the coating material; and (iii) rigidisation of the shell material or coating. The first step relates to the formation of three distinct phases namely, the core ingredient, the coating material, and the liquid manufacturing vehicle (LVM). The coating substance is an immiscible polymer in a liquid phase and it is produced by altering the temperature of the polymer solution (for example, ethyl cellulose in cyclohexane) (Dyson, 1987), addition of salt (addition of sodium sulphate to gelatine solution) and non-solvent (adding isopropyl to methyl ethyl ketone solution), addition of a polymer that is not compatible with the polymer solution (for example, adding polybutadiene to an ethycellulose solution in toluene), and induction of the polymer-polymer mixture (interaction of gelatin and Arabic gum at their isoelectric point). The core material is dispersed in the coating polymer solution. Once the liquid polymer has been formed, it is deposited on the core material. The last process involves stabilisation through thermal treatment, cross-linking, or desolvation. The schematic diagram below shows a scheme of coacervation process right from the dispersion stage through coalescence of the coacervate to make a shell material (Eghbal and Choudhary, 2018).

2. 2. 2 Factors Affecting Complex Coacervation

Some of the factors influencing complex coacervation include ionic and pH strength, charge, concentration, molecular weight, ratio, and type of the polymers used. To add on that, the extent of agitation of the system, temperature, and size of emulsion also affect the outcome of the coacervation process (Turgeon et al., 2007). It was observed by Wang et al. (1999) that polymers' molecular weights have a significant effect on the complex coacervation process. For example, large molecular weights were observed to form large-sized coacervates but with lower solubility (Wang et al., 1996). A coacervation process consisting of soy protein and dextran was observed to increase with an increase in dextran weight (Semenova and Dickinson, 2010). Concerning the effect of pH, it has been found out that the pH of the medium solution affects the polymers' charge density which in turn affects the coacervation process positively. A number of investigations report that a contracted pH range for various polymers offer good results (Turgeon et al., 2003). It is worth noting that the effective pH range also

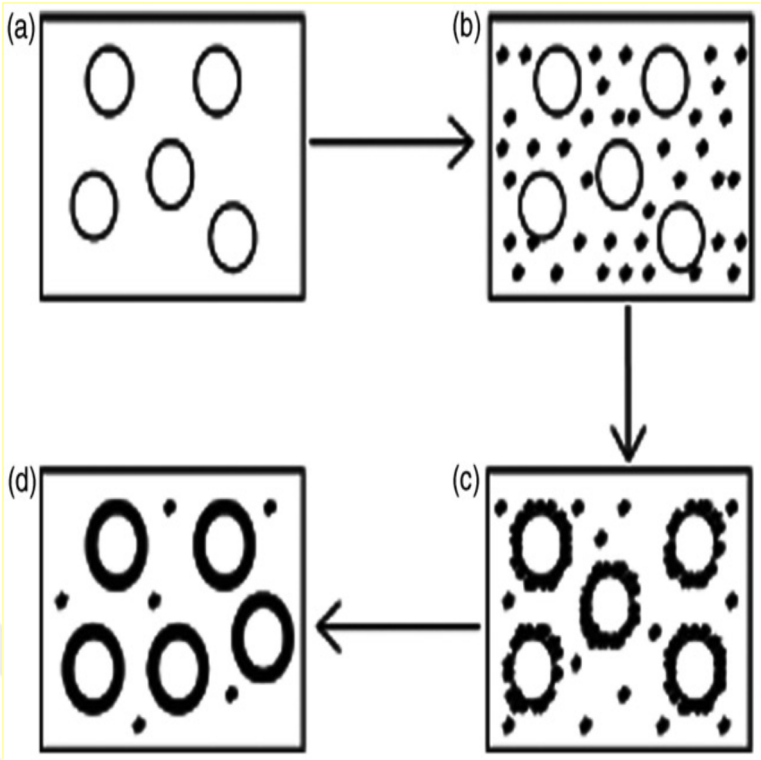

Figure 2. 4 a) Dispersion of core material in a shell polymer solution; **b)** Separation of coacervate from the solution; **c)** Coacervate micro-droplets coat the core material; **d)** The coacervates coalesce to form a continuous shell around the core particles (Ghosh, 2006)

depends on the polymers' molecular weight and distribution of reactive groups in these polymers. Take for example coacervation of chitosan and soybean protein isolate; the effective pH range is between 5.5 and 6.5 (Huang et al., 2012). In respect to how the mixing ratio of bio-polymers influence the outcome of coacervation, it was reported that the mixing ratio affected the degree of coacervation process by altering the available quantity of individual polymer prepared for electrostatic interaction. To obtain maximum coacervation, an equal ratio of biopolymers (by weight) should be used at electrical equivalence pH (this is a pH value at which charges of polymers are opposite and equal). Of key note, the stated process conditions are inter-related hence they affect the coacervation process collectively (de Kruif et al., 2004).

2. 2. 3 Heteroprotein Complex Coacervation

Coacervates associated with the heteroprotein complex and made up of globular proteins that are oppositely charged, correspond to a particular balance of short and long-range coulombic connections between proteins (Figure 2.5). The heteroprotein globular proteins normally develop at a pH range below unity (or value 1) and low

ionic strength. Another critical element considered in this coacervation is the stoichiometry of protein which helps cater for the size and charge compensation principle (Nigen et al., 2009) . Further, extreme sensitivity to ionic strength and fluctuation in pH levels implies the key role played by electrostatic interactions in production of the coacervate (Nigen et al., 2007a). Other driving forces noted in coacervation of heteroprotein are hydrophobic interactions and dipolar attraction. Addition of salts abate coulombic associations between proteins and entropic contribution associated with the release of counter-ions. In heteroprotein systems, the entropic forces linked to the discharge of counter-ions need to be significantly lower compared with the polyelectrolyte systems considering that the charge density is lower. In an event where the balance between attractive and repelling forces shift from optimum conditions, the complex coacervation process for heteroprotein reverses fully. Surface charge anisotropy (shape and size of patches, and charge density at the surface) and structural features that are constrained assist in orienting interactions to exact domains on the proteins' surface (Kurut et al., 2012; Quinn et al., 2015). Positive or negative stoichiometry is not adequate enough to understand heteroprotein coacervation. The area of heteroprotein coacervation has continued to gain much attention in the last one decade. Lactoferrin is one of the two core basic proteins.

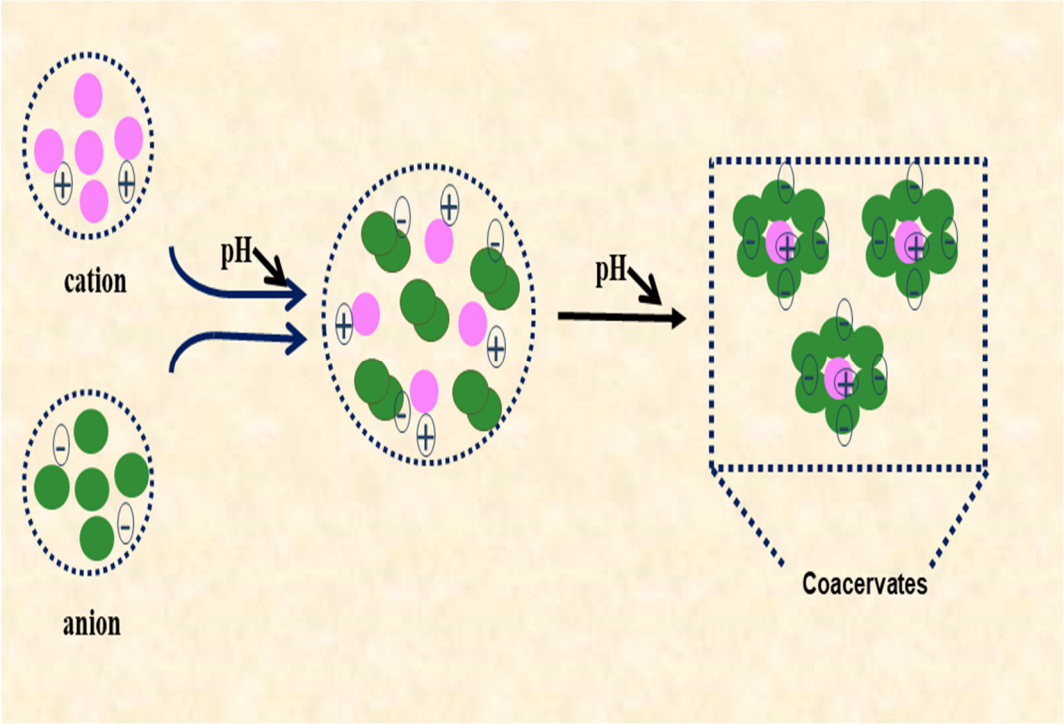

Figure 2. 5 Schematic representation of between oppositely charged proteins.

2. 2. 4 Encapsulation Studies of Oils by Complex Coacervation in the Literature

Several studies have been done regarding the application of encapsulation of oils in the food industry. This is in order to explore as many processes as possible to get the optimum encapsulation technique. While encapsulation techniques like spray drying have proved successfully, other studies are exploring multiple techniques that can be combined to achieve satisfactory results. Also, processing conditions have been investigated over years to find out how various parameters such as pH, charge density, temperature, charge, ionic strength, and polymeric concentration influence the coacervation process (Dickinson, 2008).

There are four steps involved in complex coacervation-based encapsulation of fats and oils in powder (or solid) matrix. First, two polymers are used to prepare an aqueous solution. Precisely, the protein solution is prepared at a pH level (above its isoelectric points) and a temperature above its gelling point. Once this has been achieved, the oil (hydrophobic core material) is mixed with the protein solution first followed by homogenisation to produce fine oil/water emulsion. The third step involves mixing of the aqueous solution of the biopolymer content (normally polysaccharide) with the oil-in-water emulsion. Provided the two oppositely charged biopolymers that have been selected have optimum density, complex coacervation takes place instantly with the complex coacervates producing a layer around the oil droplets. In case the biopolymers do not have an optimum opposite charge density, alteration of the temperature and pH levels is needed to attain a satisfactory level of opposite charge density for formation of complex coacervate to be initiated. Typically, the complex coacervates are not soluble in water and when they deposit on the surface of the oil droplets a precipitate is formed (separation of phases). If necessary, the coating on the complex coacervate is consolidated or hardened by cross-linking, desolvation, or heating so as to improve the thermal and mechanical stability of microcapsules (Timilsena et al., 2016b). The solid microcapsules can then be introduced in the food formulation to ensure an effective fortification process. Another compound that was found to be suitable in maintaining the stability of fish oil was incorporation of maltodextrin into a suspension of hydroxypropyl methyl cellulose (HPMC) and fish oil (Wu and Xiao, 2005). The diagram below shows the complex coacervation process of oil from the chia seed oil (Figure 2.6).

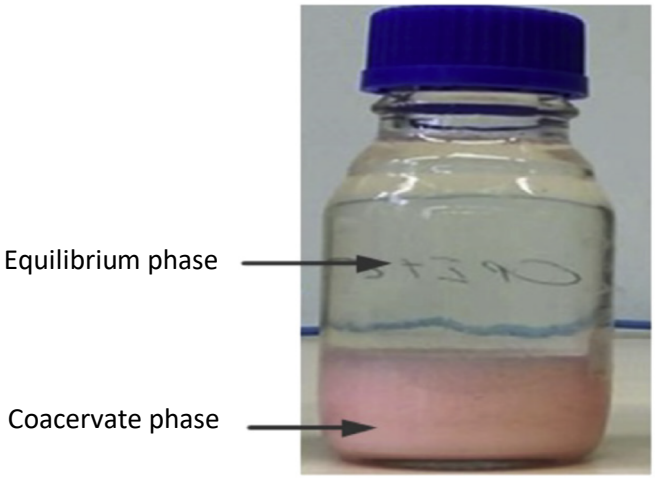

Figure 2. 6 Phase separation of chia seed oil (Timilsena et al., 2016a)

Weinbreck et al. (2004) studied microencapsulation of sunflower oil, lemon and orange oil flavour using complex coacervation of whey protein/gum arabic (WP/GA). They found that maximum coacervation occurs at pH 4 in which smooth biopolymer shell around the oil droplets was formed with high payload of oil (i.e. amount of oil in the capsule) higher than 80%. Lastly, flavoured capsules were incorporated within Gouda cheese exhibited that releasing of large capsules was faster than that the covalently cross-linked capsules.

Liu et al. (2010) worked on optimization of the encapsulation of flaxseed oil using complex coacervation of gelatin-gum Arabic (GA) matrix. The influence of homogenization rates (3,000–15,000 rpm) and total bio- polymer concentrations (1–2% w/v) on emulsion efficiency was considered to optimize the wall matrix. They found that increasing homogenization rates cause changing the structure of the capsule and the size of the capsules and amount of non-encapsulated oil was found to increase as the total biopolymer concentration was raised from 1 to 2% (w/v).

Li et al. (2018) investigated cationic lactoferrin and anionic whey protein isolate (WPI) coated Docosahexaenoic Acid (DHA) & lutein emulsions with heteroaggregation. Heteroaggregation was occurred by mixing the oppositely charged LF-lutein and WPI-DHA emulsions together at pH 6.0. Droplet size, zeta-potential, transmission-physical stability, microrheological behavior and microstructure of the heteroaggregates formed were analysed as a function of LF-lutein to WPI-DHA droplet ratio.

Marfil et al. (2018) studied on complex coacervation to encapsulate palm oil. Gelatin and gum Arabic were used as wall materials. For this purpose, the effects of wall material concentration, gelatin:gum Arabic ratio and core:wall material ratio (C:WM) (75, 100, and 125%) on the encapsulation efficiency, particle morphology, and size distribution of microcapsules were examined.

Shi et al. (2018b) encapsulated krill oil with krill protein isolate by freeze-drying in their study. Effects of oil/protein ratio on properties of microcapsules were investigated. With increased ratio, microcapsule oil loading capacity increased, loading and encapsulation efficiencies decreased.

2. 3 Lactoferrin

Lactoferrin is an iron-binding glycoprotein found in milk with a dumb-bell shape and its structure is denoted as a meaning globular and it has an isoelectric point of 8.7 with a molecular weight of 83 kDA. It has two homologous lobes, that is, C and N-lobes and each of these contain two domains; C_1, C_2 for the C-lobes and N_1, N_2 domains for the N-lobes (Figure 2.7). In between the domains is a cleft (Moore et al., 1997) and each inter-domain cleft provides a binding space for one atom of iron. Lactoferrin's tertiary structure is stabilised by approximately seventeen disulphide bounds. LF exists in two forms, that is, the *apo* and *holo* form. The former form which is metal free is more flexible but more exposed to enzymatic degradation and denaturation than the latte form. At neutral pH, LF is a carrier of positive net charge though the surface charge is randomly distributed with some patches located at inter-lobe and N-lobe region having high positive charges. Negative charges are contained in sialic acid moieties (Antonini et al., 2000). These negative charges escalates the hydration volume of LF hence improved stabilisation. LF is also ionic strength-dependent because it becomes positively charged at low ionic strength but turns negatively charge when the ionic strength is increased (Mela et al., 2010).

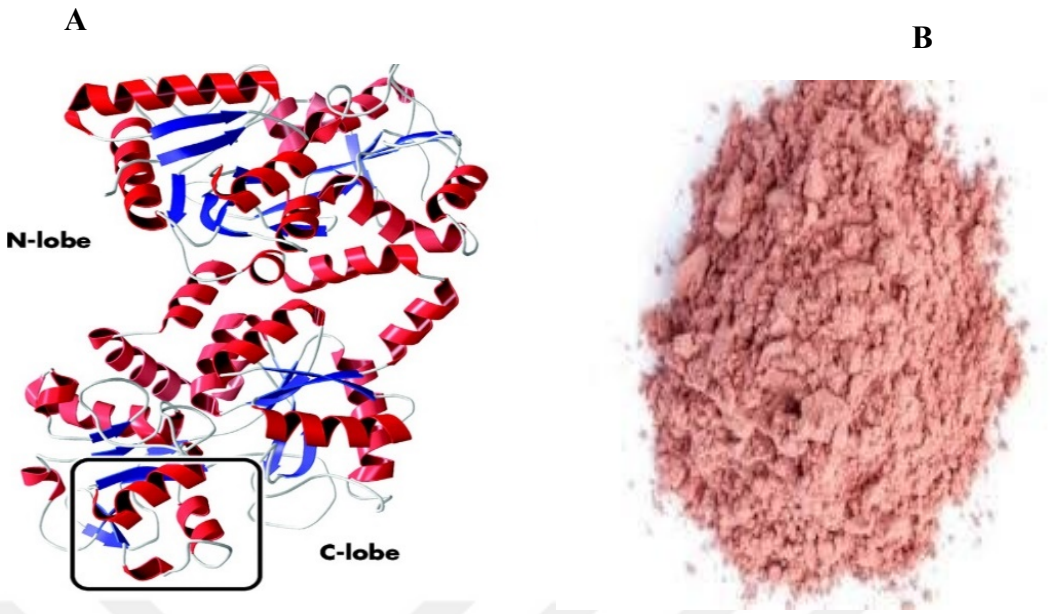

Figure 2. 7 A) Structure of Lactoferrin **B)** Powder form of Lactoferrin.

Taking into account the process conditions parameters like the protein stoichiometry and concentration, pH level, and ionic strength are fulfilled, LF was found to produce heteroprotein coacervates in the presence of β-lactoglobulin and unstructured caseins (α, β- and κ-CN) (Anema and de Kruif, 2012). For coacervation to occur, the positively charged LF mixes with the negatively charged proteins like β-lactoglobulin at the optimum protein ratio (Kizilay et al., 2014). Following the integration of the two proteins, the solution turns turbid because of formation microspheres. These microsphere continue to fuse progressively until a viscous sediment (or a continuous concentration phase) is obtained.

2. 4 Pea protein isolate

Protein is one type of protein that attracted significant interest from food scientists because of it high nutritional value, little allerginicity, low cost, and availability (Figure 2.8). Regrettably, the protein content in pea cannot be utilised sufficiently because of limitations like colour, flavour, and functionality. Pea is a food product rich in carbohydrate and protein, contains essential vitamins and minerals, and it is low in fat. Peas are consumed along with other cereal grains since they complete such a diet with important amino acids. The protein content contained in the field pea ranges between 23% to roughly 31% and fat composition of not more than 2% besides minor

ingredients such as polyphenols, minerals, phytic acid, vitamins, oxalates, and saponins (Boye et al., 2010). The carbohydrate content includes primarily starch and dietary fiber. Two groups of proteins dominate the pea protein profile, that is, globulins and albumins representing 80% and 20% respectively. Albumins are metabolic proteins that are soluble in water, and they contain higher levels of vital amino acids like lysine, tryptophan, methionine, and threonine compared to globulin. Major pea storage proteins, legumin, vicilin and convicilin are globulins and represent 65-85% of total proteins. According to sedimentation properties these proteins are classified into two fractions, 7S (vicilin, convicilin) and 11S fraction (legumin) (Barac et al., 2015). Molecular forms of the three major proteins are based on the extraction process applied to produce the protein ingredient, extrinsic variables like salts, temperature, and the pH, and modification of the ingredient, the protein structure may deviate from the usual protein structure. This leads to varied surface characteristics and conformation, that is the hydrophobicity and charge in the solution which can have alter the protein functionality. Protein ingredients in pea can be quantified in terms of ratio, and one of the procedures utilises the chemical properties and molecular weights of the two constituents. Consider for example the ultracentrifugation process where protein fractions are separated in line with their sedimentation coefficients. In this particular procedure, strong centrifugal force and density gradient medium work on the proteins to determine rate of settling and concentration distribution. The refraction and absorption of light is used to measure concentration distribution (Lam et al., 2016).

2. 5 Rasberry Seed and Sour Cherry kernel oils

2. 5. 1 Omega-3 rich oils

Epidemiological and clinical studies have unveiled that oils and fats that are rich in polyunsaturated fatty acids (PUFAs) such as omega-3 (ω-3) and omega-6 (ω-6) can provide health benefits in addition to providing energy and being a carrier of lipid soluble nutrients. PUFAs are abundantly present in marine fish, algae and some plant seeds. Fish oils possess important PUFAs including omega-3 (ω-3) PUFAs docosahexaenoic (DHA) and eicosapentaenoic acid (EPA). Omega-3 PUFAs have a long-chain are associated with a myriad of benefits because they play an essential role in foetal, cognitive, and early child development (McLennan and Abeywardena, 2005; Weitz et al., 2010). They also assist in protection human cell lines from various cancers

Figure 2. 8 Image of yellow pea A) Seed form B) Powder form

because they have anti-inflammatory effect in addition to improvement mental and cardiovascular health. Clinical studies indicate that ω-3 fatty acids from the fish oil has the capability to improve brain function and averting diseases like immune response disorders, Chrohn's infection, and ulcerative colitis (Jordan, 2010). Omega-6 fatty acids are represented by linoleic acid (LA; 18:2 ω6) and omega-3 fatty acids by a-linolenic acid (ALA; 18:3 ω3). Due to the opposing effects of omega-3 and omega-6 fatty acids, a healthy diet should contain a balanced omega-6:omega-3 ratio. In the human body, LA and ALA compete for metabolism by the enzyme Δ6-desaturase. It has been suggested that this is important to health, as too high an intake of LA would reduce the amount of Δ6-desaturase available for the metabolism of ALA, which may increase the risk of heart disease. This was supported by data showing that over the last 150 years, intakes of omega-6 have increased and intakes of omega-3 have decreased in parallel with the increase in heart disease. Thus, the concept of an "ideal" ratio of omega-6 to omega-3 fatty acids in the diet was developed. Because of the increased amounts of omega-6 fatty acids in the Western diet, the eicosanoid metabolic products from arachidonic acid (AA), specifically prostaglandins, thromboxanes, leukotrienes, hydroxy fatty acids, and lipoxins, are formed in larger quantities than those formed from omega-3 fatty acids, specifically Eicosapentaenoic acid (EPA). The

eicosanoids from AA are biologically active in very small quantities and, if they are formed in large amounts, they contribute to the formation of thrombus and atheromas; to allergic and inflammatory disorders, particularly in susceptible people; and to proliferation of cells (Simopoulos, 2008).

As the body of evidence that links health benefits to the consumption of vegetable oils continues to grow, many consumers now prefer to use vegetable oils instead of animal fats. Several phytochemicals that have been detected in edible seed oils may include tocopherols, carotenoids, phenolic and polyphenolic compounds, and especially fatty acids such as linolenic acid (18:3, ω -3) (Micić et al., 2015). Table 2.3 shows a list of natural sources of omega-3 oil.

Table 2. 3 Natural sources of ω-3 fatty acids

ω-3 fatty acid	**Sources**
Alpha-linolenic acid (ALA)	Certain nuts, flaxseed, canola, kiwifruit, raspberry, blackberry, chia, perilla, walnut, seeds and their oils, hempseed, and dark green leafy vegetables
Docosahaxaneoic acid (DHA)	Algal species and blubber of marine mammals like seals and whales
Eicosapentaenoic acid (EPA)	Liver of lean white fish and Fatty fish like mackerel and herring

2. 5. 2 Sour Cherry kernel Oil

Sour cherries belong to the *Cerasus* subgenus and *Prunus* genus and are cultivated globally. They are usually consumed as processed products such as sour cherry juice or frozen and canned sour cherry. The kernel extract from sour cherry which is made up 32% to 36% oil contain bioactive compounds (anthocyanidins and hydroxycinnamates) that have protective effects. The oil is also rich in "ϒ-sitosterol, β-tocopherol and unsaturated fatty acids, with high content of oleic acid (50–53%) and linoleic acid (35–38%)" (Bak et al., 2010). An investigative study conducted by Yılmaz and Gökmen (2013) shows some important insights about the composition of the oil extracted from the sour cherry seed kernel. After analysis, the results indicated

that the kernel oil is majorly comprised of palmitic acid (6.4%), stearic acid (1.2%), oleic acid (46.3%), linoleic acid (41.5%), and linolenic acid (4.6%). Studies have proved that the ratio ω-6 to ω-3 fatty acids is between 4.5 and 5.0. Lack of these fatty acids in the diet may negatively affect human health leading to skin lesions and cardiovascular disorders (Bozan and Temelli, 2008).

2. 5. 3 Raspberry Seed Oil

Berry seeds can have oil content of about 11% to 23% and the seed oil has gain significant attention based on its nutritional benefits. One of the unique features of berry seed oils is the high content of PUFAs. Despite the high value of PUFAs, they are susceptible to oxidation which may compromise the shelf life of the oils. This problem is neutralised by high contents of anti-oxidants found in the oil. Even though most oxidants are left in the meal once the extraction has been done, some ingredients including phenolic compounds, carotenoids, and vitamin E remain in the berry seed oil. Cold-pressed oils are more preferable because they retain high quantities of natural antioxidants which are also linked to high nutritional value (Van Hoed et al., 2011).

Raspberry originated from the Latin word, Rubusidaeus, is a rich plant product and it has diverse phytochemical content, for instance, ellagic acid, anthocyanin, querceting, and phenolic compound. These compounds play an important role in that they have antioxidant properties and facilitate cell protection from oxidative factors in addition to minimising various types of cancer. Seed oil from the raspberry is rich in ω-3 and ω-6 essential fatty acids, elements that help in the growth and development and reduction of the impacts of oxidative stress in living organisms (Oomah et al., 2000). Other than that, they assist in prevention of cancer infections and cardiovascular illnesses. Raspberry seed oil contains approximately 30% α-linolenic acid and 50-55% linoleic acid, and the ratio ω-6 to ω-3 fatty acids is between 1.5 and 1.9 (Bada et al., 2013). Initially, the ratio of ω-6 to ω-3 was believed to be 1:1 though this is not the case today since that ratio has change to 1:2.5; the ideal ratio ranges between 1:4 and 1:10. This seed oil is also rich in the a-tocopherol and g-tocopherol. The latter is essential in abating diabetic disorders, cancer, Alzheimer's disease (AD), and skin eczema. Vitamin E present in the raspberry seed oil makes it a valuable product in the cosmetic and pharmaceutical industry citing its anti-inflammatory properties. Oomah

et al. (2000) notes that the anti-inflammatory effects of the raspberry seed oil is stronger that hazelnut, avocado, and the grape seed oil.

CHAPTER 3
MATERIALS AND METHODS

3. 1 Materials

The bovine lactoferrin (LF) was kindly donated by Ingredia Nutritional (Arras, France). According to the technical specification provided by the supplier, it was purified from bovine milk and contained 96% protein, 0.5% ash and iron saturation was 10-20%. Pea protein isolate (PPI) (Nutralys®) was obtained from Roquette (Lestrem, France) and contained 85% protein, 7% moisture, and 4% ash. Raspberry seed oil (RSO) was provided by Aprés-Vin enterprises (Prosser, WA). Sour cherry seed oil (CHSO) was purchased from Çiftçizade company (Antalya, Turkey). Sodium azide and all other chemicals including solvents were purchased from Sigma-Aldrich Chemical Company (St. Louis, MO, USA). Milli-Q water (water purified of 18.2 M Ω.cm by Milli-Q apparatus, Millipore Corp., Bedford, MA, USA) was used as a solvent in all experiments. Hydrochloric acid (1 N HCl) and sodium hydroxide (1 N NaOH) were diluted from concentrated ~37% w/w) HCl-water solution or 10 M NaOH solution (Sigma-Aldrich), respectively.

3. 2 Characterization of Raspberry Seed and Sour Cherry Kernel Oils

3. 2. 1 Fatty Acid Composition

The fatty acid composition of RSO and CHSO were analyzed on Agilent GC7890A gas chromatography equipped with a flame ionization detector and capillary column 100 m in length and 0.25 mmHP-88 column (88% cranopylarly) in diameter. The analytical conditions were as seen Table 3.1. Fatty acid methyl esters (FAME) were extracted with n-heptane after cold methylation with 2N KOH in methanol.

Standards of each fatty acid were used to identify the fatty acids. Fatty acids were identified in the samples by comparing retention times for standards and samples. The area was expressed as a percentage of areas of the total fatty acids (IUPAC, 1987).

Table 3. 1 GC operating condition for free fatty acid determination.

Parameters	Condition
Flow rate of carrier gas (helium)	1 mL/minute
Detector temperature	260°C
Injector temperature	250°C
Column temperature	175°C(10 min.), 5°C/min. to 210°C, 5°C/min. to 230°C
Injection volume	1µL
Column type	HP-88 Capillary column

3. 2. 2 Refractive Index and Density

The density of the RSO and CHSO were measured using pycnometric methods according to the International Organization of Standardizations ["Methods for determining the density of non-cellular plastics, Part 1: Immersion method, liquid pycnometer" (ISO 1183-1:2012)]. Measurements were taken as the volume of the oil displaced by a known mass of the samples at 25ºC. Then reading the density value of the oil samples were calculated by taking the ratio of mass to volume.

Refractive indices (optical measurements) of the oil samples were measured by using Abbe Refractrometer (ATAGO NAR 1T-LIQUID, Tokyo, JAPAN). A halogen lamp was used for the high bright white light source.

3. 2. 3 Peroxide Value

1-2 grams of the each oil sample, in duplicate, was weighed in a glass 250 mL of erlenmeyer flask. 10 mL of chloroform was added and dissolved quickly by stirring. Then, 15 mL of glacial acetic acid and 1 mL of saturated potassium iodide (KI) were added. The flask was immediately closed, stirred for 1 minute and left to stay 5 minute in a dark place at ambient temperature. A 75 mL of distilled water was added to mixture and by addition 0.5 ml 1% starch solution was titrated with 0.01N sodium thiosulphate ($Na_2S_2O_3$) solution. A blank test was carried out. Results were expressed as milliequivalents of peroxide per kilogram of sample BS (684, 1987). The peroxide value (PV) was calculated as follows;

$$PV = \frac{(S - B)xNx1000}{m}$$

where;

S= volume of sodium thiosuphate used for sample.

B= volume of sodium thiosuphate used for blank.

N= normality of sodium thiosuphate used for titration.

m=mass of sample, in grams

3. 2. 4 Colour Measurement

Color measurements of RSO and CHSO were performed using HunterLab ColorFlex (A60-1010-615 Model Colorimeter, HunterLab, and Reston VA). The L*, a*, b* color space (also referred to as CIELAB) was used to expressed the color changes. The color values were expressed as L* (darkness/whiteness), a* (greenness/redness), b* (blueness/yellowness) values and yellowness index (YI). Three measurements were taken for each sample. The instrument was calibrated against the standard reference white tiles (L*= 93.41, a* =-1.12, b* =1.07) (Timilsena et al., 2016a).

3. 2. 5 Induction Time (IT) Measurement

A metrohm Rancimat model 743 (Herisau, Switzerland) capable of operating over a temperature range of 50-220°C was used to measure IT of oil samples. A stream of air was bubbled into 3 g of oil samples in a reaction vessel placed in an electric heating block. Filtered, cleaned, dried air was allowed to bubble through the hot oil at rates of 20 L/h. Effluent air containing volatile organic acids from the oil sample were collected in a measuring vessel containing distilled water (60 mL). The conductivity of water was measured automatically as oxidation proceeded. The induction time of the oil samples were automatically recorded at 110°C (Farhoosh, 2007).

3. 3 LF-PPI Complex and Coacervate Preparation

Dispersions of LF (4 g/L) and PPI (4g/L) were prepared by dissolving an exact amount of LF powder or PPI powder in Milli-Q water, respectively for 2 h at 25°C using a magnetic stirrer to ensure complete solubilisation. The dispersions were centrifuged at 20,000 × g for 30 minutes, filtered through Whatman No. 4 filter paper and 0.22 µm syringe filter to remove any residues. The resultant LF stock solution showed 99.8%

soluble protein yield, whereas PPI showed 30% soluble protein yield i.e. 1.2 g/L measured using Kjeldahl analysis (AOAC 981.10) (AOAC, 1995). This soluble fraction of PPI is referred to as the PPI stock solution hereafter. The mineral composition analysed using ICP-MS (Inductively Coupled Plasma Mass Spectrometry) of the stock solutions was the following (g/100 g): LF: Na 0.0568, K 0.0017, Mg < detection limit (0.00004), Ca 0.0022, Fe 0.025, P 0.050 and PPI: Na 0.2542, K 0.0588, Mg 0.0086, Ca 0.0077, Fe 0.00043, P 0.1637. Different semi-dilute concentrations of PPI working solutions (0.00035-0.07 mM) were prepared by dilution of the PPI stock solution (1.2 g/L i.e. 0.07 mM) using Milli-Q water. Appropriate volumes of PPI and LF at pH 7.0 were mixed for the molar ratio study. The molar concentrations of LF and PPI were calculated using respective molecular weights (discussed in SDS-PAGE section) and the molar ratio was based on the assumption that all different fractions of PPI (legumin, vicilin, convicilin) participated equally in complex formation with LF in the same ratio as they existed in the working solutions. For the pH study, pH of PPI/LF ratio of 0.15 (mmol/ mmol) i.e. mixture of 0.047 mM LF and 0.007 mM PPI was adjusted to target pH from pH 2-9 using 1 N standard HCl or NaOH as shown in Figure 3.1 magnetic stirring conditions (500 rpm). Appropriate volumes (5.0 mL) of LF stock solution was rapidly poured into an equal volume of freshly prepared PPI working solutions in a beaker followed by mixing at 500 rpm. As described in previous literature (Yan, Y. et al., 2013), for “high to low”, PPI and LF working solutions at pH 9.0 were mixed and then the mixtures were rapidly adjusted to a target pH while mixing. For “low to high”, LF and PPI solutions were mixed at pH 2.0 and then the mixtures were adjusted to a target pH quickly while mixing. The polymer-rich phase (coacervate) was collected using mild centrifugation at 500 × g for 10 minutes and characterized using AFM, SAXS and TEM. Sodium azide (0.02 wt%) was added to prevent any bacterial growth in samples only at ≥ pH 7.0. No significant difference in coacervate structure were observed in terms of sizing, turbidity measurements and zeta potential as compared to fresh samples without the addition of 0.02 wt% azide in above-mentioned pH conditions.

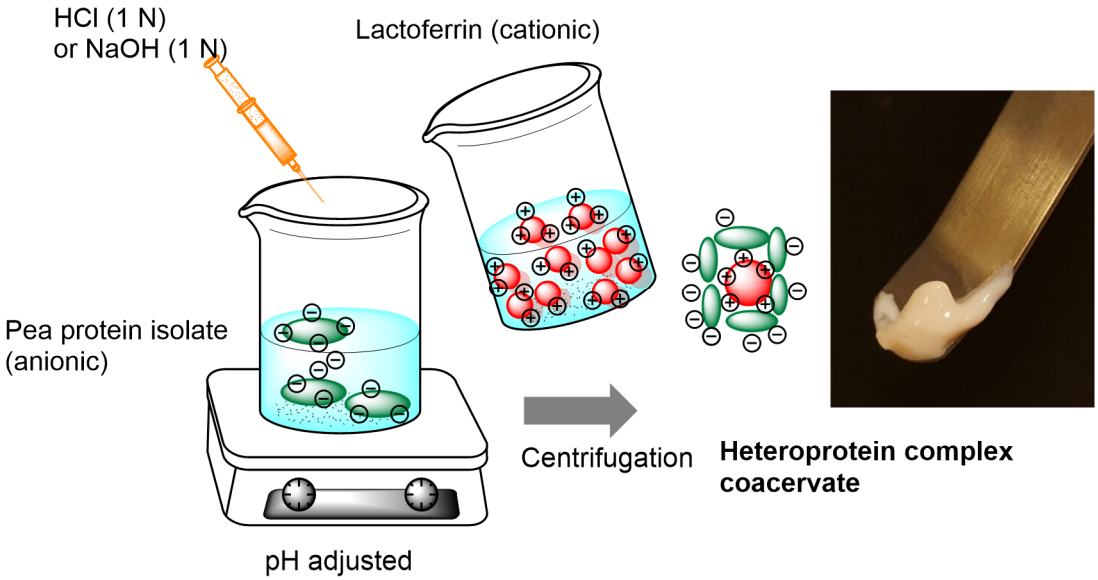

Figure 3. 1 Schematic illustrations of steps of production of heteroprotein complex coacervate showing the visual aspect of the viscous phase (macroscale)

3. 4 Protein Content, Solubility Curve and Composition

Both the stock protein solutions (LF and PPI) after centrifugation and filtration were examined for crude protein content. The PPI stock solution (1.2 g/L) was analyzed for its solubility as a function of pH from pH 2-9 (AOAC, 1995). The composition was assessed using sodium dodecyl sulphate polyacrylamide gel electrophoresis (SDS-PAGE) technique. 50 µL of protein solution (at 4 g/L for LF, 1.2 g/L for PPI) was mixed with 50 µL of Laemmli sample buffer (62.5 mM Tris-HCl, 2% SDS 25% glycerol, 0.01% bromophenol blue, 5% β-mercaptoethanol) and the mixture was heated at 95 ° C for 5 min. The samples were cooled to room temperature and 20 µL was loaded onto SDS gels previously prepared on a Mini-PROTEAN II system (Bio-Rad Laboratories). Gels were run for 10 min at 100 mV followed by a phase of 30 minutes at 200 mV. The gels were stained with Coomassie Blue R-250 [0.05% (w/v) in 25.0% (v/v) isopropanol 10.0% (v/v) acetic acid] for at least 4 hours, after which they were destained with water for one hour. Gels were scanned using a flat-bed scanner (Bio-Rad Molecular Imager, Chemi-Dco XRST) and the intensities of the protein bands were quantified using Image LabTM software version 5.1 Beta. The percentage composition of each sample was determined by scanning the areas for each band.

3. 5 Emulsions Preparation for Method Optimization

Aqueous emulsifier solutions were prepared by dispersing either LF powder or PPI powder into Milli-Q water, and then stirring for at least 2 h at room temperature to ensure complete dispersion. The pH of the protein solutions was then adjusted to 7.0 using 0.1 M NaOH or 0.1 M HCl. In this section, Raspberry Seed Oil (RSO) was utilized to prepare emulsions. 10 gr of RSO and 90 gr of protein solution mixture were mixed. The mixture was pre-homogenized by Ultra Turrax T25 basic disperser tool (IKA®-WERKE GMbH & Co. KG, Germany) at 17.000 rpm for 2 minutes and then passed 2-times through a laboratory scale jet homogenizer (LAB 1000, APV-Gaulin, Wilmington, MA) at operating pressure of 350 bar. The emulsions were then stored for 24 h prior to utilization. Final protein solution was 1 wt% while oil was 10 wt% (**Identity 1 and 2** in Table 3.2).

We applied 4 different formulations and processes for mixed-protein emulsions. Initially, LF and PPI solutions were mixed on magnetic stirrer for 30 minutes and then pH of the mixtures were adjusted to 5.4 and 7 by using 1 M NaOH or 0.1 M HCl (**Identity 3 and 4** in Table 3.2) . Then, raspberry seed oil was added on the mixtures and emulsions were prepared as described above. Final pH of the emulsions were adjusted again to 5.4 and 7 by using 1 M NaOH or 0.1 M HCl. Final protein solution was 1 wt% (LF:PPI=1:1) while oil was 10 wt% (Table 3.2).

In **Identity 5** in Table 3.2, pH of LF solution was adjusted to 7 by using 1 M NaOH. Then, raspberry seed oil was added on the solution and LF-stabilized emulsion was prepared as described above. Then, PPI solution at pH 7 was added slowly to LF-coated droplets. Final pH of the emulsion was adjusted again to 7 by using 1 M NaOH or 0.1 M HCl. Final protein solution was 1 wt% while oil was 10 wt% (Table 3.2).

In **Identity 6** in Table 3.2, pH of LF solution was adjusted to 7 by using 1 M NaOH. Then, raspberry seed oil was added on the solution and LF-stabilized emulsion was prepared as described above. Then, PPI solution at pH 7 was added slowly to LF-coated droplets. Final pH of the emulsion was adjusted again to 5.4 by using 1 M NaOH or 0.1 M HCl. Final protein solution was 1 wt% while oil was 10 wt% (Table 3.2).

Table 3.2 Formulation and process conditions of single and mixed protein solutions

Identity number	Protein	Protein pH	Protein Conc. (wt%)	Oil Conc. (wt%)	Pre-mixing	Homogenization	Final pH	Protein Addition
1	LF	7	1	10	Ultraturrax (17,000 rpm, 2 min.)	350 bar, 2 times	7	No
2	PPI	7	1	10	Ultraturrax (17,000 rpm, 2 min.)	350 bar, 2 times	7	No
3	LF-PPI	5.4	1	10	Ultraturrax (17,000 rpm, 2 min.)	350 bar, 2 times	5.4	No
4	LF-PPI	7	1	10	Ultraturrax (17,000 rpm, 2 min.)	350 bar, 2 times	7	No
5	LF	7	1	10	Ultraturrax (17,000 rpm, 2 min.)	350 bar, 2 times	7	Yes (PPI 1 wt% at pH 7)
6	LF	7	1	10	Ultraturrax (17,000 rpm, 2 min.)	350 bar, 2 times	5.4	Yes (PPI 1 wt% at pH 7)

3. 6 Emulsion Preparations for Oil/Wall Material Concentration Optimization

Aqueous emulsifier solutions were prepared by dispersing either LF powder or PPI powder into Milli-Q water, and then stirring for at least 2 h at room temperature to ensure complete dispersion. The pH of the protein solutions was then adjusted to 7.0 using 0.1 M NaOH or 0.1 M HCl. In this section, Raspberry Seed Oil (RSO) was utilized to prepare emulsions. LF solution were mixed with raspberry seed oil at different concentration, respectively. The mixture was pre-homogenized by using lab scale homogenizer (Art-Miccra D-8, Germany) at 17,000 rpm for 2 minutes (Figure A4) and then ultrasound at 10% amplitude was applied for 1 minute to each emulsions (Soniprep 150 Ultrasonic Disintegrator, UK) (Figure A3). Then, PPI solution at pH 7 was added slowly to LF-coated droplets. Final pH of the emulsion was adjusted again to 5.4 or 7 by using 1 M NaOH or 0.1 M HCl. The emulsions were then stored for 24 h prior to utilization. Final protein solution was 2 wt% while oil was 2, 4, 6, 8, 10 wt %.

Two sets of emulsions were prepared. In the first set, soluble LF-PPI complexes were used to form emulsions. The content of RSO was varied (2, 4, 6, 8, 10 wt %) and emulsions were prepared at pH 7 as described above (Set 1). For the second set, emulsions were formed by heteroprotein complex coacervation. The method was adapted from study of Kermasha et al. (2018) studies. The content of RSO was varied (2, 4, 6, 8, 10 wt %) as well and emulsions were prepared at pH 5.4 as described above (Set 2). After emulsions were agitated for 2 hours under continuous stirring at 300 rpm and pH was adjusted to5.4 to complete coacervation process. The particle suspension was then slowly cooled further, with continuous stirring, to 5°C, using an ice-bath.

3. 7. Freeze Drying of Encapsules

Freeze drying of RSO with LF-PPI complexes were carried out by the method described by Kermasha et al. (2018). Emulsions prepared in Section 3.5 at different oil ratios (Set 1 and Set 2) were put into round aluminium plates (4 cm diameter, 2 cm height) (Figure A6-A) and placed in freezer at -22°C for 24 h. Frozen emulsions were freeze dried (CHRIST Alpha 1-4 LDPlus, Martin Christ, Germany) (Figure A5) . After freeze drying (Figure A6-B), the encapsules were immediately transferred to desiccator including silica beads at room temperature. At that point, the freeze dried

encapsules were ground to smaller size by using glass rod and put into tightly sealed plastic cups for further analysis.

3. 8 Formation of Encapsulated Raspberry Seed and Sour cherry Kernel Oils

As described above, only raspberry seed oil (RSO) was used to identify optimum conditions. In the last part of our study, RSO and CHSO encapsules were formed at optimum conditions (6 wt% oil and 2 wt% protein concentration) as in Section 3.5 followed by Section 3.6. at pH 7 and 5.4. Single protein coated RSO and CHSO encapsules were produced as controls.

3. 9 Storage Conditions for Oxidative Stability

2 g bulk and encapsulated RSO and CHSO were transferred to 10 mL loosely capped glass bottles. Samples were stored at 45°C for 16 days. Oxidative stability was examined by measurement of Peroxide value of samples.

3. 10 Size and ζ-potential Measurements

The mean hydrodynamic radius (R_h) of the pure protein solutions, complex and coacervate was measured by dynamic light scattering (DLS) at 25 °C equipped with a 4 mW helium/neon laser at a wavelength output of 633 nm. Sizing was performed at 10 s intervals in disposable plastic cuvettes (ZEN 0040) using noninvasive backscattering at a detection angle of 173 °C. Assuming the scattering particles to be spherical, their apparent hydrodynamic radius was calculated from the diffusion parameters using Stokes-Einstein equation, i.e. $R_h = k_BT/(6\pi\eta DT)$, where k_B is the Boltzmann constant, T is absolute temperature, and η is solvent viscosity, D is diffusion coefficient (Bengoechea et al., 2011).

The ζ-potential values of the pure protein solutions, their complexes and coacervates, emulsions were measured using a laser Doppler velocimetry and phase analysis light scattering (M3-PALS0) using disposable electrophoretic mobility cells (DTS 1060). Z-potential was calculated based on the Henry equation:

$$U_E = 2\varepsilon z f(\kappa a)/3\eta$$

where U_E is the electrophoretic mobility, ε is the dielectric constant, z is the zeta potential, f(κ a) is Henry's function and η is the dispersion viscosity. F(κ α) is related to the particle radius (α) and κ is the Debye length, where equal to 1.5 is referred to as

Smoluchowski approximation in this study. For emulsions, samples were diluted to a droplet concentration of 0.001% oil (v/v) using water, and then pH adjusted to the specific pH. The results were reported as mean Z-average mean diameter or mean ζ-potential of five readings and standard deviations were calculated (Anema and de Kruif, 2014; Can Karaca et al., 2011).

3. 11 Turbidity Measurements

The turbidity of pure protein solutions and their complex/ coacervate were measured by a Jenway 6715 UV-Visible Spectrophotometer (Bibby Scientific Limited, Beacon Road, Stone, Staffordshire, ST15 OSA, UK) using 1 cm disposable plastic cuvette at 600 nm (Flanagan, S. E. et al., 2015). Milli-Q water was used as blank reference resulting in 100% transmittance. The turbidity (OD_{600}) was calculated using equation (3):

$$OD_{600} = -\ln \frac{I}{I_0} \tag{3}$$

where, I is the transmitted intensity and I_0 is the incident light intensity.

3. 12 Small-Angle X-ray Scattering

Small angle X-ray scattering (SAXS) patterns were recorded in order to determine the size (radius of gyration) of 0.007 mM PPI stock solution, 0.047 mM LF at pH 7.0 and their complexes or coacervates at pH 5.4, 5.8, 6.2 and 7.0, respectively. The SAXS camera set-up (SAXSpace, Anton Paar, Austria) is described in great detail elsewhere (Patil-Sen et al., 2016). Briefly, the collimation block unit vertically focuses a line shaped beam of Cu-K_α radiation with a wavelength, $\lambda = 0.154$ nm on to the detector plane. For the SAXS experiments the high resolution mode was chosen, which permits to detect a minimum scattering vector, q_{min}, of 0.04 nm^{-1} ($q = (4\pi/\lambda) \sin\theta$, where 2θ is the scattering angle). All studied samples were filled into the same vacuum-tight, reusable 1 mm quartz capillary to guarantee exactly the same scattering volume. The capillary was placed in the temperature controlled sample stage at 25 °C ± 0.1 °C. All samples as well as the aqueous buffers and empty capillaries were exposed for 120 minutes. The SAXStreat software (Anton Paar) was used to correct the scattering patterns with respect to the position of the primary beam. The SAXS data was further transmission-corrected by setting the attenuated scattering intensity at q = 0 to unity

and the background was subtracted using the SAXS Quant software (Anton Paar). The scattering vector q was calibrated with silver-behenate, which has a known lattice spacing of 5.84 nm. The reduced scattering pattern were finally analyzed with the GIFT software package in order to fit the scattering data by Indirect Fourier Transformation (IFT), generate the Pair-Distance Distribution Functions (PDDF) and to determine the radius of gyration (Rg) of the pure proteins and their coacervates.

3. 13 Transmission Electron Microscopy

Transmission electron microscopy (TEM) was employed to observe the microstructure of the complexes and complex coacervates. The LF-PPI complexes or coacervates at different pH (5 μL) were deposited onto a 400-mesh carbon-copper coated grid for 1 minute. This was followed by two washings with 5 μL of distilled water for 5 seconds, each. Finally, the grids were stained with 1 wt% Uranyl Acetate for 60 seconds and blotted with filter paper. Images were recorded using a CM10 TEM microscope (Philips, Surrey, UK) operating at 120 kV (Priftis et al., 2015).

3. 14 Atomic Force Microscopy Measurements

Complexes, coacervate and pure proteins were investigated with an Icon Fast-Scan Bio Atomic Force Microscope (AFM) (Bruker Nano Surfaces, Santa Barbara, CA). Samples were prepared for deposition by serial dilution of the stock solutions at the required pH. Good dispersions were generally found at a dilution of 1×10^6 times, and continuous films at 100× dilution. 20 μL of each diluted sample was pipetted onto a freshly cleaved ruby mica disc and incubated for 5 minutes, before rinsing with approximately 5 mL of Milli-Q water, drying by wicking onto filter paper followed by a stream of nitrogen. The LF and LF-PPI complex at lower pH value (pH 5.4) adhered well, but the complex at pH 7.0 would only adhere to the mica if it had been pre-treated with Mg^{2+} ions (50 μL of 5 mM $MgCl_2$ solution for half an hour), the rationale being that the charge on the complex was negative hence repelling from the mica which is also negatively charged at neutral pH. Pure PPI did not adhere well to the mica, although lower quality images could be obtained by drying the sample without rinsing. Samples were scanned using TESPA-V2 probes (Bruker) with tapping mode in air, at a resonant frequency of 340-350 kHz and minimum set point, at a typical scan rate of 3-4 Hz depending upon image size. Multiple scans across the samples were obtained

to ensure good statistics, typically at 2 μm scan size and 1536 or 2048 pixel resolution. AFM images were analysed using the Particle Analysis function in ImageJ (NIH). Each image was converted into a binary image using a manual threshold to prepare for the automated analysis. The outline of each complex was fitted with an ellipse, with the major and minor axes describing the length and width of each complex respectively. Sizing of the individual proteins was carried out in Nanoscope Analysis software (Bruker, version 1.5) using the manual ruler tool (Nigen et al., 2010).

3. 15 Droplet Size Analysis

Emulsion droplet size distribution was measured using a Mastersizer 3000 laser light scattering instrument (Malvern Instruments Ltd., Worcestershire, United Kingdom). This instrument measures the angular dependence of the intensity of light (λ=632.8 nm) scattered from a stirred diluted emulsion. The refractive indices of water and raspberry seed oil were taken as 1.330 and 1.480, respectively (Can Karaca et al., 2011). Average droplet sizes were characterized in terms of the Sauter mean diameter d_{32} or volume mean diameter d_{43} defined by:

$$da,b=\sum d_i n_i^a / \sum d_i n_i^b$$

All datas were collected over 5 readings at room temperature.

3. 16 Microstructure Analysis

For microscopy of the emulsions, a Leica TCS SP2 confocal laser scanning microscope (CLSM), mounted on a Leica Model DM RXE microscope base, was operated in fluorescence mode. 1 mL of sample, 100μL of Nile Red and 100μL of Fast green FCF were mixed in a sample cap. Approximately 300 μL of the mixture was placed into a laboratory made welled slide, filling it completely. A coverslip (0.17 mm thickness) was placed on top of the well, ensuring that there was no air gap (or bubbles) trapped between the sample and coverslip. The samples were scanned at 25°C, using 40 oil-immersion objective lenses, of numerical apertures of 0.3 and 1.25, respectively, approximately 10–20 μm below the level of the coverslip, in order to minimize hydrodynamic (and other) interactions with the coverslip. Fluorescence from the sample was excited with the 488 nm Ar and 633 nm He–Ne laser lines. Images were recorded at a resolution of 1024x1024 pixels (Lamprecht et al., 2000).

3. 17 Emulsion Stability

Emulsion samples were transferred to sealed plastic caps (inner diameter=1 cm, height=5 cm) and then stored at room temperature. After seven days of storage, the extent of separation was examined and photographs of emulsion samples were taken over a period of 7 days using a digital camera to record the separation (Sarkar et al., 2016).

3. 18 Optical Microscopy

The emulsions with 1, 2 and 3 wt% LF-PPI complexes and 10 wt% RSO at pH 7 were prepared as described in Section 3.5.1. A small drop of emulsion was placed onto the microscope slide and carefully covered with a cover slip. After being equilibrated for a few minutes, photomicrographs (20× magnification) were taken using Olympus BX 51 microscope (Tokyo, Japan) equipped with a camera (Pixera PVC 100C, USA) (Erçelebi and Ibanoglu, 2009).

3. 19 Rheological Measurement

Rheological properties of emulsions were analysed with a RheoStress RS-1 controlled stress rheometer (HAAKE, Karlsruhe, Germany), using a cone and plate geometry (cone diameter 35 mm, angle 2°) at 25 ± 0.01°C . For each measurement, 2.0 ml of emulsion were carefully deposited over the plateau of the rheometer.

Stress sweep tests (1 Hz at 25°C) were used to determine the linear viscoelastic region of all samples; a stress value of 1 Pa were chosen for all the frequency tests. All the dynamic frequency sweep tests were done inside the linear viscoelastic region in a frequency range of 0.01 to 10 Hz. and the elastic (G′) and viscous (G″) moduli were recorded versus frequency. All data analysis were made by a software (Reowin Pro Data Manager Version 2.64).

Steady flow measurements were carried out in the range of 0-300 s^{-1} during 60 sec and rheological parameters (shear stress, shear rate, apparent viscosity) were obtained from the software. Flow curves were fitted to power law model ($\eta = K * \gamma^{n}$) using Sigma Plot (Version 12, UK) software. The K and n parameters which are consistency and flow index, respectively, were calculated (Erçelebi and Ibanoglu, 2009).

3. 20 Moisture Content Determination of Powders

The moisture content of powdered encapsules were determined by drying them in the oven according to Official method of analysis (AOAC, 1995). 1 g of sample was put into an aluminium petri and oven dried at 105°C for 24 h. The measurements were carried out in triplicate.

3. 21 Encapsulation Yield Calculation

The solid content of the wall materials (LF and PPI) and the amount of core material (RSO) added during encapsule formation were used to calculate the encapsulation yield as follow (Rutz et al., 2017).

$$\text{EY (\%)} = \frac{\text{Final weight of encapsules}}{\text{Initial weight of LF, PPI and RSO}} * 100$$

3. 22 Loading Capacity, Loading Efficiency and Encapsulation Efficiency

The oil loading capacity (LC), loading efficiency (LE) and encapsulation efficiency (EE) of encapsules were determined as follows (Aziz et al., 2016; Shi et al., 2018)

$$\text{LC (\%)} = \frac{\text{Wt}}{\text{Wm}} * 100$$

$$\text{LE (\%)} = \frac{\text{Wt-Wf}}{\text{Wm}} * 100$$

$$\text{EE (\%)} = \frac{\text{Wt} - \text{Wf}}{\text{Wt}} * 100$$

Where Wm is the weight of RSO encapsules used for calculation of total RSO content (Wt) and Wf is the surface RSO content of encapsules.

The surface oil, also known as the non-encapsulated oil fraction, was determined according to the method described by Frascareli et al. (2012). 15 mL of hexane is added to 1 g of powders in a 50 mL of centrifuge, which was shaken for 2 min at room temperature in order to extract the free oil. Then, the dispersion was passed through Whatman filter paper No:4. The powder collected on the filter was washed three times with 20 ml of hexane. The filtrate was gathered and the solvent was removed using rotary evaporator (Heidolph Laborota 4000 Efficient, Germany) at 60°C.

The total oil content was determined according to the method described by Shi et al. (2018) with some modifications. 500 mg of RSO encapsule was mixed with 15 mL HCl (4 mol/L) with vortex for 5 minutes at room temperature. To extract RSO, 15 mL of hexane was added on it and shaken for 2 min at room temperature in order to extract the free oil. Then, the dispersion was passed through Whatman filter paper No:4. The powder collected on the filter was washed three times with 20 ml of hexane The filtrate was gathered and the solvent was removed using rotary evaporator (Heidolph Laborota 4000 Efficient, Germany) at 60°C.

3. 23 Morphological Analysis by Scanning Electron Microscopy

Morphological analysis of RSO encapsules was performed using Scanning Electron Microscopy (SEM) (Zeiss Gemini SEM 300, Germany) at an accelerating voltage of 15.0 kV. Produced RSO encapsules were placed on circular aluminium stub and coated with gold palladium in an argon atmosphere. Digital images were taken at magnification 250, 800 and 1200 (Shi et al., 2018).

3. 24 Peroxide Value Determination

Before measurement of Peroxide value oils from freeze dried (encapsulated) samples were extracted as described by Shi et al. (2018). Briefly, 5 g of sample was mixed with chloroform: methanol (2:1, v/v) and placed to dark place for overnight. The dispersion filtered through Whatman No:42 filter paper by twice. The residue was re-extracted twice by same solvent; the filtrates from three extractions were combined. The solvent-oil mixture was then passed through over anhydrous sodium sulphate placed over a filter paper in a funnel. The solvent was removed using rotary evaporator (Heidolph Laborota 4000 Efficient, Germany) at 50°C.

Peroxide values of bulk and extracted RSO and CHSO were evaluated as Section 3.2.3 during storage.

3. 25 Fourier Transforms Infrared Radiation Analysis

Fourier transforms infrared radiation (FTIR) spectra of oils and encapsules were recorded using FTIR spectrometer (FTIR 100, Perkin Elmer Incorporation, USA). Samples were placed directly onto the Universal diamond ATR crystal and all spectra

were measured against a background spectrum of air in the wavenumber range from 4000 to 650 cm^{-1} (Santos et al., 2015). .

3. 26 Statistical Analysis

The results were analyzed by one-way analysis of variance (ANOVA) to test for significant difference. Means of the groups the groups were compared using Duncan's multiple range test using a SPSS statistical packet (Version 22, Polar Engineering and Consulting, Nikiski, USA). Differences among sample means were reported to be significant when $p<0.05$ and Sigma Plot (Version 12, UK) program used for drawing plots.

CHAPTER 4
RESULTS AND DISCUSSIONS

4. 1 Characterizations of Oils

Raspberry Seed and Sour Cherry Kernel are mainly classified as by product from fruit processing. They contain high amount of ω -6 and ω -3 fatty acids contained oil which cannot be synthesized in the human body in their oil content (10-23%). Fatty acid compositions of RSO and CHSO were presented in Table 4.1. RSO is mainly composed of linoleic (ω-6) (51.6 %) and linolenic acid (ω-3) (31.37 %). CHSO contains oleic acid (57.2 %), linoleic (ω-6) (23.1 %) and linolenic acid (ω-3) (5.34 %). RSO had higher ratio of ω -6/ ω -3 fatty acids than CHSO. The results are in agreement with previous studies (Dimic et al., 2012; Oomah et al., 2000; Yılmaz and Gökmen, 2013)

The peroxide value (PV) is an indicator of the initial stages of oxidative change. The PV represents the total hydroperoxide content and is one of the most common quality indicators of fats and oils during production and storage (Chandrasekara and Shahidi, 2011). Initial PV values of RSO and CHSO were 3.42 and 1.34 meq O_2/kg oil, respectively as shown in Table 4.2. Those values are in range of PV found in other studies for these oils (Dimic et al., 2012; Parry et al., 2005; Yılmaz et al., 2018).

The oxidation of lipids has several important consequences for food quality and acceptability. The oxidative stability of a food is therefore an important parameter in determining its shelf life and quality. Induction times (IT) of the oils, which is a result of Rancimat methods, were measured to examine secondary products of lipid oxidation at accelerated conditions. The end point of the IT (h) was characterized by the sudden increase of water conductivity (µS/cm), due to the dissociation of volatile carboxylic acids which is indicator of presence of aldehyde and ketones. The IT of RSO was higher than CHSO which means that CHSO is more prone to oxidation (Table 4.2). Uluata and Ozdemir (2012) and Šućurović et al. (2009) were studied CHSO and RSO, respectively and similar results found by them.

Table 4. 1 Fatty acid composition of studied cold pressed oils (%)

Fatty acids	RSO	CHSO
C12:0 (Lauric acid)	0	0
C14:0 (Myristic acid)	0	0
C16:0 (Palmitic acid)	2.38	7.03
C18:0 (Stearic acid)	0.15	2.08
C18:1 (Oleic acid)	10.45	57.2
C18:2ω-6 (Linoleic acid)	**51.6**	**23.1**
C18:3 ω -3 (Linolenic acid)	**31.37**	**5.34**
C20:0 (Arachidic acid)	0.1	0
ω -6/ ω -3 ratio	1.64	4.32

Table 4. 2 Quality parameters of studied seed oils

Oil type	PV (meq O_2/kg oil)	Induction Time (h) at 110 °C	Refractive Index	Density (g/mL)
Raspberry seed oil	3.42 ± 0.02	1.94 ± 0.05	1.4810 ±0.01	0.968 ± 0.002
Sour cherry seed oil	1.34 ± 0.01	1.18 ± 0.07	1.4700 ± 0.01	0.954 ± 0.001

The density of RSO and CHSO were shown in Table 4.2. It is also important as quality parameter because the increasing of density cause an increase in the unsaturation of the oils (Šućurović et al., 2009). Values of Refractive Index of RSO and CHSO were measured as 1.4810 and 1.4700, respectively which were used later for droplet size and droplet charge measurements of emulsions and protein complexes

Table 4. 3 Color value of studied oils

Oil type	L*	a*	b*
RSO	1.45±0.09	-0.80±0.12	1.25±0.07
CHSO	4.31±0.06	-1.57±0.23	1.07±0.25

Color perceptions of the RSO and CHSO were investigated because of the importance of visual presentations for potential applications. The Hunter L* (lightness), a* (redness) and b (yellowness) values were listed in Table 4.3 represent the color spectrums of the oils tested. CHSO was lighter than RSO as indicated in L value. Negative a* values indicate green color of the oils and Positive b* values indicate yellow color of the oils.

Multi-component analyses of the RSO and CHSO were analyzed by Fourier transform spectroscopy (FTIR). The spectral regions were chosen for developing the regressions with including the fingerprint regions were selected according to the previous researcher's observations (Monica et al., 2007; Santos et al., 2015). The spectra in the FTIR region have well-resolved bands that can be assigned to present functional groups of the oils. The spectra are dominated by some peaks which shown in Table 4.4 for both oils.

The spectra of the RSO and CHSO have been shown on Figure 4.1 and Figure 4.2, respectively. Those observations are supported by the results of the other researchers performed with oils (Monica et al., 2007; Yeboah et al., 2017).

Table 4. 4 Assigment of absorption bands in the IR spectra of the oils

Peaks (cm^{-1})		Assignment of absorption bands
Cherry seed oil	Raspberry seed oil	
3007.91	3010.14	C-H stretching vibrations of the cis double bond (=CH)
2922.92 2853.68	2924.59 2854.39	Symmetric and asymmetric stretching vibrations of methylene (-CH2) groups
1743.91	1743.29	Ester carbonyl (-C=O functional group of the triacylglycerols) stretch
1463.52	1460.34	Bending vibrations of the CH_3 and CH_2 aliphatic groups
1377.64	1377.30	Bending vibrations of the CH_3 groups
1234.2	1236.68	Stretching vibrations of the C-O ester groups
1161.08	1159.57	Stretching and vibration of C=O group
1096.22	1098.21	-CH bending and -CH deformation vibration of fatty acids
721.68	720.91	CH_2 rocking vibration and out of plane vibration of cis-disubstituted olefins

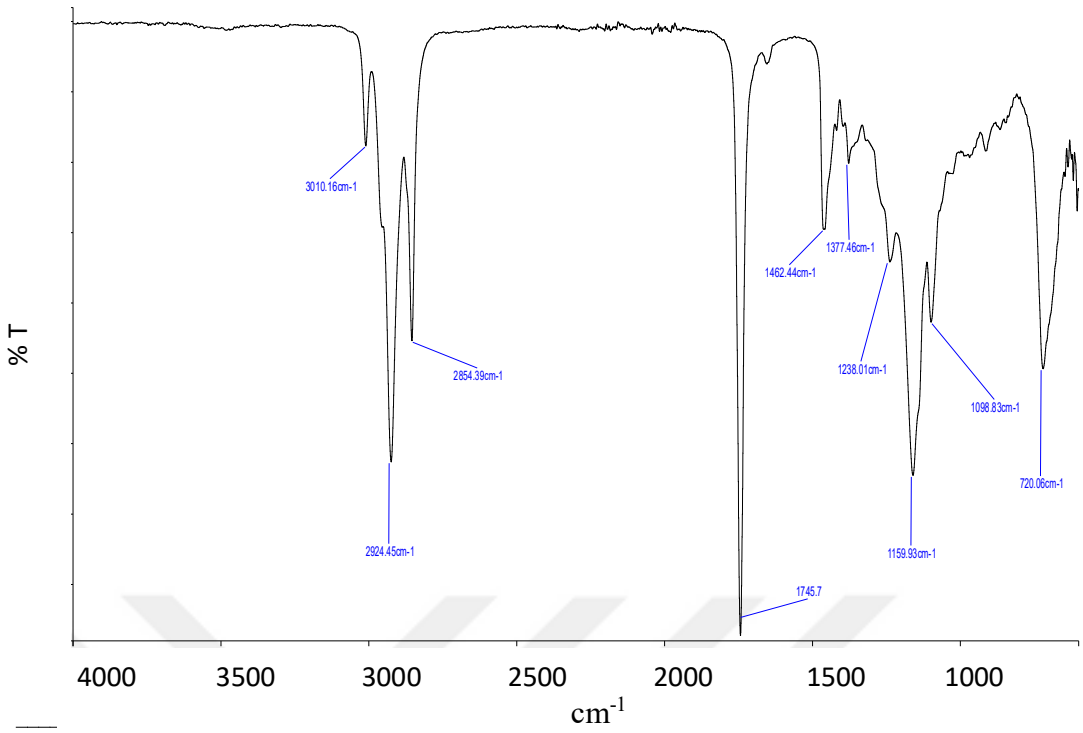

Figure 4. 1 FTIR spectra of RSO

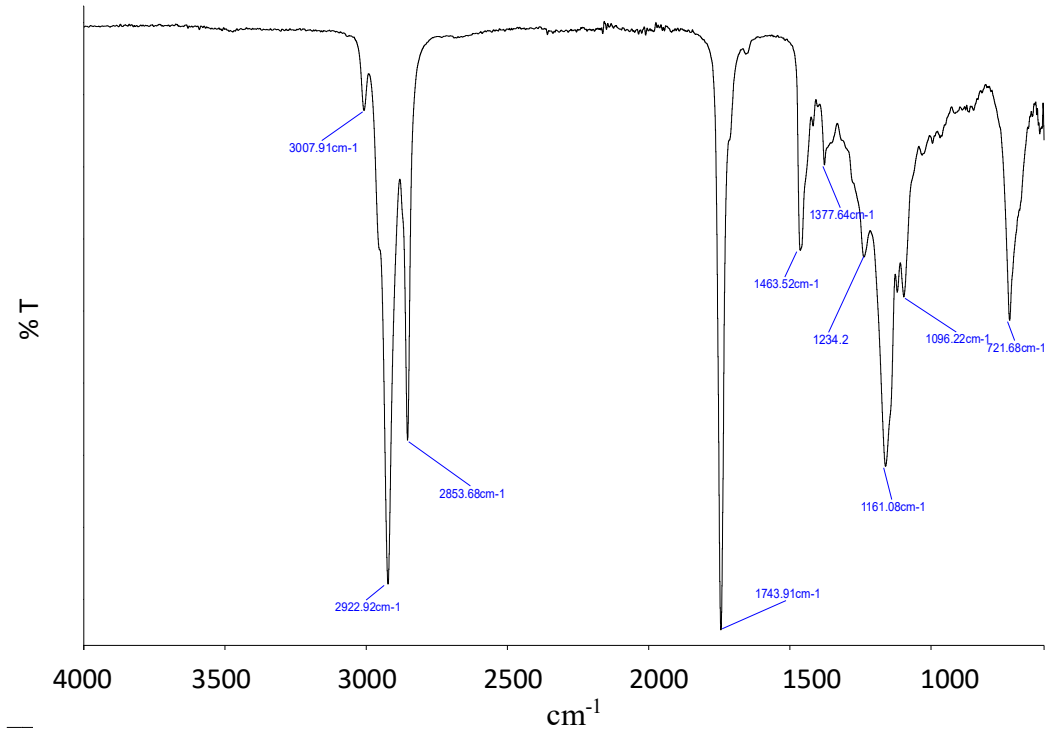

Figure 4. 2 FTIR spectra of CHSO

4. 2 Formation of Heteroprotein Complexes and Coacervates

4. 2. 1 Protein Content, Solubility Curve and Composition

Figure 4.3 shows the SDS-PAGE electrophoretogram of the LF and PPI stock solution tested. Lactoferrin (LF) stock solution (0.047 mM) had protein content of 96% (Kjeldahl, N×6.38), in agreement with the specification stated by the manufacturer, of which 95% was lactoferrin (Figure 4.3). On the other hand, pea protein isolate stock solution (0.007 mM) had protein content of 97% (Kjeldahl, N×6.25) and exhibited a wide variety of polypeptide subunits of molecular weight (M_w) ranging from 20 to 75 kDa, consisting of three main sets of protein subunits i.e. convicillin (72.4-77.9 kDa, 13.5%), vicillin (28.7-47.3 kDa, 33.2%) and legumin (α-subunits, 40.9 kDa, 21.2%; β-subunit, 22.3-23.1 kDa, 18.1%), which is in agreement with findings of previous authors (Barac et al., 2010). The legumin/vicillin (L/V) ratio was 1.2 which is within the lower range of values reported in literature (Mertens et al., 2012). The solubility curve of PPI stock solution is shown in Figure 4.4 showing isoelectric point (pI) at pH 4.0, which is in accordance with previous report (Liu et al., 2009).

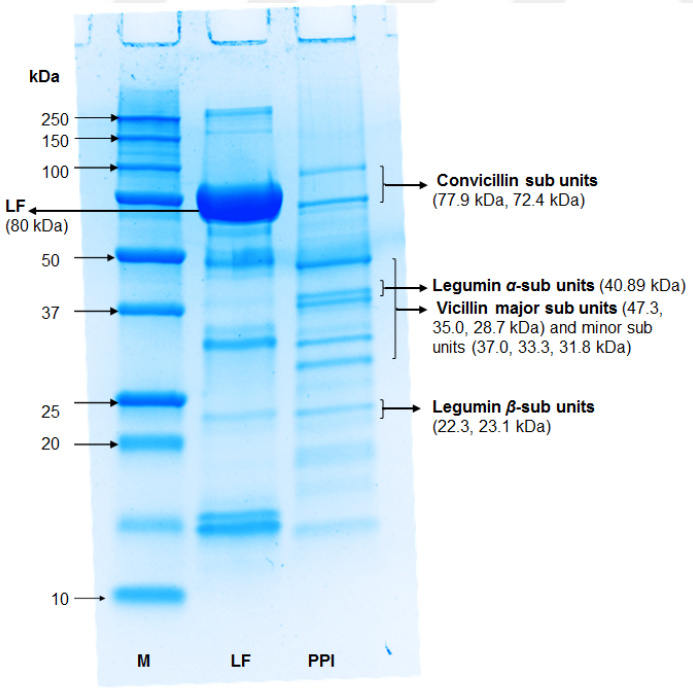

Figure 4. 3 SDS-PAGE of LF (0.047 mM) and PPI (0.007 mM) stock solutions. M is the molecular weight marker (10–250 kDa).

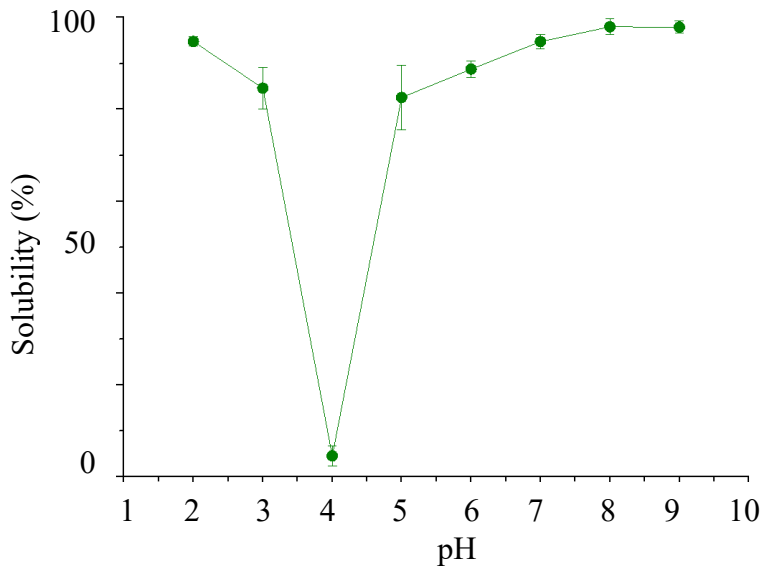

Figure 4. 4 Solubility curve of PPI stock solution after centrifugation and filtration (1.2 g/L).

Structure of coacervates formed by proteins with complementary charges are driven by electrostatic interactions. Hence, it is obvious that pH, ionic conditions, molar ratio of the charged moieties, protein characteristics (type, size, shape, molecular weight, and surface charge density) etc. may strongly influence the kinetics and thermodynamics of complex coacervation, and most of these parameters cannot be varied independently of each other (Qazvini et al., 2012). The approach toward charge neutralization can be via alteration of the charge of one or both partner macroions, or alteration of the combining ratio (microstoichiometry) within the complex (Kizilay, Ebru et al., 2011*)*. In this study, we first discuss the effect of different molar ratio of PPI/ LF on complex and/or coacervate formation at pH 7. This sets the scene for understanding the effect of the pH on the structure of LF-PPI complexes and coacervates at a fixed PPI/ LF molar ratio and identifies the boundary pH conditions leading to LF-PPI complex coacervation.

4. 2. 2 Effects of Biopolymer Mixing Ratio on LF-PPI Complex Formation

Typically, complexation occurs under solvent conditions, where both biopolymers have opposing charges. Selection of pH 7 was justified for the biopolymer mixing ratio as LF and PPI have a net positive and negative charge, respectively. Figure 4.5 shows the influence of PPI addition on the hydrodynamic radius and turbidity of the LF as a function of PPI/ LF ratio varying from 0.007 to 0.15 mM at neutral pH.

Almost optically clear LF-PPI solutions (Figure 4.5A) underwent a turbidity onset at > 0.04 mM PPI solution that was measurable with increase of optical density OD_{600} (Figure 4.5B). The turbidity corresponds to appearance of scattering particles in the medium and the formation of LF-PPI complexes. The OD_{600} exhibited its highest value (0.39) at PPI/LF molar ratio of 0.06, making the solution significantly cloudy indicating the maximum formation of insoluble complexes. Beyond PPI/ LF ratio of 0.06, intermediate levels of turbidity were observed with less cloudy appearance.

To assign the macroscopic turbidity data to hetero-protein coacervation, we used DLS and ζ-potential measurements. As shown in Figure 4.5B, in agreement with the turbidity data, R_h increased slowly from 51 nm to 57.6 nm as PPI/LF ratio increased by one order of magnitude, followed by maxima (~ 82 nm) at PPI/ LF ratio of 0.06 and then a decrease. At and above molar ratio of PPI/ LF of 0.08, the R_h reached a plateau. The effect of biopolymer mixing ratio was critical for controlling the charge balance within the mixed systems.

Zeta potential (ζ), the electro-kinetic potential difference between the dispersion medium and the slip plane (stationary layer of fluid attached to the dispersed particle) of moving particles confirmed an associative driving force for complexation between the positively charged amino acids of LF and the negative charges on PPI at very low biopolymer concentrations (Figure 4.6). In absence of added PPI, 0.047 mM LF was cationic at pH 7 and the ζ-potential was +12 mV. On addition of PPI, the positive charge of the mixture decreased to be electrically neutral (-2.5 mV) at 0.007 mM.

This means that at molar ratio of PPI/ LF of 0.06, the number of positively charged amino groups were nearly equivalent to that of the carboxylic acid groups, validating charge neutral complex formation, in agreement with the largest R_h and turbidity maxima. Above PPI/LF molar ratio of 0.06, the negative ζ-potential increased steadily to -12.3 mV, which might be attributed to LF molecules being covered by PPI moeties and thus formation of soluble complexes. Similar behavior for mixtures of LF and other proteins showing inter-protein interactions with increase in negative charge of mixed solutions have been observed previously (Anema and de Kruif, 2016). We selected this PPI/LF ratio of 0.15 to investigate the behavior of rather "soluble LF-PPI complex" with almost no visible turbidity (OD_{600} <0.15) as a function of pH drift in the next section.

A

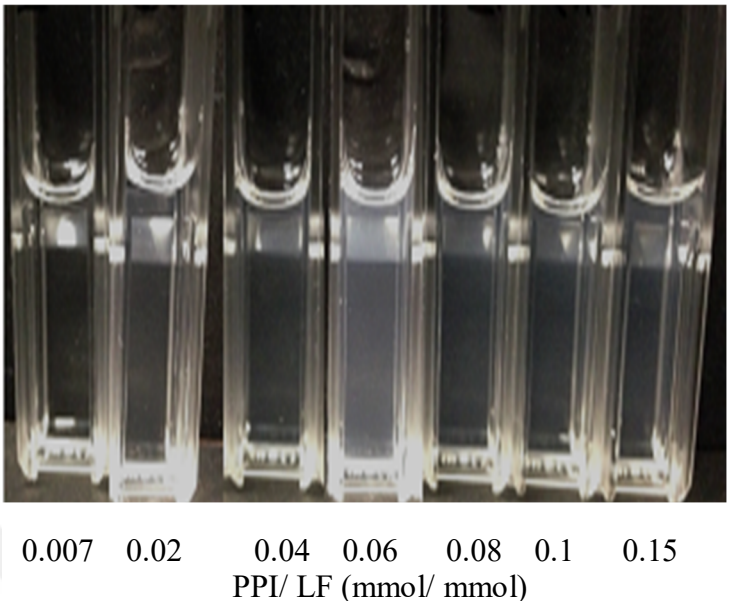

B

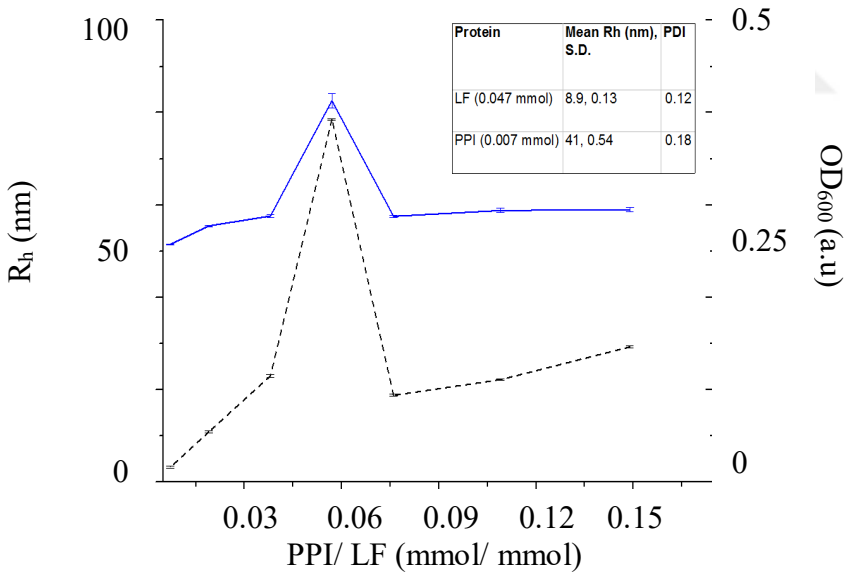

Figure 4. 5 Visual images (A) and dependence of hydrodynamic radius, R_h (bold line), turbidity (dotted line) (B) on PPI/ LF ratio on mixing LF (0.047 mM) with different concentrations of PPI at pH 7. Error bars represent standard deviations. Table inset shows the Rh and PDI (polydispersity index) of the pure LF and PPI stock solutions, respectively at pH 7

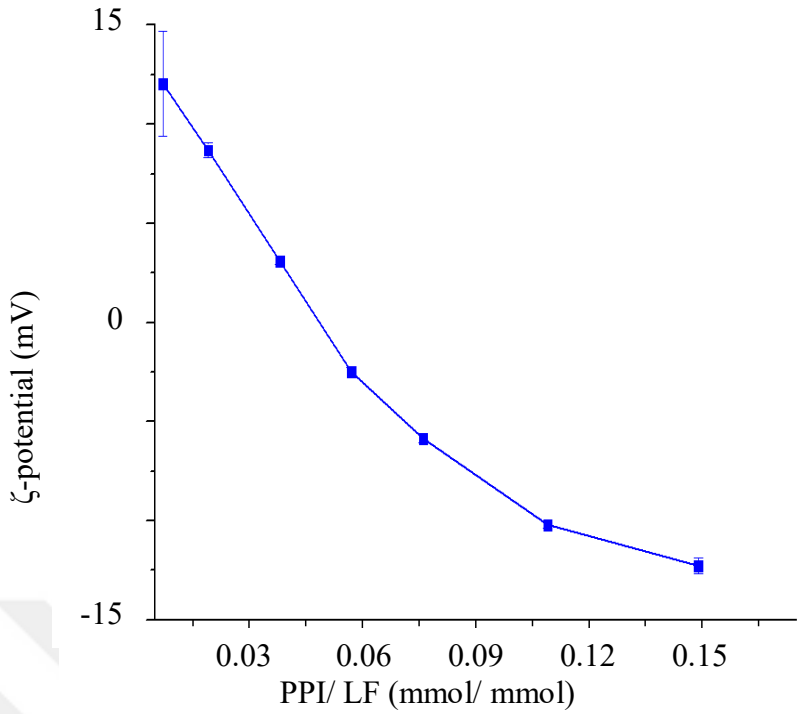

Figure 4. 6 Mean ζ-potential values as a function of PPI/ LF ratio on mixing LF (0.047 mM) with different concentrations of PPI at pH 7. Error bars represent standard deviations

4. 2. 3 Effects of Ph on Coacervate Formation

Heteroprotein coacervation differs from native protein self-aggregation based on the degree of pH-dependence of complex and kinetics of aggregation (Flanagan, Sean E. et al., 2015; Yan, Y. et al., 2013). It is known that coacervation can get overshadowed by protein self-aggregation. Hence, the hydrodynamic radius of native LF (0.047 mM), PPI (0.007 mM) and their mixtures at PPI/ LF ratio of 0.15 were measured as a function of pH 2-9 (Figure 4.7A) to discriminate between self-aggregation (if any) and LF-PPI interaction.

There was no significant change in hydrodynamic radius of LF as a function of pH (< 50 nm). In the case of PPI, the hydrodynamic radius remained below 70 nm at pH 6 to 9. However, the particle size was higher in the acidic region with possible PPI-PPI self-aggregation and reached the maximum at pH 4 (~ 332 nm), being the isoelectric point of PPI (Gharsallaoui et al., 2009), in line with the solubility curve (Figure 4.2). In the case of LF-PPI mixtures, the hydrodynamic radius remained below 75 nm in all pH except at pH 5-6, where the larger aggregates seemed to appear with maxima at pH 5.4 (Figure 4.7B). These large sizes might be attributed to the scattering from particles

of turbid LF-PPI mixtures (Figure 4.8). The interaction between LF and PPI did not readily lead to a new “liquid” phase. However, when these turbid materials at pH 5.4 and 5.8 were separated by mild centrifugation, presence of viscous liquid (Figure 4.7A, zoomed image in Figure) in the Eppendorf tubes had the clear signature of formation of coacervates (Anema and de Kruif, 2016). As observed in several LF-based coacervate studies (Croguennec et al., Accepted, In Press), the coacervates created might have coalesced into this concentrated viscous phase. Post pH 6.2, the samples were exhibiting rather “one-phase” with 35 nm complex.

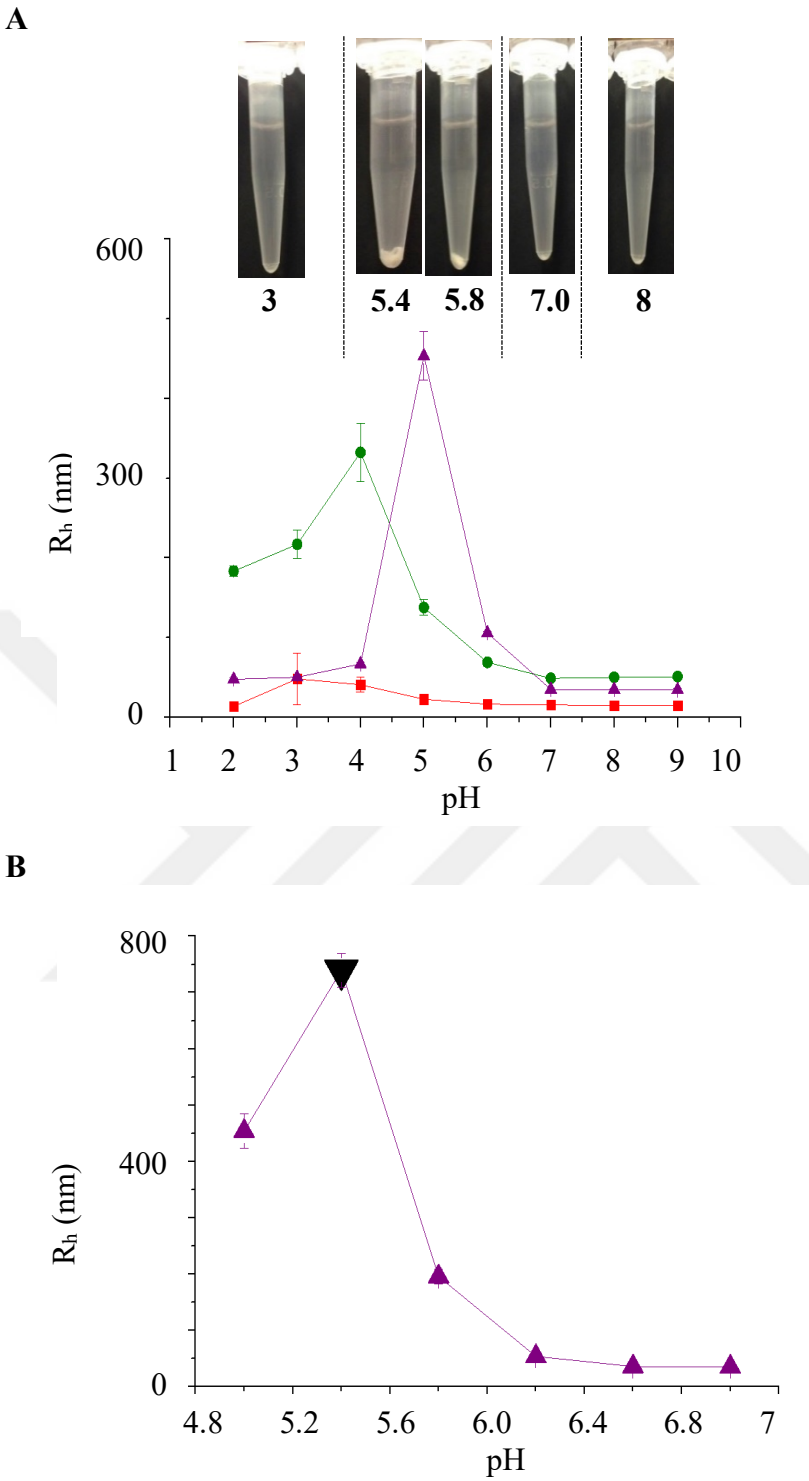

Figure 4. 7 Evolution of hydrodynamic radius, R_h of 0.047 mM LF solution (■), 0.007 mM PPI solution (●) and mixture of 0.047 mM LF and 0.007 mM PPI solutions (▲) (PPI/ LF molar ratio of 0.15 mmol/ mmol) as a function of pH with corresponding visual images taken after mild centrifugation of the LF-PPI mixtures (A) and zoomed-in mean hydrodynamic diameter of LF-PPI mixtures in pH 5-7 region (B). Error bars represent standard deviations.

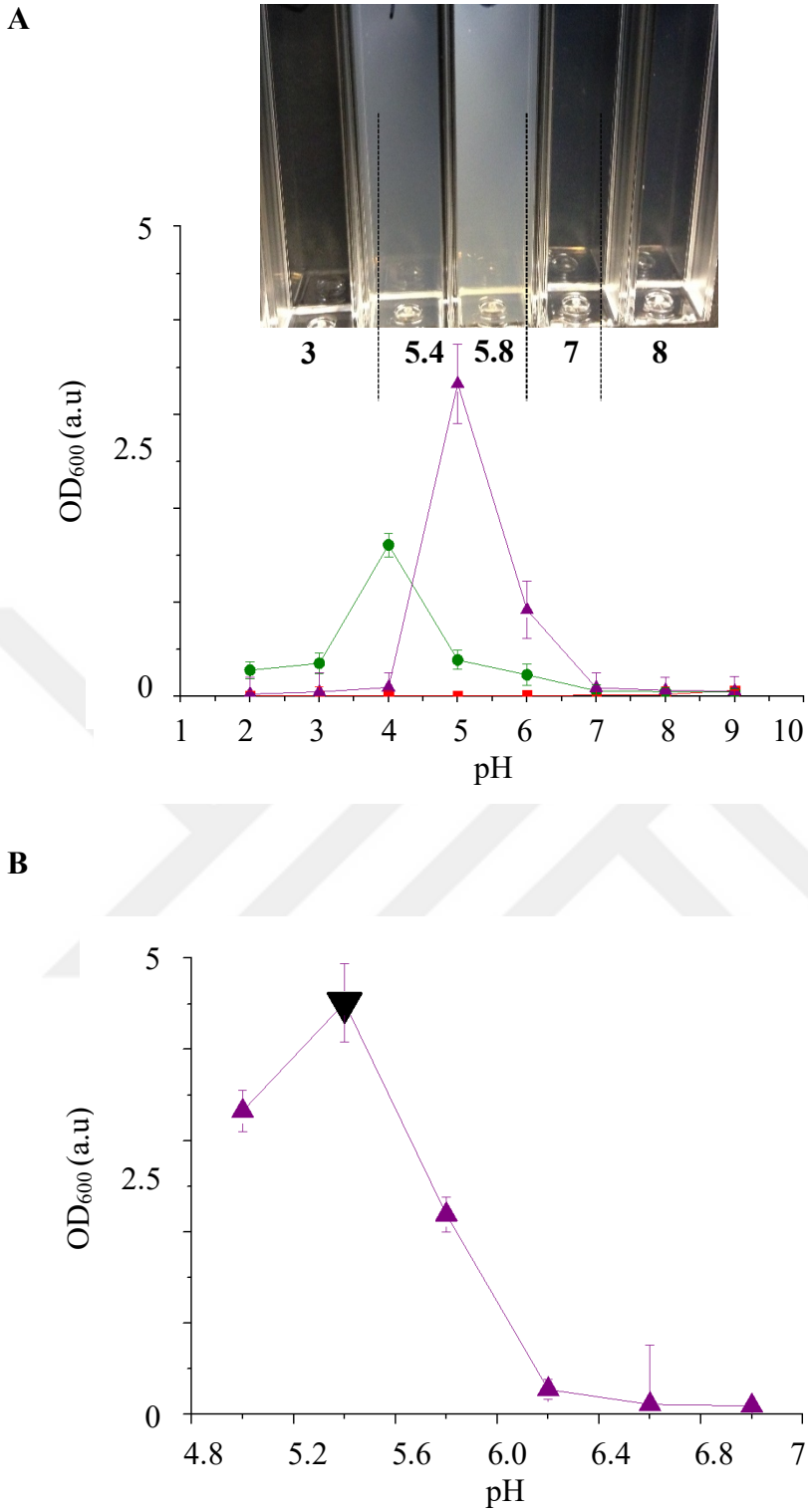

Figure 4. 8 Turbidity of 0.047 mM LF solution (■), 0.007 mM PPI solution (●) and mixture of 0.047 mM LF and 0.007 mM PPI solutions (▲) (PPI/ LF molar ratio of 0.15) as a function of pH with corresponding photographs of cuvette taken immediately after mixing (a) and the zoomed-in turbidity values of coacervates in pH 5-7 region highlighting the isoelectric point (▼) (b). Error bars represent standard deviations

4. 2. 4 Identification of Boundary Conditions for Coacervate Formation

Since complex coacervation between LF and PPI is due to electrostatic interaction between oppositely charged proteins, the charge characteristics of the individual components were measured by Doppler electrophoresis in a wide pH range of 2.0–9.0. (Figure 4.9). The ζ-potential of LF decreased from +24.8 mV to -1.5 mV as pH increased from 2 to 9 and reached zero at around pH 8.5, which is the isoelectric point of LF. The isoelectric point of LF is in line with the theoretical net charge and fits closely with the pI value reported previously (Yan, Y. et al., 2013).

On the other hand, ζ-potential value of PPI changed from +23.2 mV to -28.2 mV as pH increased and close to zero around pH 4 (pI). This is in line with the increase in R_h data, solubility curve validating the aggregation of pea protein molecules near its isoelectric point. The observed pI of PPI is within the range reported by previous authors (Liu et al., 2009). When the LF (0.047 mM) and PPI (0.007 mM) were mixed, the ζ-potential decreased from +32.5 mV to -18.6 mV as a function of pH, with values approximately zero in the pH range from 5-6. Zooming in further the ζ-potential values in pH 5-6 (Figure 4.9B), it can be observed that from pH 5-5.8, the ζ-potential values remained ≤ -5 mV and it is only at pH 6.2 and beyond, the negative charge started increasing.

Although the mechanism of the complex coacervate formation is not fully understood, we hypothesize the following sequential processes based on previous literature. Below pH 4, both LF and PPI molecules being cationic molecules (pH> pI) appear to repel each other and this prevents the formation of a complex between the two protein molecules.

A

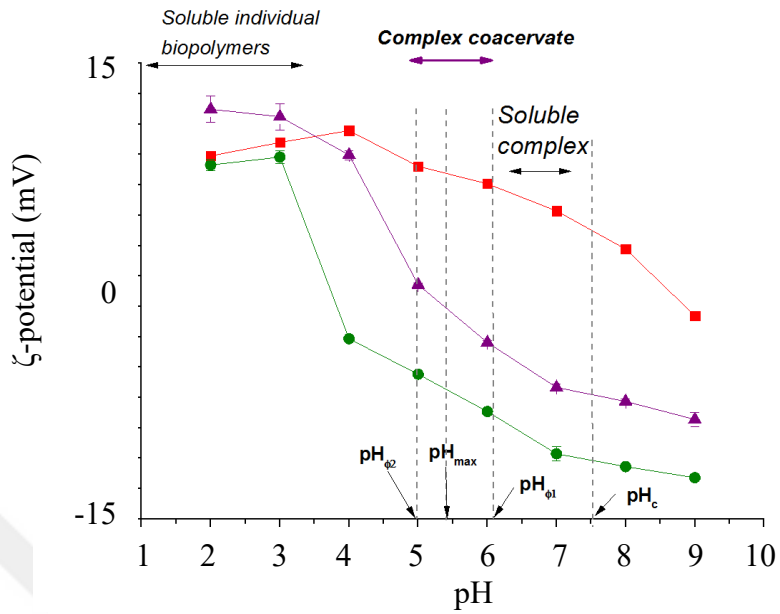

B

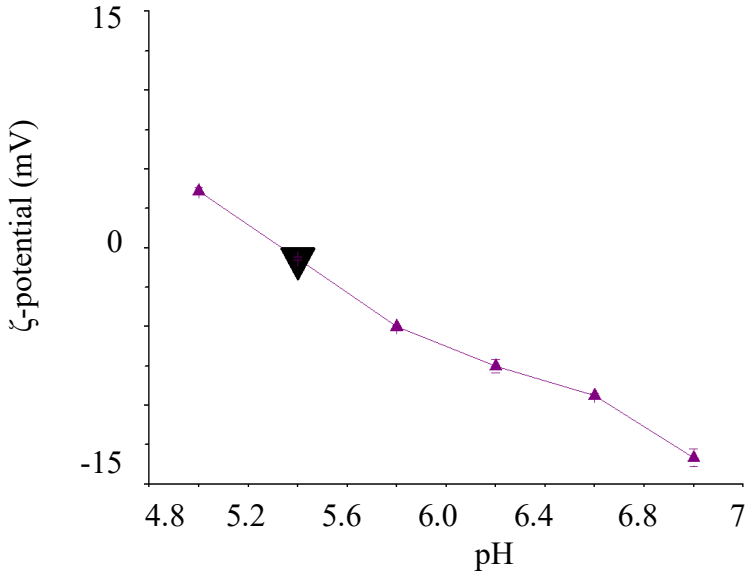

Figure 4. 9 Mean ζ-potential values of 0.047 mM LF solution (■), 0.007 mM PPI solution (●) and mixture of 0.047 mM LF and 0.007 mM PPI solutions (▲) (PPI/ LF molar ratio of 0.15 mmol/ mmol) as a function of pH showing pH_c, $pH_{\varphi 1}$, pH_{max}, and $pH_{\varphi 2}$ (A) and the zoomed-in mean ζ-potential values of LF-PPI mixtures in pH 5-7 region highlighting the isoelectric point (▼) (B). Error bars represent standard deviations.

This is in line with the low particle size, turbidity measurements and transparent appearance of the mixed biopolymer solutions (Figure 4.7 and 4.8). Dublin et al. (1994) showed that two polyelectrolytes that contain like (negative or positive) charge could form soluble complex. Hence, in our case, the LF and PPI might be present as individual biopolymer molecules or as soluble complexes below pH 4. Above pH 5.0, hydrodynamic radius (*R*h) gradually increased above the value that corresponds to the *R*h of LF or PPI alone observed for pH < $pH_{\phi 2}$ *(*Kizilay, E. et al., 2011*)*. The pure (precipitate-free) coacervate formation appeared to be initiated above pH 5.0, followed by growth of primary complexes to form quasi-neutralized insoluble complexes ($pH_{\phi 2}$), with a depletion of charge at pH 5.0. Further kinetic experiments should be performed to confirm this growth mechanism. At pH 5.4 (pH_{max}), electrical equivalence was achieved between the proteins with ζ-potential reaching zero and the scattering of particles being highest with rapid rise in R_h (Figure 4.7B) and maximum turbidity (Figure 4.7). This is seen in other studies where LF has been shown to form coacervate with anionic proteins at this pH range. For instance, Anema and de Kruif (2016) observed maximum coacervation for β-lg (β-lactoglobulin)-LF complexation at pH 6.3, where the ζ-potential was nearly zero. In our case, coacervation was maximum at pH 5.4, which is more closer to the pI of PPI, as halfway between respective pI's would be pH 6.25 (=(4+8.5)/2).

Soluble complexes are formed between biopolymers when net charge is high and electrostatic interaction is lower whereas insoluble complexes and coacervate formation occurs when electrostatic interaction between molecules is strong and net charge was low. In our case, we suggest that at pH 5.0-6.0 there was formation of coacervate, whereas pH ≥ $pH_{\phi 1}$ (6.2), soluble complexes were formed and the boundary is designated as pH_c (pH 7), *i.e.* 1.5 units away from isoelectric point of LF. Above pH 8.5, both LF and PPI carried a similar net charge. To reveal the distribution of size of these complexes and/or coacervates, small angle X-ray scattering (SAXS), atomic force microscopy (AFM) and electron microscopy was used.

4. 2. 5 Small Angle X-ray Scattering (SAXS)

The SAXS pattern of pure dispersions of LF and PPI were recorded at pH 7 at 25 °C and analyzed by the Generalized Indirect Fourier Transform (GIFT) method (Bergmann et al., 2000) (Figure 4.10). The determined SAXS data of LF and of PPI

(Figure 4.10A) compared well to previous literature data (Anderson et al., 1987; Grossmann et al., 1992; Welland et al., 1989). As revealed in the PDDFs (Figure 4.10B) LF was not perfectly globular, but composed of two globular lobes, which are compactly arranged in protein crystals, but under solution conditions can open up. In solution, Grossmann et al. (1992) determined a radius of gyration, Rg = 3.3-3.6 nm for human lactoferrin measured at pH 7.5. Since our samples were measured at a slightly lower pH, the difference in our observed value of Rg = 4.2 nm for bovine lactoferrin might be related to a bigger opening of the inter-domain cleft (Table 4.5). Note, that the smallest cleft is observed in the crystal form of lactoferrin, in which the corresponding Rg is smaller than 3 nm (Anderson et al., 1987; Grossmann et al., 1992) Concerning PPI, a maximum extension of about 25 nm and furthermore a double peak distribution is apparent in the PDDF. Pea consisted of legumin, vicilin and convicilin, as discussed before (Mession et al., 2013) Legumin has Rg = 4.45 nm (Plietz et al., 1984) and and vicilin has Rg = 4.4 nm (I'Anson et al., 1988).

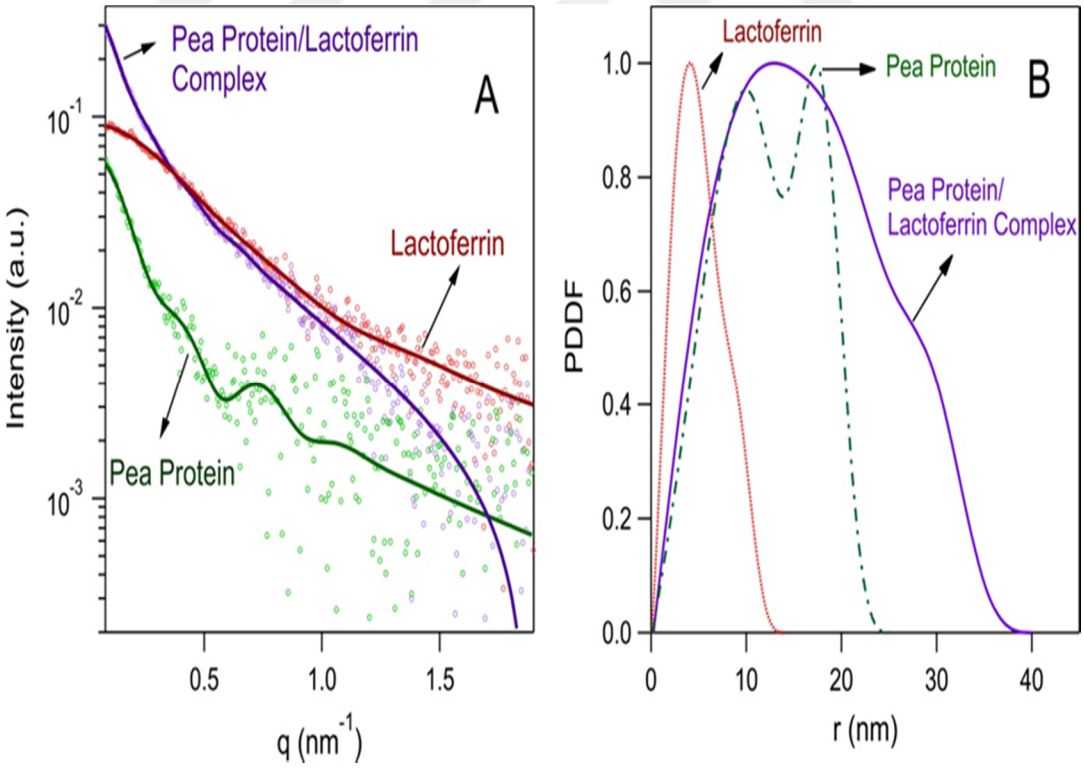

Figure 4. 10 A) SAXS curves of 0.007 mM PPI, 0.047 mM LF and their complex formed at pH=7. The solid lines represent the fitted curves obtained by Indirect Fourier Transformation (IFT) analysis. B) The corresponding Pair-Distance Distribution Functions (PDDFs) are displayed as a function of the radial distance (r).

Thus, the PDDF confirms that the PPI aggregates into oligomers (about 3-6 proteins), which was first shown as a pseudo-hexagonal, ring-like appearance by scanning electron tunneling microscopy (Welland et al., 1989). The extension of PPI aggregates is in the order of 20-25 nm, which compares well to a maximum extension of about 25 nm displayed in the PDDF (Figure 4.10B).

Table 4. 5 Radius of gyration of PPI, LF and their complex at pH 7.0

Sample	Radius of gyration (nm)
LF	4.22
PPI	9.47
LF-PPI complex	13.1

Figure 4. 11 gives an overview of all measured LF-PPI complexes and coacervates at various pH values. As clearly shown at pH 7.0, complexes were composed of both LF and PPI, since a simple superposition of the individual LF and PPI scattering curves would not lead to a SAXS curve with Rg = 13.1 nm. Therefore, the amount of self-aggregated protein can practically be ignored. In accordance with the ζ-potential measurements (compare Figure 4.9), the biggest coacervates were formed at pH 5.4. Their maximum extension reached values of about 80 nm (Figure 4.9B), leading to rough estimate of coacervate radius of 40 nm. Since all involved proteins have similar radii (Rg = 4.0 to 4.5 nm, which relates to R = $\sqrt{\frac{5}{3}}$ Rg = 5.2 to 5.8 ≈ 5.5 nm), we can roughly estimate the number of proteins involved in the biggest coacervates: Vcoacervate /Vprotein ≈ 380 proteins. Assuming a protein packing density similar to the closest packing density of spheres (0.74), we obtain a corrected estimate of about 280 proteins per coacervate. The highest solubility of proteins was determined for pH 6.2 (smallest Rg = 7.7 nm), which corresponds to about 4-5 proteins per complex. Further increasing the pH increases the size of the complexes again: at pH 7, roughly 36 proteins were observed in an aggregate. We note though, that these estimates protein numbers have to be taken with due care, since these complexes were not exclusively spherical. A closer inspection of the PDDF's in Figure 4.11B reveals that the size distributions were bimodal instead (note, that each PDDF displayed a shoulder

at higher distances). This bimodal size distribution was further confirmed by AFM measurements and might be assigned to differently shaped spherical "coacervates" and elongated shaped "complexes", respectively (Svergun and Koch, 2003).

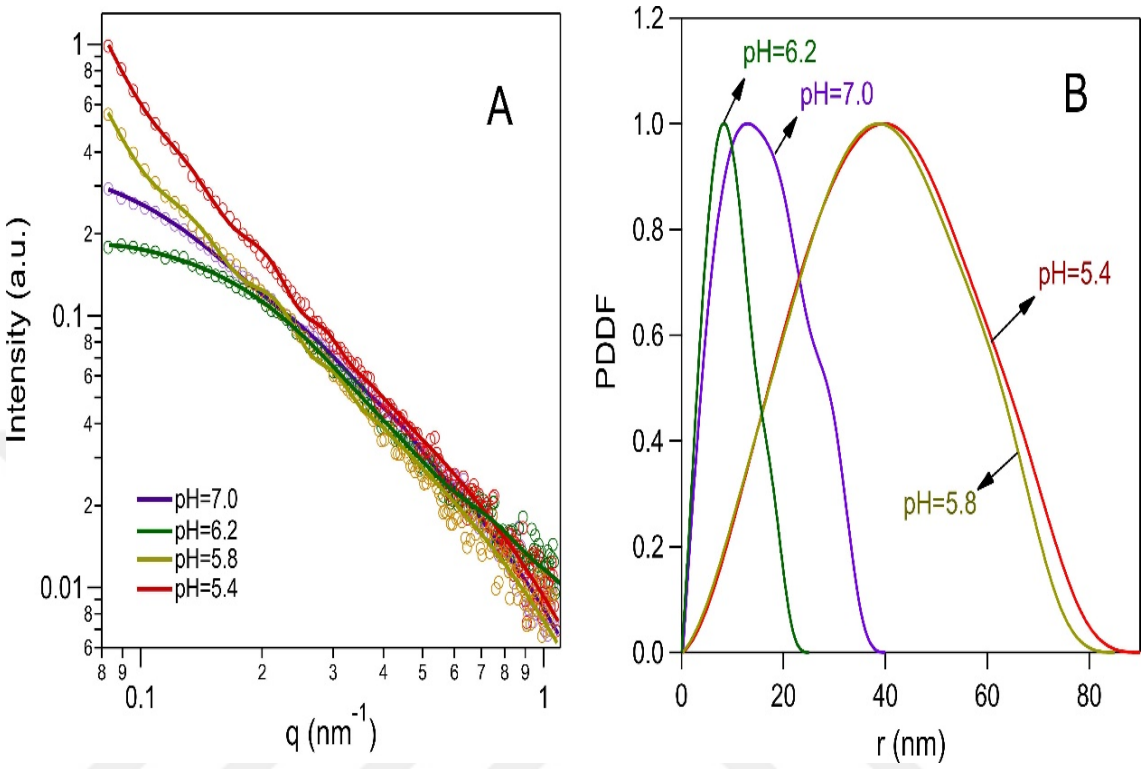

Figure 4. 11 A) Small angle scattering curves of the LF-PPI coacervates and/or soluble complexes at various pH values. B) The corresponding Pair-Distance Distribution Functions (PDDFs) were evaluated based on Indirect-Fourier Transformation and show that the largest coacervate formed at pH=5.4

Table 4. 6 Radius of gyration of LF-PPI coacervates (at pH 5.4 and 5.8) and soluble complexes (at pH 6.2 and 7.0)

pH	Radius of Gyration (nm)
7.0	13.1
6.2	7.7
5.8	30.3
5.4	31.3

4. 2. 6 Electron Micrographs of The Coacervates

To investigate the microstructure of the coacervate, negative stained TEM micrographs of mixtures at PPI/LF molar ratio of 0.15 at different pH are shown in Figure 4.12. Dense coacervates with partially inter-connected "chain" like clusters as well as "spherical shaped" structures can be observed at the pH 5.4 (Figure 4.12A), which is consistent with near zero ζ-potential and high R_h. However, at pH 7.0 (Figure 4.12B), the overall negative charge was relatively high leading to more separated micro-clusters which did not separate out even after centrifugation.

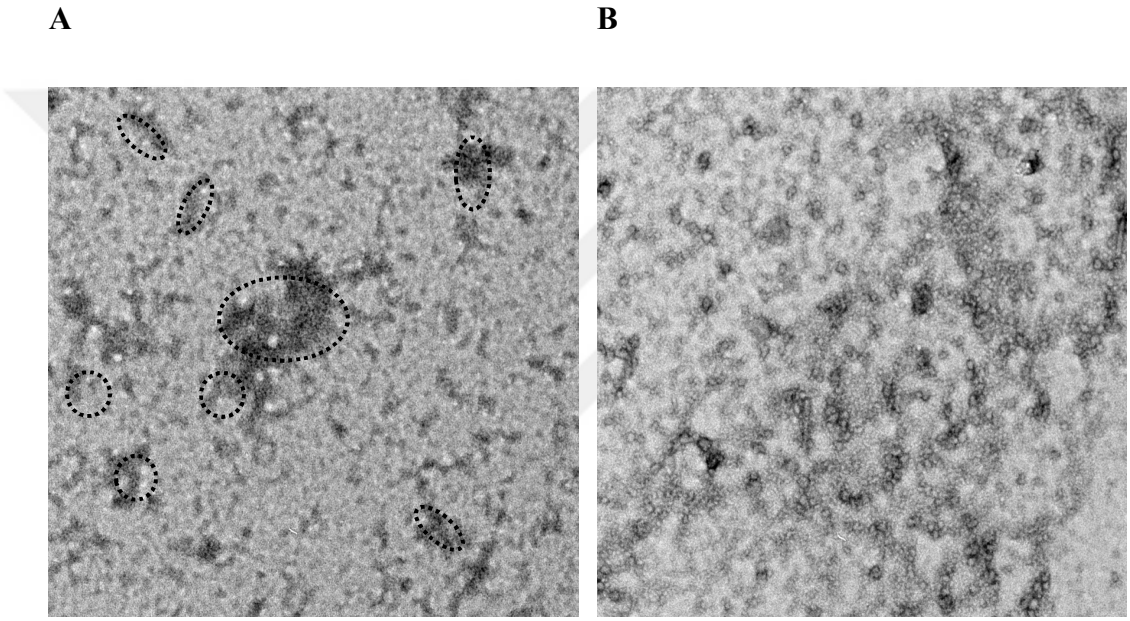

Figure 4. 12 TEM micrographs of LF-PPI mixtures (PPI/LF molar ratio = 0.15) at pH 5.4 (A) and pH 7.0, (B). Scale bars 500 nm

Additionally, AFM images were analyzed to investigate structure of LF, LF-PPI complex (pH 7.0) and LF-PPI coacervate (pH 5.4) adsorbed to mica surfaces (Figure 4.13). As can be observed from Figure 4. 13A and histogram a, LF showed uniform spherical particles, with a mean radius of 6.2 nm. From SAXS, the lactoferrin radius was 4.2 nm. This increase in apparent size can be described by the well-known tip-magnification effect in AFM. A tip radius of 7.5 nm, typical of the TESPA-V2 (Bruker) probes used in this study, would result in an apparent size of 6.2 nm for the lactoferrin. The complexes formed at pH 7.0 were very sparse owing to a weak electrostatic attachment, despite the use of the divalent cation Mg^{2+} to modify the surface of mica (Pastre et al., 2003). This may be because of the influence of ionic

strength change on the narrow boundary conditions of LF-PPI complex and coacervate formation.

The radius of the soluble complexes (Figure 4.13Bb) from AFM images was found to lie in the broader range between 9-15 nm (mean radius = 11.2 nm) which is in close agreement with SAXS data (PPI: R_g = 9.5 nm, LF-PPI complex at pH 7.0: R_g = 13.1 nm). The coacervates formed at pH 5.4 were clearly visible as groups of individual proteins forming complexes of greater than 40 nm in size. The analysis of complex morphology is shown in Figure 4.11. While a dense and space filling structure of coacervates was formed at pH 5.4 (Figure 4.13C), the complexes produced at pH 7.0 (Figure 4.13B) were less clustered, which is in line with the electron micrographs (Figure 4.12A and B). Figure 4.13D shows the detail of the large single coacervate in topography and AFM phase contrast. Below, we present a schematic representation created from circular unit with measurements taken from the AFM images of pure LF and PPI and overlaid onto the image (Figure 4.13D top) as closely as possible. The underlying image was then deleted to reveal a stylised cartoon of the coacervate, which suggests that LF were forming bridges between predominantly PPI moieties forming the structural units. Bottom panel is a cartoon illustration of the same complexes, made up of LF (red small circles) and PPI (blue large circles) scaled using the mean individual protein size from the histograms.

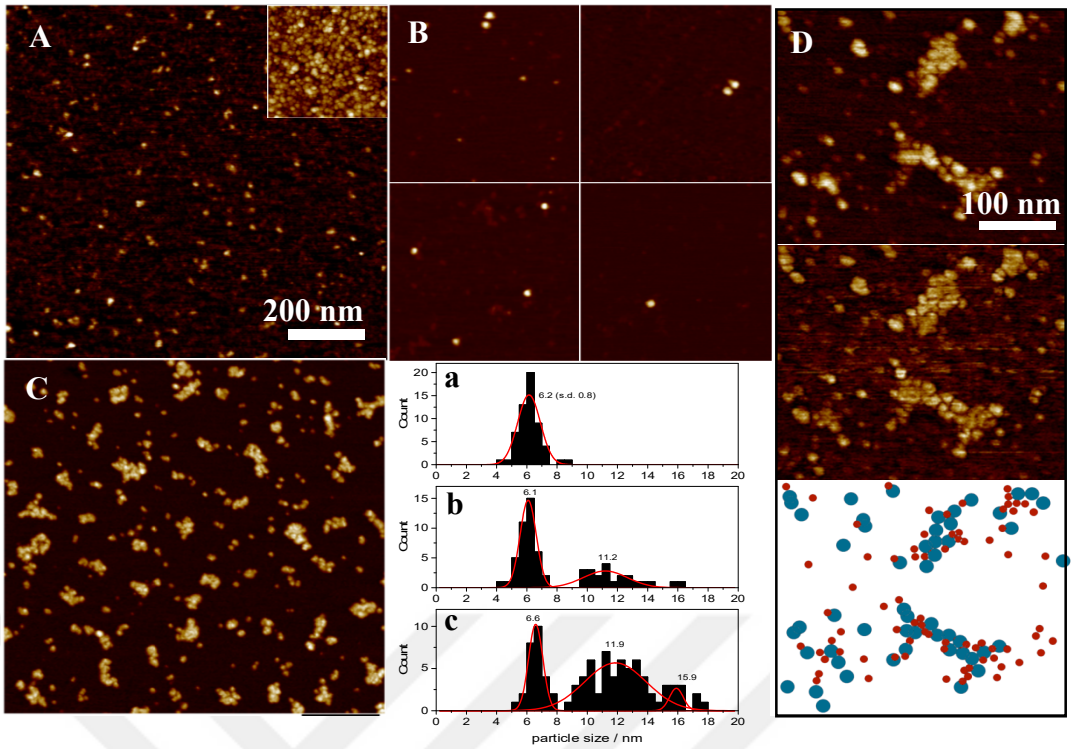

Figure 4. 13 Tapping mode AFM images with size analysis histograms of individual proteins, either as isolated particles or when they can be clearly discriminated within complexes. A-a LF at pH 7.0 (inset shows image of continuous close packed layer of LF prepared from a higher concentration solution), B-b LF-PPI complex at pH 7.0 (the pH 7.0 complex did not bind well to mica and were sparsely distributed, so shown here are a composite of 4 separate 500 nm scans), C-c LF-PPI coacervate at pH 5.4. Histogram of diameters, a-c, is for entities < 20 nm radius only. Images A-C are to the same scale. D Coacervates at pH 5.4 at higher resolution. Top panel is AFM topography, middle panel is an AFM phase contrast image of the same area, which shows the protein has a different material response to the background mica substrate (as expected) and the sensitivity of the mode to gradient helps discriminate individual proteins

The distribution of particle sizes is represented in Figure 4.14D, which shows the length and width of each particle. As there are many more individual particles of smaller size, and a fewer number of large aggregates containing much more of the total mass of coacervate, the size of each data point was scaled to be directly proportional to the size of each particle. This better represents the most likely size and shape of the coacervate, and hence directly comparable to SAXS data. Overall, the distribution contains strong clusters around 40-50 nm and 60-70 nm. More spherical clusters are represented by the straight line with the major and minor axes of the same size, whilst the extending chain like complexes by the distribution along the x-axis, with no further increase in width. Interestingly, the complexes appeared to grow directionally forming ordered chains with width of 30-50 nm. In fact, once the clusters start to grow, they

were more likely to elongate, which might be linked to PPI-PPI aggregation. The concentration of ordered-chain like aggregates with length being 140 nm and minor axis of 40 nm dominated over the spherical nanocomplexes of 40 nm. We believe that the connection between these spherical nanocomplexes were responsible for the formation of coacervate, shown by the liquid behavior of the dense phase at a macroscopic scale post centrifugation. Similar spherical to elliptic shaped clusters have also been reported in other coacervate systems, such as bovine serum albumin (BSA) and poly (dimethyldiallylammonium chloride) (Kaibara et al., 2000), polyelectrolyte-mixed micelle (Liberatore et al., 2009). The self-aggregation of PPI particularly that elongates could not be fully ignored although their abundance was limited. However, to our knowledge this is the first study that reports such hierarchy of morphology in LF-mixed plant protein coacervate system, where PPI self-aggregates and LF-PPI coacevates do coexist.

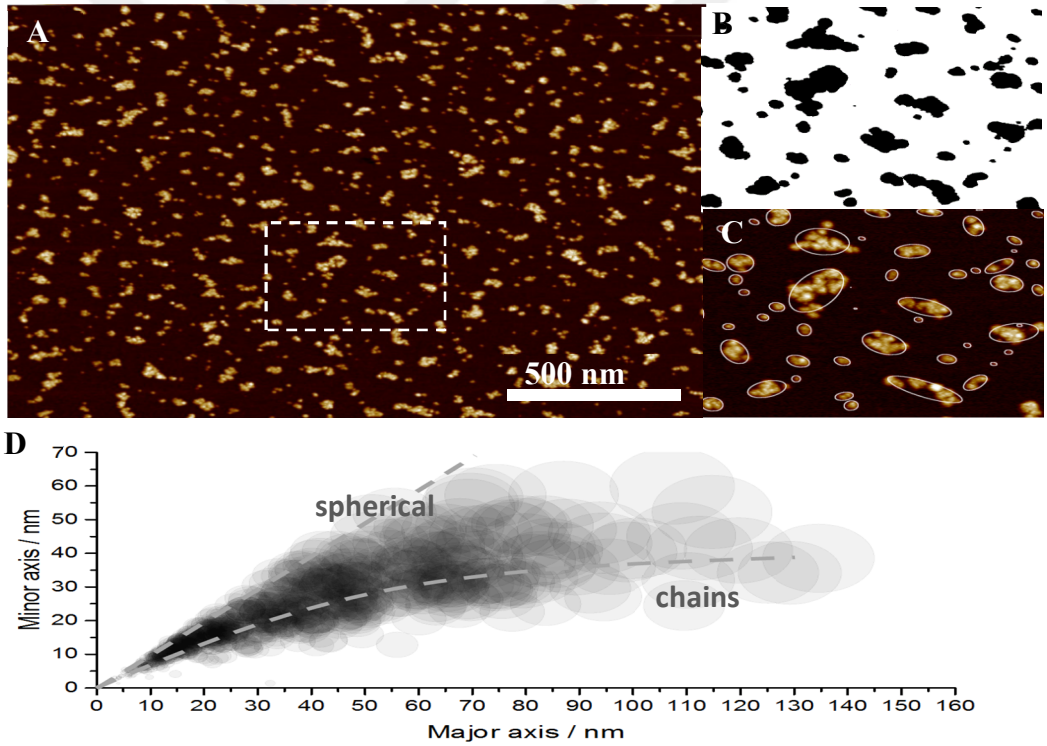

Figure 4. 14 A) AFM topography image of pH 5.4 coacervate at 2048 pixel resolution, B) digital zoom of area highlighted in panel A, thresholded to create a binary image before automated particle analysis, C) software fits ellipses to each aggregate, shown here overlaid upon the digital zoom of the original image. The major and minor axis of each ellipse is used to generate panel D), describing the size and shape distribution of >1000 complexes. The size of each data point has been scaled to the size of the complex, hence the intensity reflects the probability of each protein particle to be aggregated within a complex of a particular size/shape. Complexes up to 140 nm in length were found, which tended to be limited to a width of around 40 nm

4. 3 Emulsion studies Part I: Method optimization

4. 3. 1 Droplet Size of Emulsions

Emulsions are often used to encapsulate and deliver bioactive components within the food industry, such as ω-3 fatty acids, carotenoids, flavonoids, and phytosterols. It is therefore important to understand how heteroprotein emulsions formed.

The particle size is usually reported as either the volume-weighted ($d_{43}=\sum d_i n_i^4/\sum d_i n_i^3$) or surface-weighted mean diameter ($d_{32}=\sum d_i n_i^3/\sum d_i n_i^2$), where ni is the number of droplets of diameter d_i. The mean particle diameter of emulsion droplets depends on emulsifier type and formation method. The particle size distribution (PSD) defines the fraction of particles in different size ranges. The particle size distribution is usually measured using light scattering or microscopy methods (McClements et al., 2009).

Six different emulsions were prepared as indicated in Table 3.2. We have chosen total protein concentration as 1 wt% while oil concentration was 10 wt% oil from previous studies based on LF stabilized emulsions (Sarkar et al., 2009; Tokle and McClements, 2011). Our aim was here to examine effect of different methods on droplet size of emulsions prepared by RSO. Sauter mean diameter (d_{32}) and volume mean diameter (d_{43}) of emulsions were presented in Table 4.7. PPI coated emulsion (Identity 2) had higher diameter than LF coated emulsion (Identity 1) as expected because of moleculer size of them. But the both results were lower than 1 µm as Mao and McClements (2011) found in their study. In the Identity 3 and 4, interaction of LF-PPI was occurred before emulsion preparation. Afterwards, oil was added and emulsion was prepared. For these samples, the results of d_{43} were lower than 1µm at pH 7 whereas slightly higher than 1µm at 5.4. This might be due to aggregation of free proteins in this pH region (Mao and McClements, 2013). In the 5th and 6th samples, we prepared LF coated emulsion at pH 7 and then added PPI solution at 7. Then pH of the emulsions were adjusted to pH 7 and 5.4, respectively. The d_{43} of these samples were lower than samples which called as Identity 3 and 4.

Table 4. 7 Sauter mean diameter (d_{32}) and volume mean diameter (d_{43}) of emulsions 1) LF coated RSO at pH 7, 2) PPI coated RSO at pH 7, 3) LF-PPI coated RSO at pH 5.4 (complex formed before emulsion forming), 4) LF-PPI coated RSO at pH 7 (complex formed before emulsion forming), 5) LF-PPI coated RSO at pH 7 (complex formed after emulsion forming with LF), 6) LF-PPI coated RSO at pH 5.4 (complex formed after emulsion forming with LF)

Identity number	d_{32} (µm)	d_{43} (µm)
1	0.105 ± 0.000	0.432 ± 0.021
2	0.100 ± 0.001	0.983 ± 0.011
3	0.073 ± 0.002	1.380 ± 0.109
4	0.083 ± 0.001	0.647 ± 0.023
5	0.119 ± 0.001	0.867 ± 0.038
6	0.129 ± 0.006	0.703 ± 0.011

4. 3. 2 Droplet Charge of Emulsions

The mean electrical charge (ζ-potential, mV) on droplets of individual LF, PPI and LF-PPI stabilized emulsions are presented in Table 4.8. As can be seen from Table 4.8, droplet charge of native LF and PPI coated emulsions were +52.3 and -40.7 (mV), respectively at pH 7. Gharsallaoui et al. (2009) found that the ζ-potential of droplets in a PPI stabilized emulsion was nearly -40 mV. Singh and Sarkar (2011) studied on protein-stabilised emulsions and found ζ-potential of LF stabilized emulsion as +52 mV. For mixed emulsions, charge is negative at pH 7 and positive (almost zero) at pH 5.4. These results are in accordance with our previous finding (Figure 4.9). In soluble complex region, pH 6.2-7.2, there were still free PPI in the solution could be reason of the negative droplet charges.

Table 4. 8 Droplet charge (ζ-potential) of emulsions 1) LF coated RSO at pH 7, 2) PPI coated RSO at pH 7, 3) LF-PPI coated RSO at pH 5.4 (complex formed before emulsion forming), 4) LF-PPI coated RSO at pH 7 (complex formed before emulsion forming), 5) LF-PPI coated RSO at pH 7 (complex formed after emulsion forming with LF), 6) LF-PPI coated RSO at pH 5.4 (complex formed after emulsion forming with LF)

Identity number	Zp (mV)
1	52.3 ± 1.7
2	-40.7 ± 0.7
3	0.4 ± 0.1
4	-21.7 ± 0.6
5	-20.1 ± 1.0
6	1.2 ± 0.4

4. 3. 3 Emulsion Stability

The emulsion stability of emulsions prepared with different methods after 1 day and 7 days are shown in Figure 4.15 and 4.16, respectively. Visual observation of the all samples indicated that all of them were stable to gravitational separation after 1 day (Figure 4.16).

After 7 days, Sample 2, Sample 3 and Sample 6 were separated after 7 days. The emulsions prepared with native LF and prepared mixed protein at pH 7 were stable after 7 days (Figure 4.16). The emulsion prepared with LF and PPI solution added afterward sample (Sample 6) was showed highest phase separation which expected. Because phase separation of two polymers in water occurs if there is a strong electrostatic attraction (de Kruif et al., 2004).

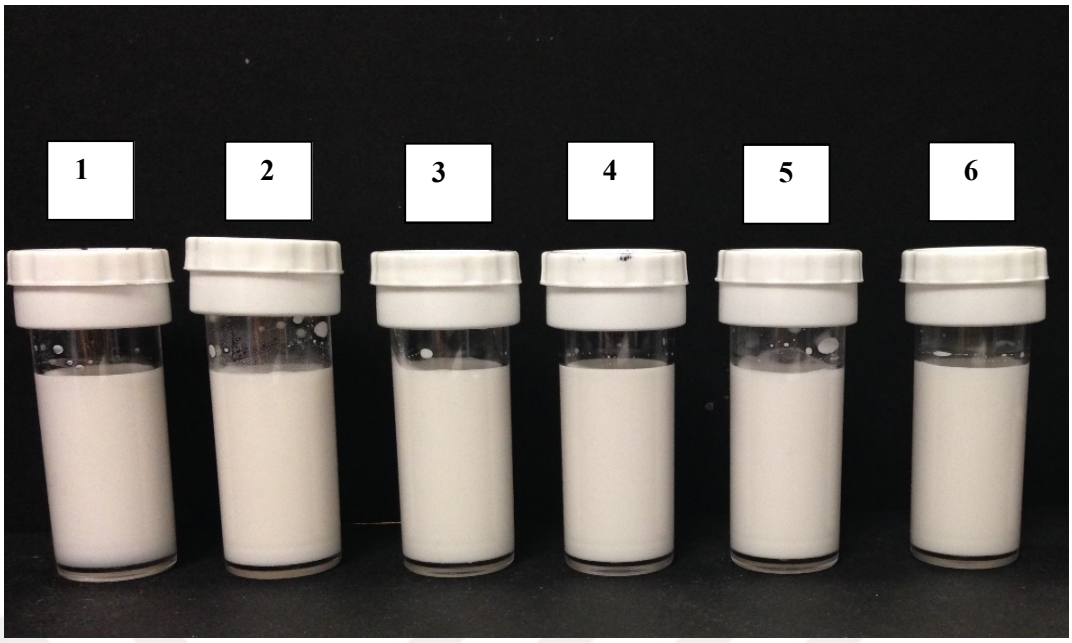

Figure 4. 15 Visual appearance of emulsions after 1 day 1) LF coated RSO at pH 7, 2) PPI coated RSO at pH 7, 3) LF-PPI coated RSO at pH 5.4 (complex formed before emulsion forming), 4) LF-PPI coated RSO at pH 7 (complex formed before emulsion forming), 5) LF-PPI coated RSO at pH 7 (complex formed after emulsion forming with LF), 6) LF-PPI coated RSO at pH 5.4 (complex formed after emulsion forming with LF)

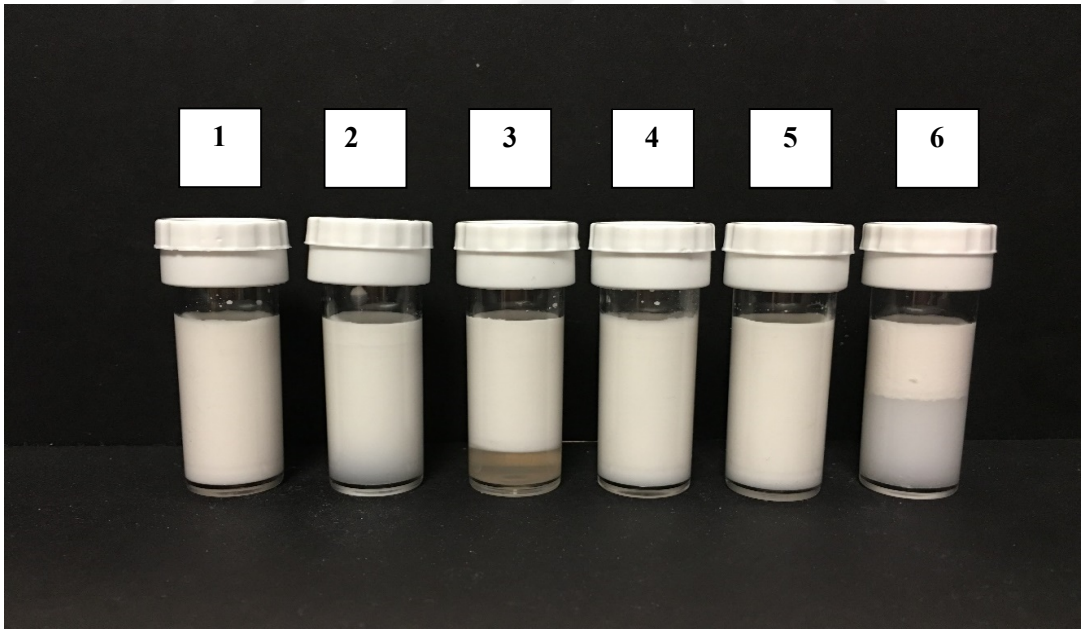

Figure 4. 16 Visual appearance of emulsions after 7 days 1) LF coated RSO at pH 7, 2) PPI coated RSO at pH 7, 3) LF-PPI coated RSO at pH 5.4 (complex formed before emulsion forming), 4) LF-PPI coated RSO at pH 7 (complex formed before emulsion forming), 5) LF-PPI coated RSO at pH 7 (complex formed after emulsion forming with LF), 6) LF-PPI coated RSO at pH 5.4 (complex formed after emulsion forming with LF)

4. 3. 4 Microstructure Results

Confocal fluorescent images of samples were shown in Figure 4.17. Emulsions made with individual LF and PPI had fine and rather monodisperse droplets. However, PPI adding to LF stabilized emulsions at pH 5.4 showed a significant populations of larger droplets in agreement with droplet size results (d_{43} value of sample 3 and 6: 1.380-0.703 µm, respectively).

All the results suggest that LF, PPI molecules and LF-PPI complexes were able to coat the surface of the oil droplets. Because of the better phase separation and uniform size distrubition, making preliminary emulsions with LF and then adding PPI which followed by forming complexes and coacervates were chosen as method for further studies.

4. 4 Emulsion Studies Part II: Oil/Wall Material Concentration Optimization

The purpose of this section was to optimize amount of oil that required the saturate 2 wt% of protein. The concentration of protein had been chosen according to droplet size measurement and optical microscopy images of emulsions that prepared with 1, 2 and 3 wt% of LF-PPI complexes and 10 wt% RSO, respectively. The volume mean diameter (d_{43}) of the emulsions prepared with 1, 2 and 3 wt% of LF-PPI were 0.92, 0.44 and 0.52 µm, respectively. As seen in Figure 4.18, emulsion prepared with 1 wt% had larger droplet size due to insufficient saturation of oil with protein. The smallest droplet size was observed in emulsion prepared with 2 wt% LF-PPI complex which is important for emulsion stability and encapsulation efficiency. For these reason, the protein concentration was used as 2wt% and oil concentration was changed from 2 wt% to 10 wt%. We prepared emulsions for both soluble complexes and complex coacervate between LF and PPI (1:1 wt/wt ratio). The biopolymer ratio (1:1) and pH value had been chosen according to previous study in Section 4.2.

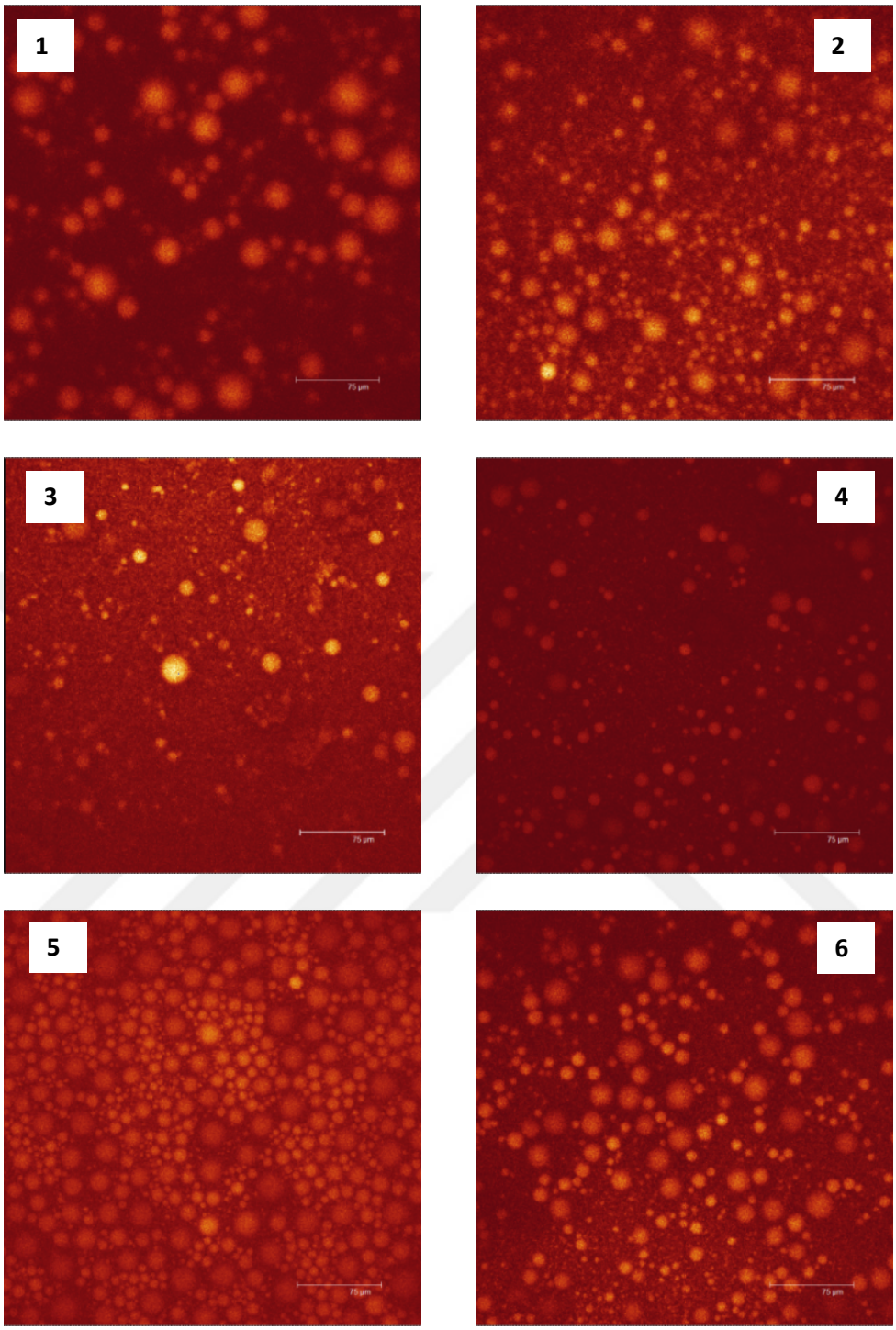

Figure 4. 17 Micrustructure of emulsions 1) LF coated RSO at pH 7, 2) PPI coated RSO at pH 7, 3) LF-PPI coated RSO at pH 5.4 (complex formed before emulsion forming), 4) LF-PPI coated RSO at pH 7 (complex formed before emulsion forming), 5) LF-PPI coated RSO at pH 7 (complex formed after emulsion forming with LF), 6)LF-PPI coated RSO at pH 5.4 (complex formed after emulsion forming with LF) (75µm scale)

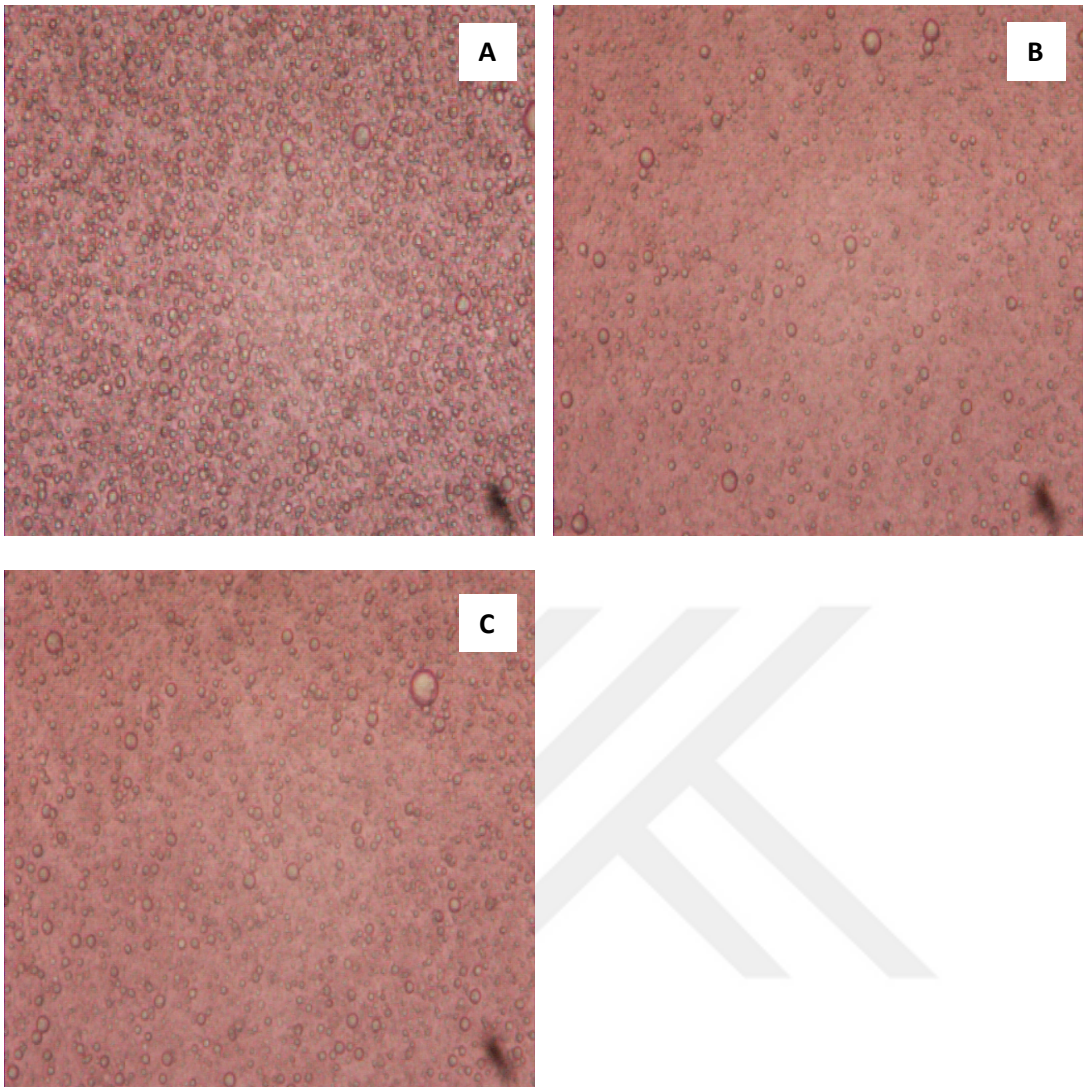

Figure 4. 1188 Optical microscopic images of emulsions prepared with 10 wt% RSO and A: 1 wt% LF-PPI complex B: 2 wt% LF-PPI complex C: 3 wt% LF-PPI complex at pH 7 (scale: 50 µm)

4. 4. 1 Droplet Size of Emulsions

Sauter mean diameter (d_{32}) and Volume mean diameter (d_{43}) values of the emulsions were presented in Figure 4.19 and 4.20, respectively. According to ANOVA results, both values were significantly affected by the oil content in the emulsions at pH 5.4 and pH 7 ($p<0.05$) (Table A5-A12). For pH 7, encapsules d_{43} varied from 1.33- 1.76 µm whereas d_{32} varied from 1.12- 1.51 µm with respect to oil concentration. For pH 5.4, encapsules d_{43} varied from 1.70- 3.14 µm whereas d_{32} varied from 0.77- 1.73 µm with respect to oil concentration (Table A1 and A2). The highest d_{43} values were observed in LF-PPI stabilized RSO emulsions at pH 5.4 for 2 and 10 wt% oil due to protein aggregation which can be seen at the particle size distribution of them (Figure

A1 and A2, respectively), they had bimodal distribution. Increasing oil content at pH 5.4 resulted in increase in droplet size of emulsions. Mao and McClements (2011) observed similar behaviour for lactoferrin and β-lactoglobulin coated corn oil samples. They prepared a series of emulsions with different oil contents (5 to 40%) but the same mass ratio of β-lg to LF (60%-to40%) coated droplets, and then measure their mean particle diameters. The d_{43} values of samples were between 10-20µm in their study and increase with increasing oil content.

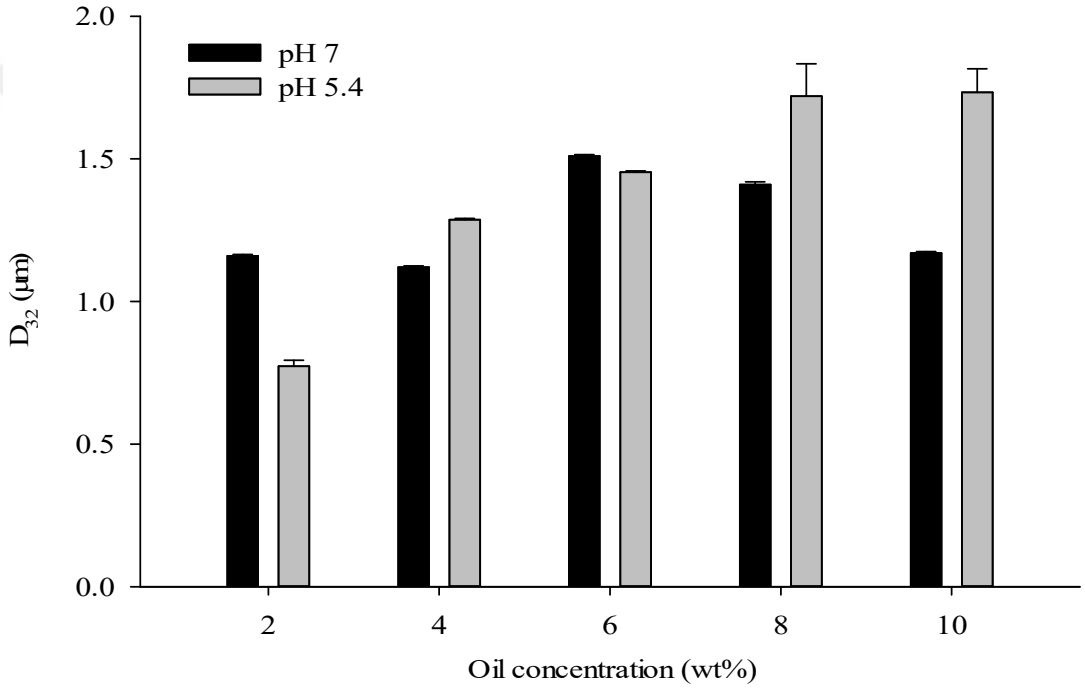

Figure 4. 19 Influence of changing RSO concentration and pH on Sauter mean diameter (d_{32}) value of emulsions prepared with LF-PPI complexes (2 wt%) and RSO (2-10 wt%). Error bars represent standard deviations

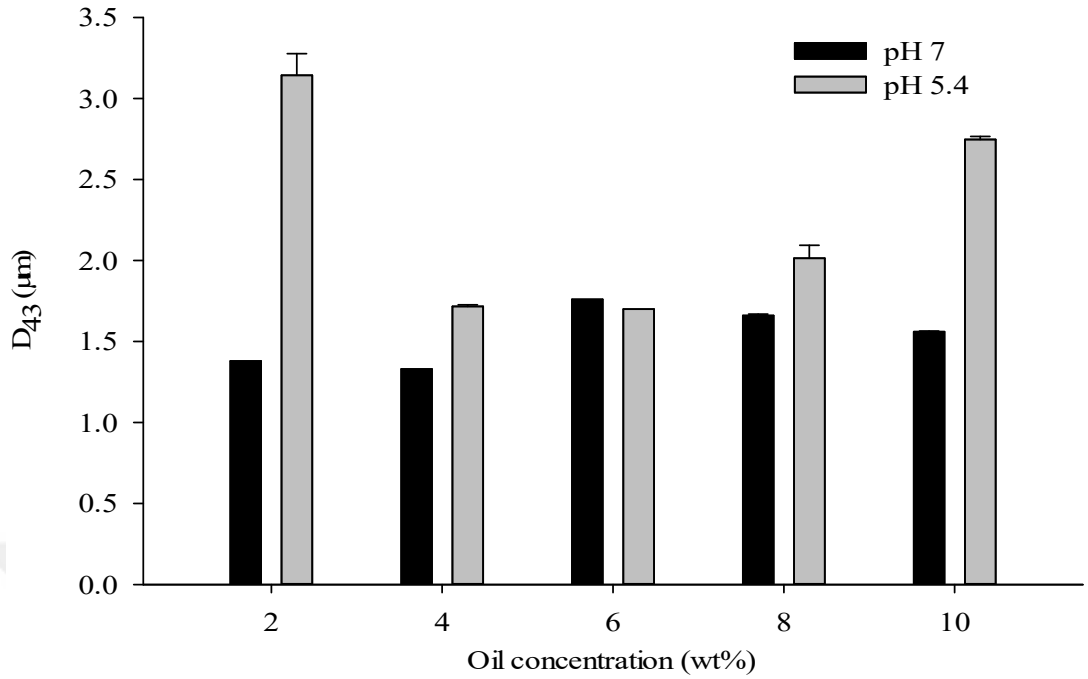

Figure 4. 19 Influence of changing RSO concentration and pH on Volume mean diameter (d_{43}) value of emulsions prepared with LF-PPI complexes (2 wt%) and RSO (2-10 wt%). Error bars represent standard deviations

4. 4. 2 Rheological Measurement

Figure 4.21 and Figure 4.22 shows that flow behaviours of emulsion prepared with 2 wt% LF-PPI and 2, 4, 6, 8 and 10 wt% RSO at pH 5.4 and pH 7, respectively. The flow behaviours of samples were described by steady shear measurement at room temperature. As seen from the Figures, the shear stress linearly increased with shear rate. Therefore, this type of flow behaviour was characterised by Power Law model;

$$\sigma = K.\gamma^n$$

Where K is the consistency index which is an indicator of the viscous nature of the emulsion, n is the flow behavior index. The flow behaviour n<1 represents a shear-thinning fluid and n=1 represents a Newtonian fluid (Erçelebi and Ibanoglu, 2009).

In all samples, shear stress showed linear dependence on shear rate. It was found that increasing oil content cause increase in shear stress. All LF-PPI stabilized emulsions show shear thinning behaviour (n<1). Furthermore, consistency index (K) values were increased with the rise of RSO concentration (Table 4.9). Besides, Emulsions prepared at pH 5.4 had higher consistency index for all samples which agreed with the results

of flow behaviour samples (Figure 4.21 and Figure 4.22). It was obvious from the Figures that higher shear stress values were observed for emulsions prepared at pH 5.4. Zhao, J. J. et al. (2015) found similar results for LF coated orange oil emulsions.

Dynamic frequency sweep tests were carried out in the linear viscoelastic range to determine the frequency dependence of the storage modulus (G´) and loss modulus (G´´). The method is useful in a variety of applications including gel strength evaluation, monitoring starch gelatinization, studying the glass transition phenomenon, observing protein denaturation and coagulation, evaluating curd formation in dairy products, cheese melting, shelf life testing, etc. In this study, storage modulus (G´) and loss modulus (G´´) of LF-PPI stabilized emulsions with different oil concentration at pH 5.4 and pH 7 were measured as a function of applied shear frequency.

Figure 4.23 and 4.24 illustrates the influence of the oil concentration on the viscoelastic properties of LF-PPI stabilized emulsions. Storage modulus G´ (represented by open symbols on the figure) represents the elastic portion or solid state behaviour. Meanwhile, the loss modulus G´´ (represented by filled symbols on the figure) characterizes the viscous behaviour or liquid state behavior.

The graphs showed that why the increasing frequency the storage modulus becomes smaller than the loss modulus at a particular point. Prior to this point of change the sample can be characterized as containing higher amounts of links and bonds. After that certain point the samples seem to get higher loss modulus compared to the strage modulus which can be interpreted as the loss of such bonds between individual molecules. As shown in the Figure 4.23 and 4.24, the crossover between G" and G' curves was observed at the different frequency ranges which 0.14, 0.14, 0.15, 0.15 and 0.23 for 2, 4, 6, 8, 10 wt% RSO contained emulsions, respectively. It was obvious from the graphs crossover between G' and G" curves shifted towards to high frequencies when oil concentration was increased to 10 wt% for both pH 5.4 and pH 7. In the frequency range studied (0.1 to 10 Hz), the storage modulus was appreciably higher than the loss modulus (G'>G") before crossover indicating that the structures formed had predominantly elastic-like characteristics.

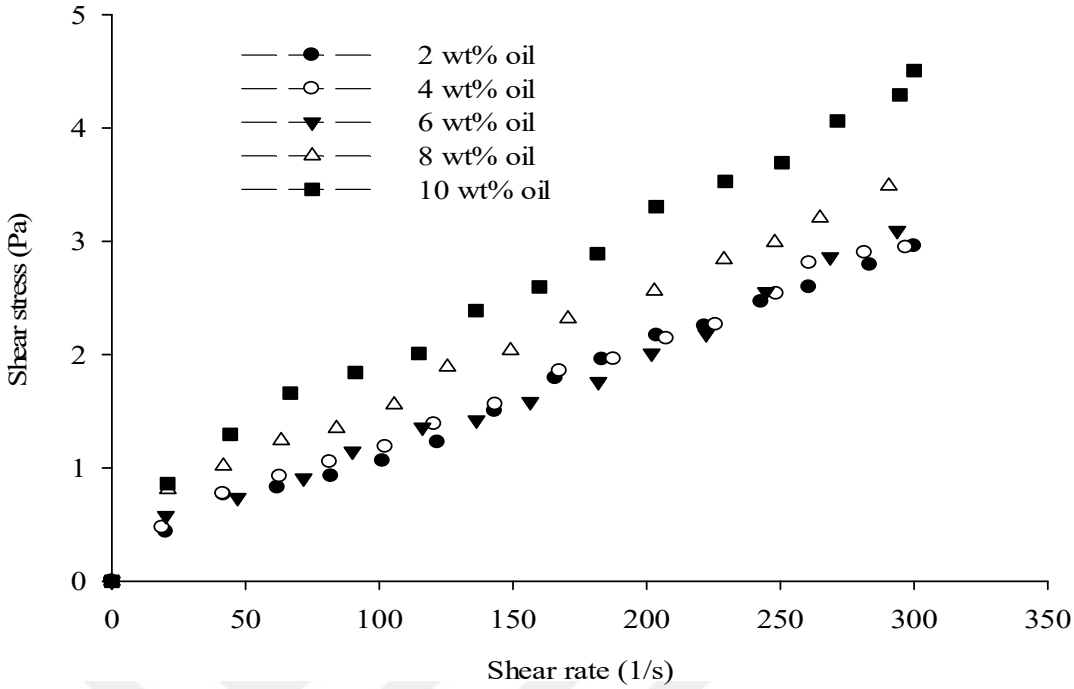

Figure 4. 21 Influence of changing RSO concentration (2-10 wt%) on Flow behaviour of emulsions prepared with 2 wt% LF-PPI complexes at pH 5.4

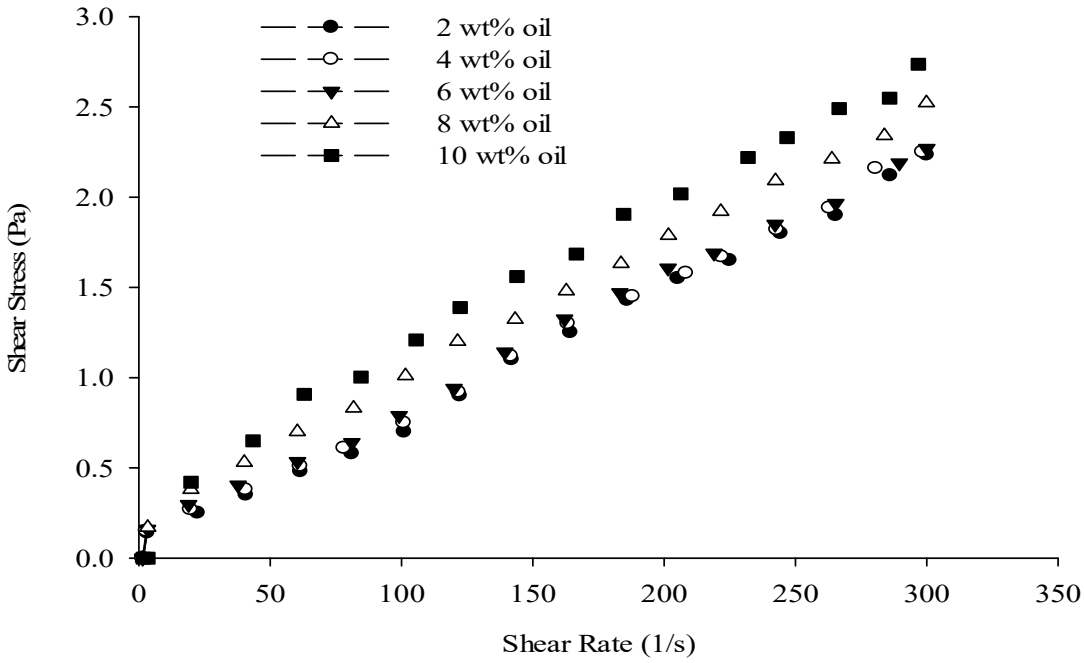

Figure 4. 22 Influence of changing RSO concentration (2-10 wt%) on Flow behaviour of emulsions prepared with 2 wt% LF-PPI complexes at pH 7

Table 4. 9 Rheological parameters of emulsions prepared with 2 wt% LF-PPI complexes and 2-10 wt% RSO at pH 5.4 and pH 7

Protein concentration (wt%)	Oil concentration (wt%)	pH	n	K	R^2
2	2	5.4	0.83	0.03	0.98
2	4	5.4	0.79	0.03	0.99
2	6	5.4	0.85	0.02	0.97
2	8	5.4	0.65	0.08	0.95
2	10	5.4	0.70	0.08	0.99
2	2	7	0.97	0.01	0.99
2	4	7	0.94	0.01	0.99
2	6	7	0.89	0.01	0.99
2	8	7	0.80	0.03	0.99
2	10	7	0.75	0.04	0.99

The magnitude of the storage and loss moduli increased with increasing oil content, which can be attributed to the formation of a network of droplets held together by attractive electrostatic interactions. As the oil content increases, the number of attractive particle-particle interactions per unit volume increases (Mao and McClements, 2013). Zhao, J. et al. (2015) studied on lactoferrin-pectin or lactoferrin-soybean stabilized orange oil emulsions. According to their study, all emulsions exhibited a liquid-like behaviour at low frequency.

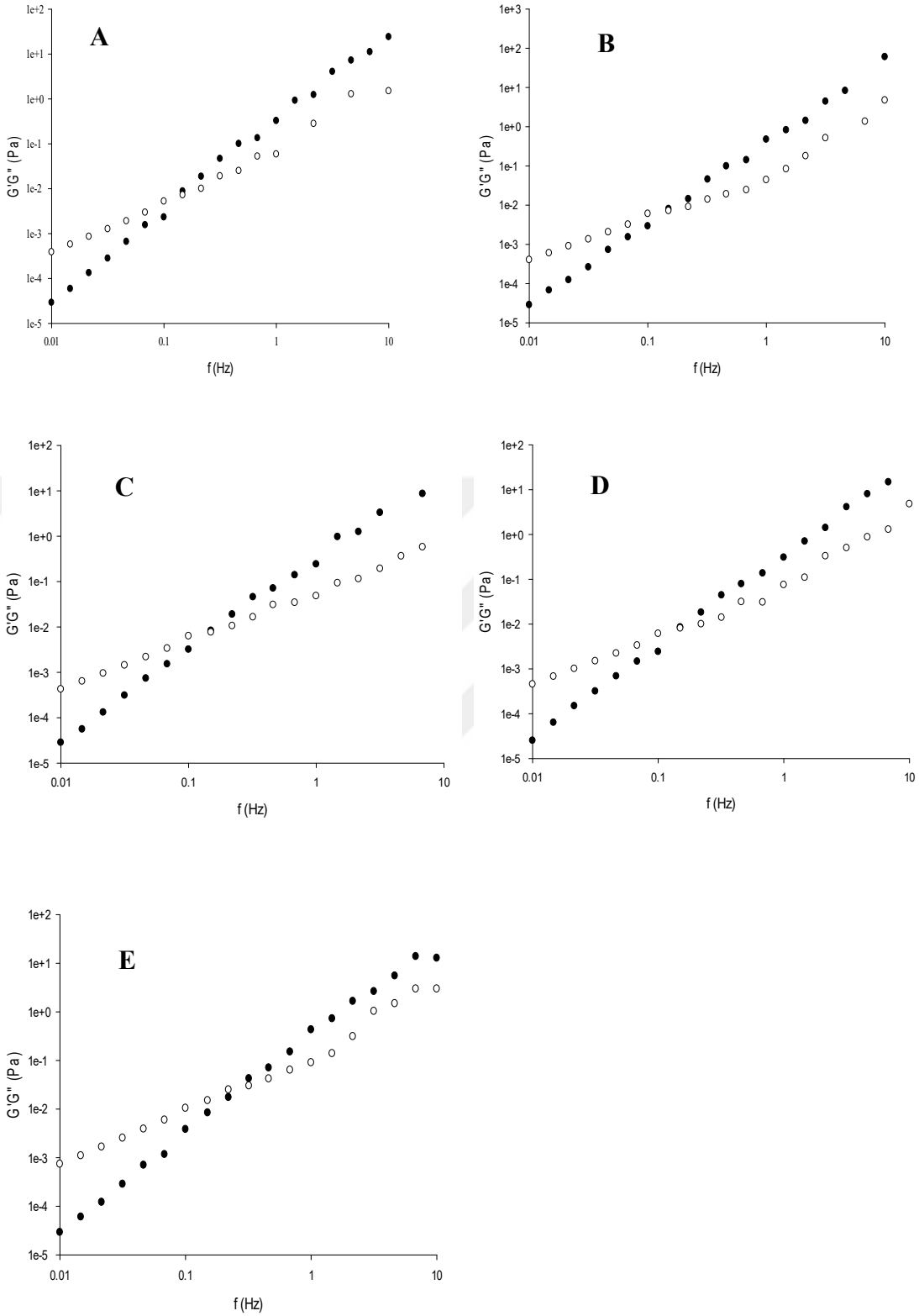

Figure 4. 23 Influence of changing RSO concentration on Viscoelastic moduli (G´-open symbols, G´´-filled symbols) of emulsions prepared with 2 wt% LF-PPI complexes at pH 5.4; A) 2 wt% RSO oil, B) 4 wt% RSO oil, C) 6 wt% RSO oil, D) 8 wt% RSO oil, E) 10 wt% RSO oil

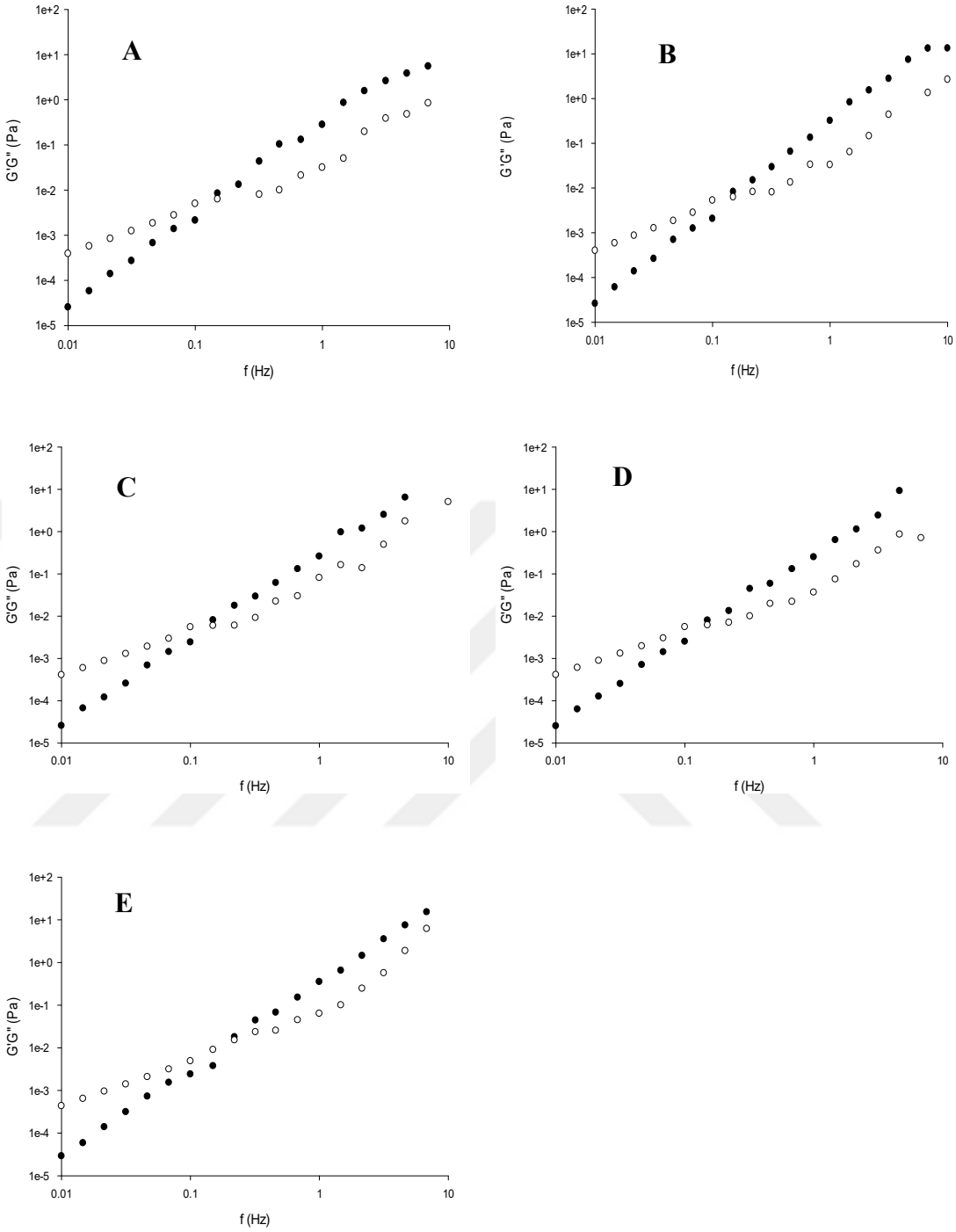

Figure 4. 24 Influence of changing RSO concentration on Viscoelastic moduli (G´-open symbols, G´´-filled symbols) of emulsions prepared with 2 wt% LF-PPI complexes at pH 7; A) 2 wt% RSO oil, B) 4 wt% RSO oil, C) 6 wt% RSO oil, D) 8 wt% RSO oil, E) 10 wt% RSO oil

4. 5 Freeze Drying of Emulsions

4. 5. 1 Moisture Content of Encapsules

After freeze drying of emulsions, total lipids of encapsules seemed to be increased because of loss water during drying. Figure 4.25 shows moisture content of RSO encapsules coated with LF-PPI at pH 5.4 and pH 7. Increasing oil concentration result in significantly decrease in MC (%) of the encapsules because of the hydrophobicity of the powders ($p<0.05$) (Table A3, A25, A26 for pH 7 and Table A4, A15, A16 for pH 5.4). Shi et al. (2018) were studied encapsulation of krill oil with krill protein isolate by freeze drying and they observed a similar decrease in MC (%) at pH 7 by increasing of oil concentration.

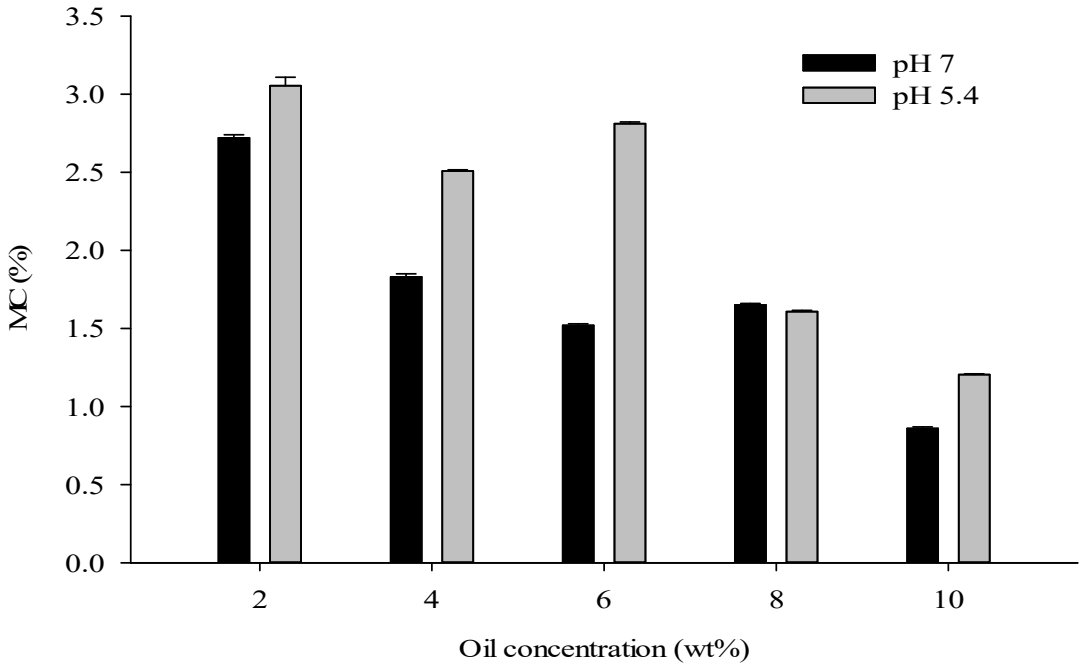

Figure 4. 25 Influence of changing RSO concentration (2-10 wt%) on Moisture Content (MC) (%) of encapsules prepared with 2 wt% LF-PPI complexes at pH 5.4 and 7. Error bars represent standard deviations

4. 5. 2 Encapsulation Yield

Encapsulation yield is one of the major parameter to evaluate the success of the encapsulated powder after freeze drying. Figure 4.26 shows the yield of the

encapsulated RSO powder based on the different oil concentration and pH. There was no significant difference between the samples according to ANOVA and Duncan's multiple range test ($p<0.05$) (Table A13, A14 for pH 5.4 and Table A23, A24 for pH 7). EY (%) values were between 92% and 99% as seen in Table A3 and A4 which expected for the freeze drying . The encapsulation yield can change according to drying method as stated by Wilkowska et al. (2016). They produced encapsules using different drying methods (Spray and freeze drying) and observed that spray dried encapsules had lower product yield. Because some amount of powder was lost due to the fact that it was not separated in cyclone and was blown with air and remained on the filter. Quispe-Condori et al. (2011) observed higher particle yield (70-78%) for zein encapsulated flaxseed oil by freeze drying.

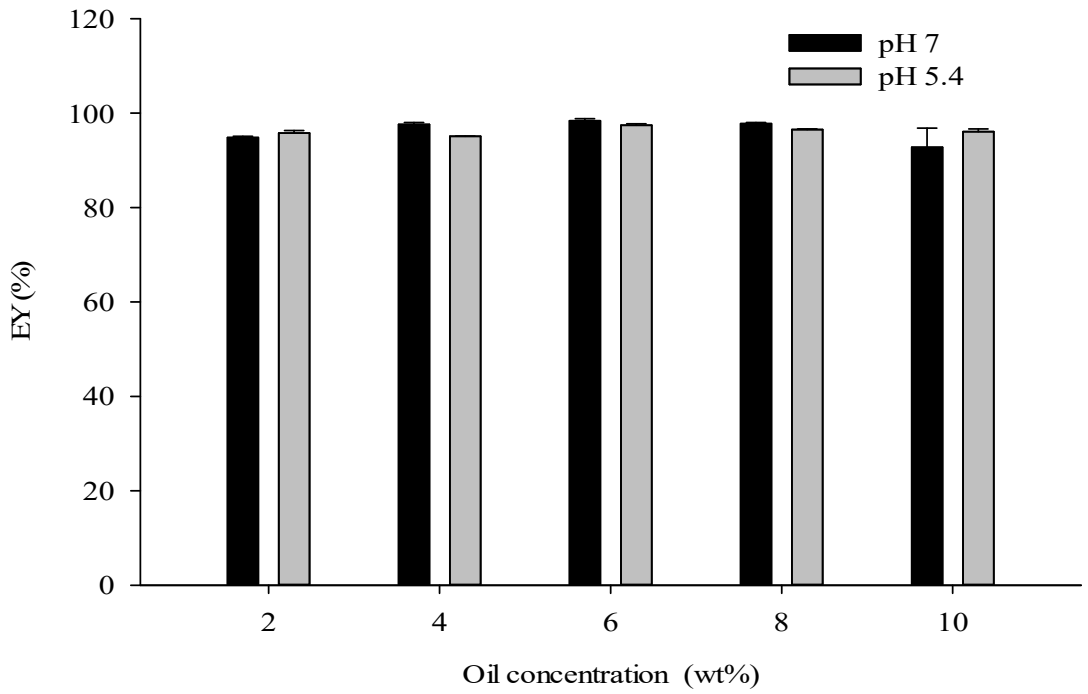

Figure 4. 26 Influence of changing RSO concentration (2-10 wt%) on Encapsulation Yield (EY) (%) of encapsules prepared with 2 wt% LF-PPI complexes at pH 5.4 and 7. Error bars represent standard deviations

4. 5. 3 Loading Capacity, Loading Efficiency, Encapsulation Efficiency

Weight of oil per 100 g encapsules is defined as Oil Loading Capacity. Higher oil loading indicates more economically feasible encapsule production and less wall material is required to encapsulate the oil (Kaushik et al., 2015). Figure 4.27 shows oil loading capacity of RSO encapsules with different oil concentration. The LC (%) was significantly increased by increasing oil amount $p<0.05$ for both encapsules prepared at pH 5.4 and pH 7 (Table A4, A21, A22 for pH 5.4 and Table A3, A31, A32 for pH 7). Aziz et al. (2014) and Shi et al. (2018) were found similar decreasing for krill oil encapsules in their studies.

Figure 4.28 implies Loading Efficiency of encapsules with different oil concentration. LE (%) indicates how much RSO was retained by protein as a portion of the total weight of encapsules. Oil types, core/wall material ratio, stirring speed and pH are some main parameters that influence LE (%) of the samples (Aziz et al., 2014). In our results, the highest LE (%) was obtained from 2 wt% oil concentration for both encapsules produced at pH 5.4 and pH 7 (Table A3-A4). Increasing oil content results in significantly decreasing LE (%) ($p<0.05$) (Table A19, A20 for pH 5.4 and Table A27, A28 for pH 7). The addition of RSO might cause protein saturation and this saturation likely resulted in decreasing emulsifying capacity. Hence, free RSO was present and a low amount of added oil was being entrapped within encapsules (Shi et al., 2018).

Encapsulation Efficiency (EE) is determined by dividing the mass of the core material encapsulated in the wall material by the core material utilised in the formulation. The mass of the free oil (non-encapsulated or surface oil) ought to be low for higher efficiency values of encapsulation to be attained. On the other hand, the mass of the completely encapsulated oil needs to have high values. It is important to assess the surface oil because it can oxidise really fast and this means that high surface oil is correlated to poor stability and flavor of encapsules (Kaushik et al., 2015). EE of RSO encapsules varied from 34.95 to 49.08% for samples prepared at pH 7 whereas ranged from 41.35 to 57.77% for samples prepared at pH 5.4 (Table A.3 and Table A.4, respectively. As can be seen in Figure 4. 29, EE (%) was significantly decreased by increasing oil content which indicates increasing free surface oil in the systems ($p<0.05$) for both encapsules produced at pH 5.4 and pH 7 (Table A17, A18 for pH

5.4 and Table A29, A30 for pH 7). Maximum EE (57.77) was achieved with 2wt % proteins and 2 wt% RSO used sample for pH 5.4. Aziz et al. (2014) found the optimal conditions for a 92% of EE of gelatin-gum arabic stabilized krill oil as 1.75:1 for ratio of core material to wall, 3.8 for pH and 3 for stirring speed. Haider et al. (2017) observed similar EE value observation for krill oil encapsulation by proteins. They found EE value of the obtained particles as 33-59 % which decreased with increasing oil content.

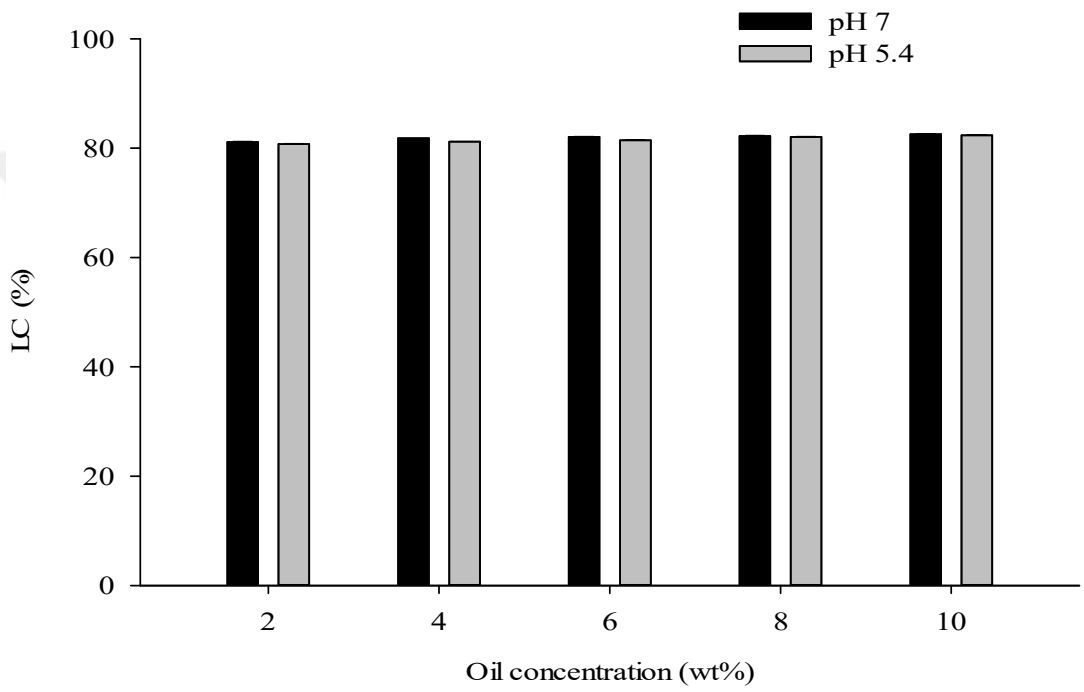

Figure 4. 27 Influence of changing RSO concentration (2-10 wt%) on Loading Capacity (LC) (%) of encapsules prepared with 2 wt% LF-PPI complexes at pH 5.4 and 7. Error bars represent standard deviations

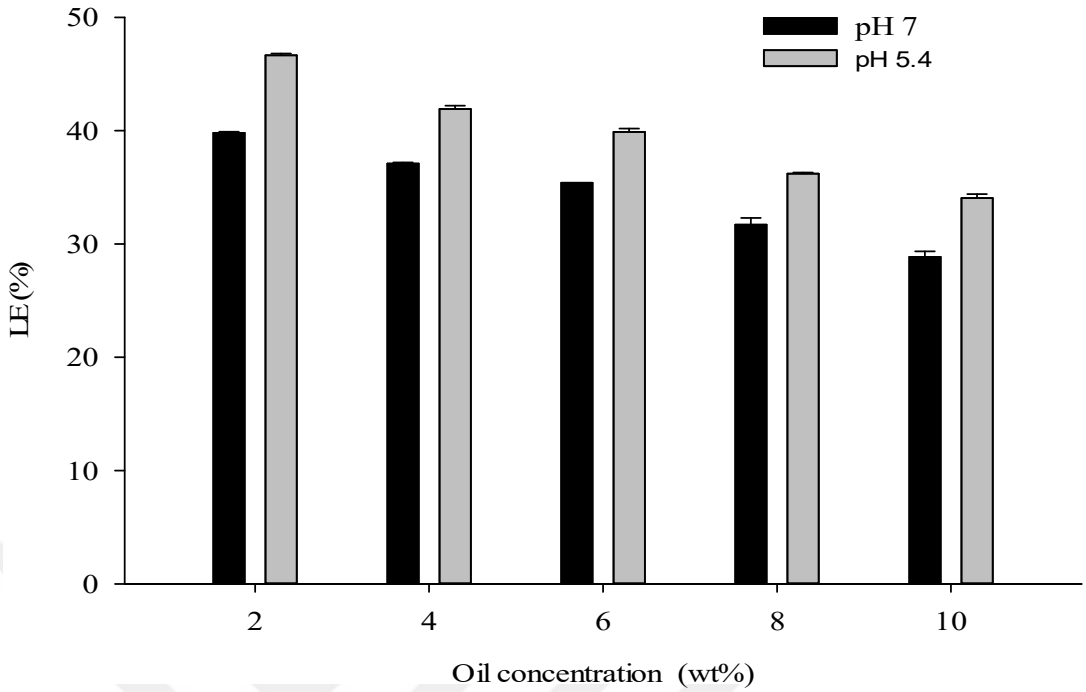

Figure 4. 28 Influence of changing RSO concentration (2-10 wt%) on Loading Efficiency (LE) (%) of encapsules prepared with 2 wt% LF-PPI complexes at pH 5.4 and 7. Error bars represent standard deviations

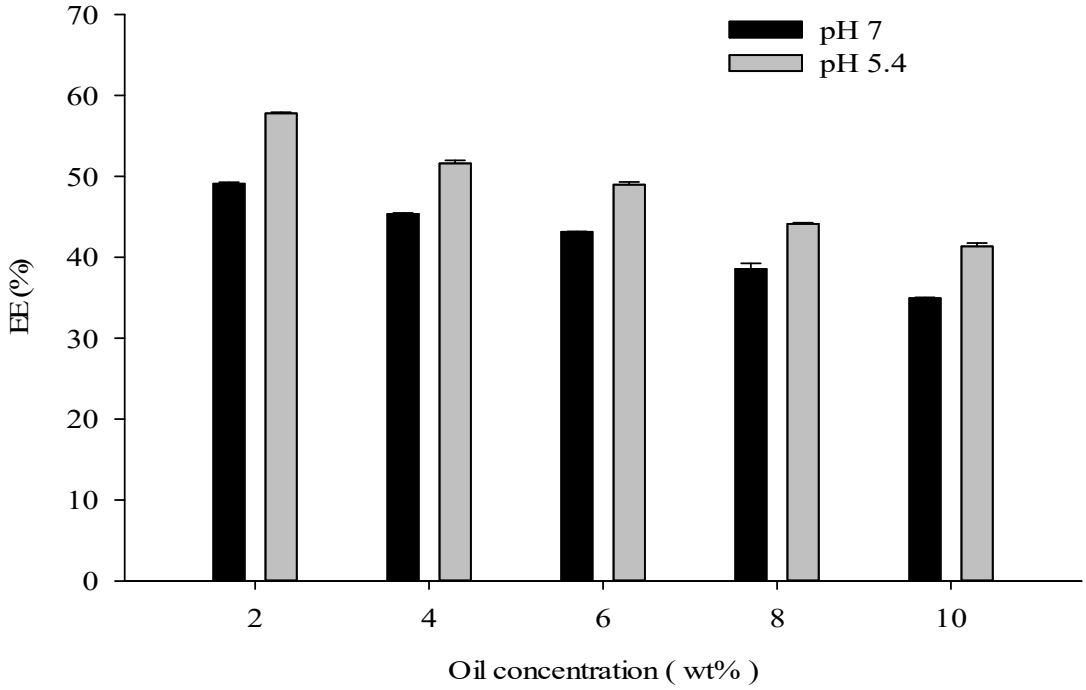

Figure 4. 29 Influence of changing RSO concentration (2-10 wt%) on Encapsulation Efficiency (EE) (%) of encapsules prepared with 2 wt% LF-PPI complexes at pH 5.4 and 7. Error bars represent standard deviations

4. 5. 4 Scanning Electron Microscopy

Surface morphology of freeze dried RSO encapsules captured with a scanning electron microscope (SEM) is shown in Figure 4.30 (250x) and Figure 4.31 (800x) at pH 7. Similarly, Figure 4.32 (250x) and Figure 4.33 (1200x) represent surface morphology of RSO encapsules at pH 5.4. Two levels of magnification (250x and 800x or 1200x) were selected to show surface morphology of RSO encapsules based on the image clarity. The particles exhibited an irregular spherical shape and various sizes. Irregularity of shapes increases by increasing oil content for both pH value which result in agglomerate-like appearance. At the 10 wt% RSO, the agglomerates became bigger due to clustering for both pH values. The results were in accordance with encapsulation efficiency results. For pH 5.4, larger particles were observed because of the protein aggregation.

We observed spongy, porous structure a with 250x magnifications due to voids left after sublimation of ice crystals during freeze drying. The irregularly shaped particles observed under the 250× magnification in the present study are probably part of the porous, spongy microstructure created during freeze-drying. Shi et al. (2018) examined microencapsulated krill oil by freeze-drying with SEM at 250× and 600x magnification. They also observed irregularly-shaped particles, clustering, voids, and oval bulges. Although different oil and wall material were used in their study, it appears that freeze-drying results in a relatively similar microstructure when oil is microencapsulated. In support, Aziz et al. (2014) showed individual droplets of krill oil microencapsulated with gelatin and gum Arabic, but without freeze-drying. Unlike the studies that used freeze-drying, Aziz et al. (2014) showed individual microcapsules. Their microcapsules did not exhibit the agglomerate-like appearance covered with oval-shaped bulges. Additionally, Aberkane et al. (2014) studied on emulsion powders produced with pea protein/maltodextrin and pea protein/ pectin/maltodextrins wall materials by spray drying. Particles showed a spherical shape and various sizes with no apparent cracks or fissures. Pea protein /pectin /maltodextrins mixture resulted in microspheres with smoother surface and fewer teeth or roughness in their study.

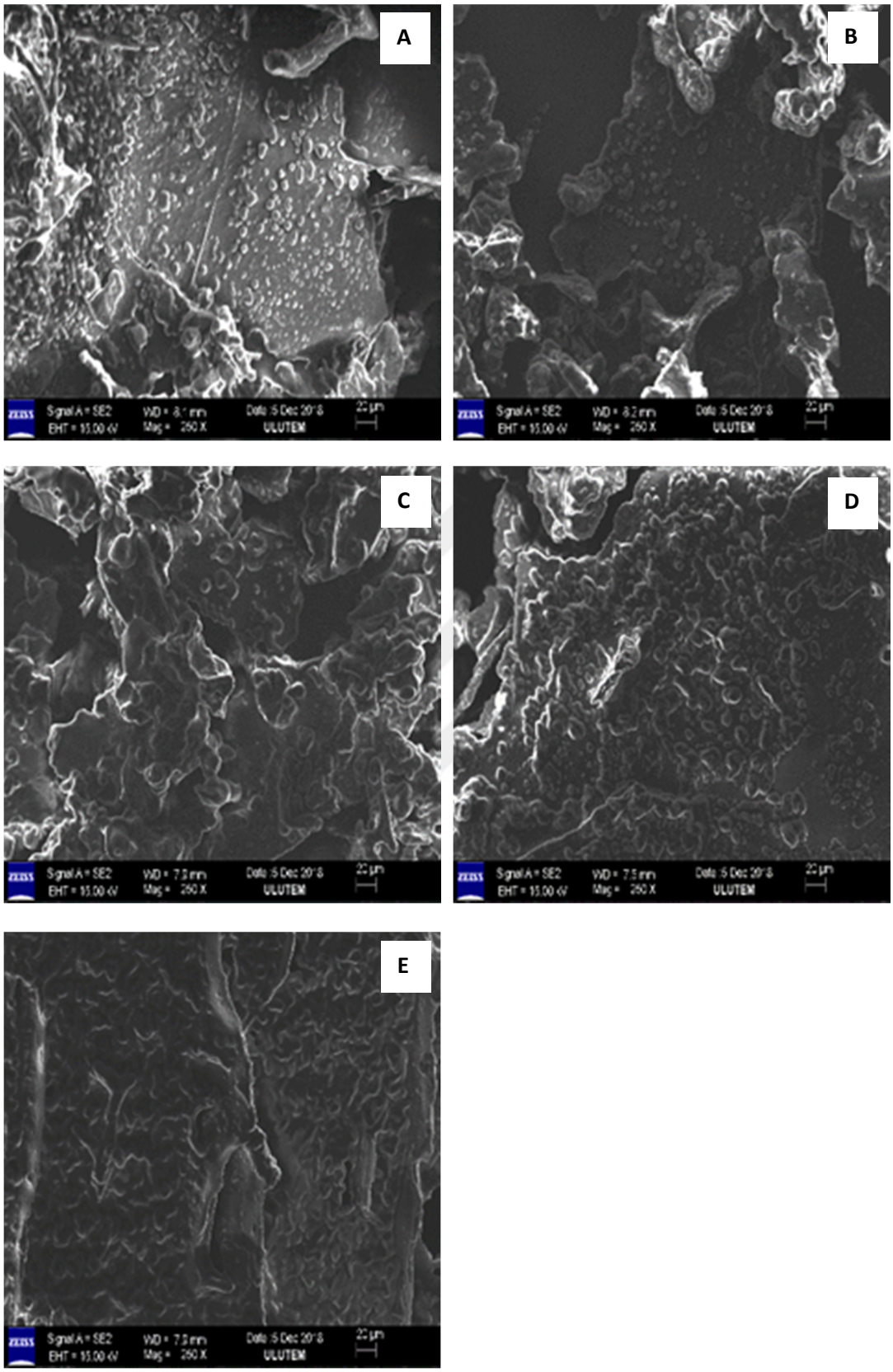

Figure 4. 30 Influence of changing RSO concentration on Microstructure of encapsules prepared with 2 wt% LF-PPI complexes at pH 7 A) 2 wt% RSO oil, B) 4 wt% RSO oil, C) 6 wt% RSO oil, D) 8 wt% RSO oil, E) 10 wt% RSO oil (A-E for 250x images, 25 µm scale)

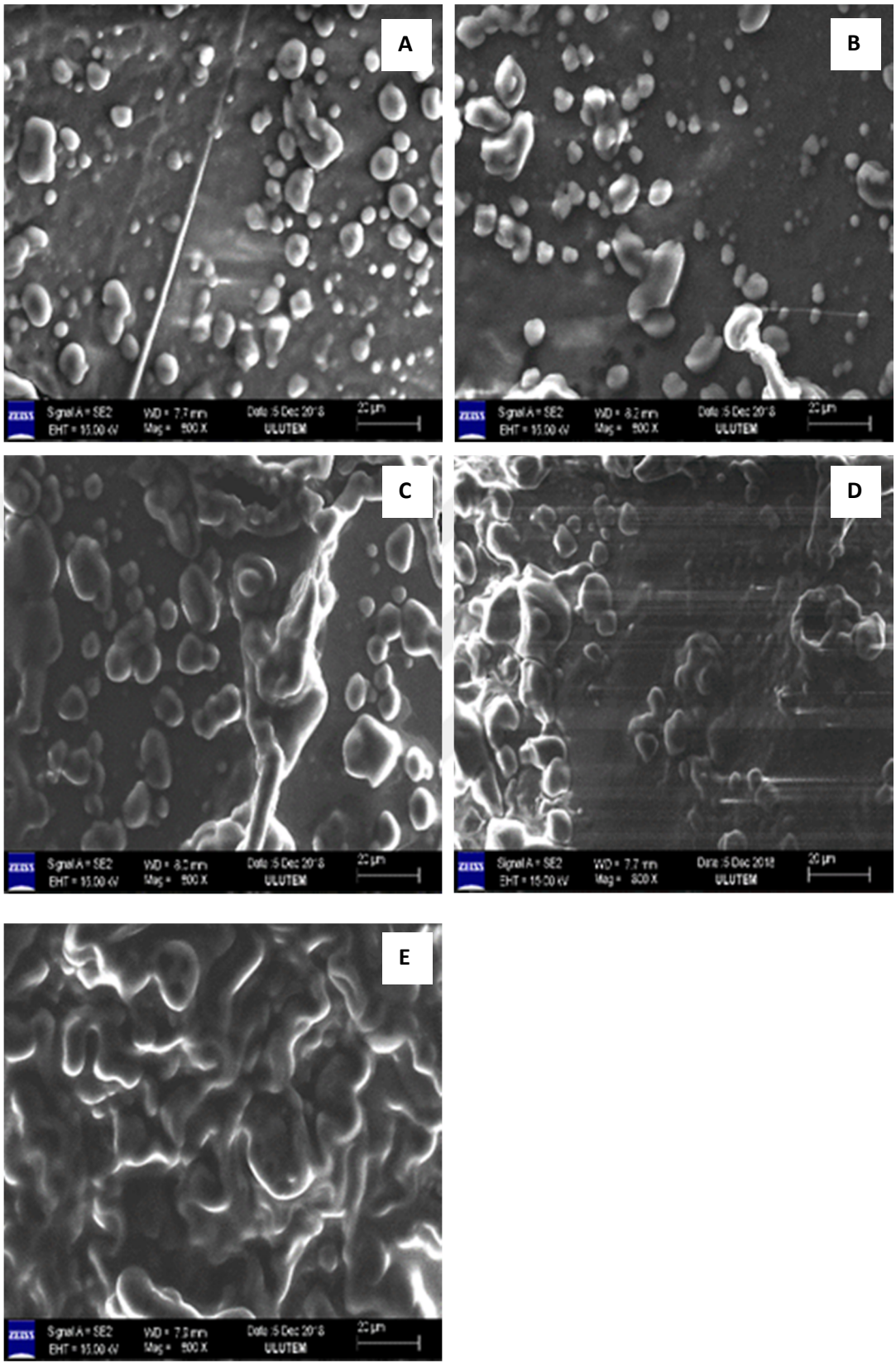

Figure 4. 31 Influence of changing RSO concentration on Microstructure of encapsules prepared with 2 wt% LF-PPI complexes at pH 7 A) 2 wt% RSO oil, B) 4 wt% RSO oil, C) 6 wt% RSO oil, D) 8 wt% RSO oil, E) 10 wt% RSO oil (A-E for 800x images, 25 µm scale)

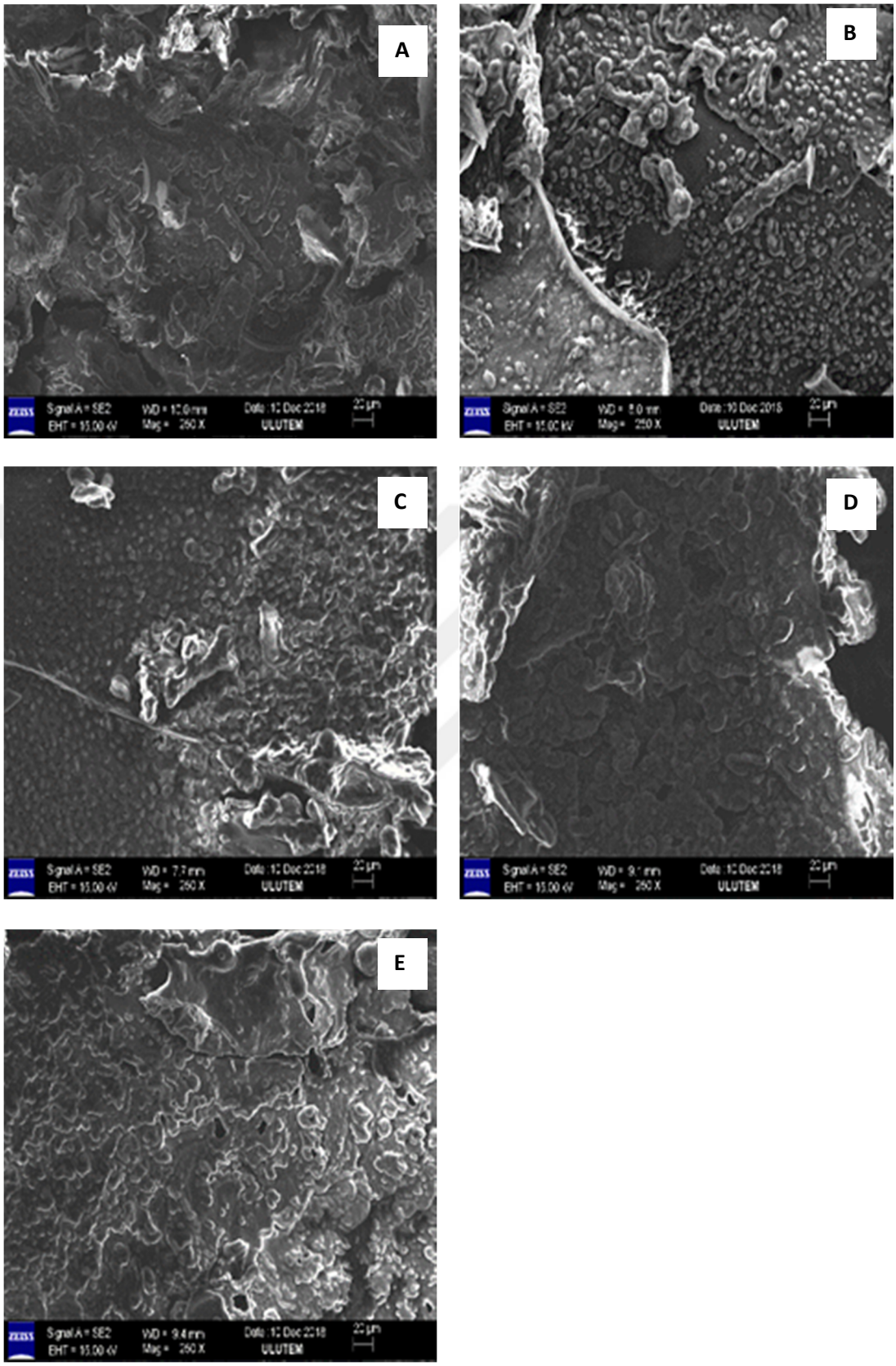

Figure 4. 32 Influence of changing RSO concentration on Microstructure of encapsules prepared with 2 wt% LF-PPI complexes at pH 5.4 A) 2 wt% RSO oil, B) 4 wt% RSO oil, C) 6 wt% RSO oil, D) 8 wt% RSO oil, E) 10 wt% RSO oil (A-E for 250x images, 25 µm scale)

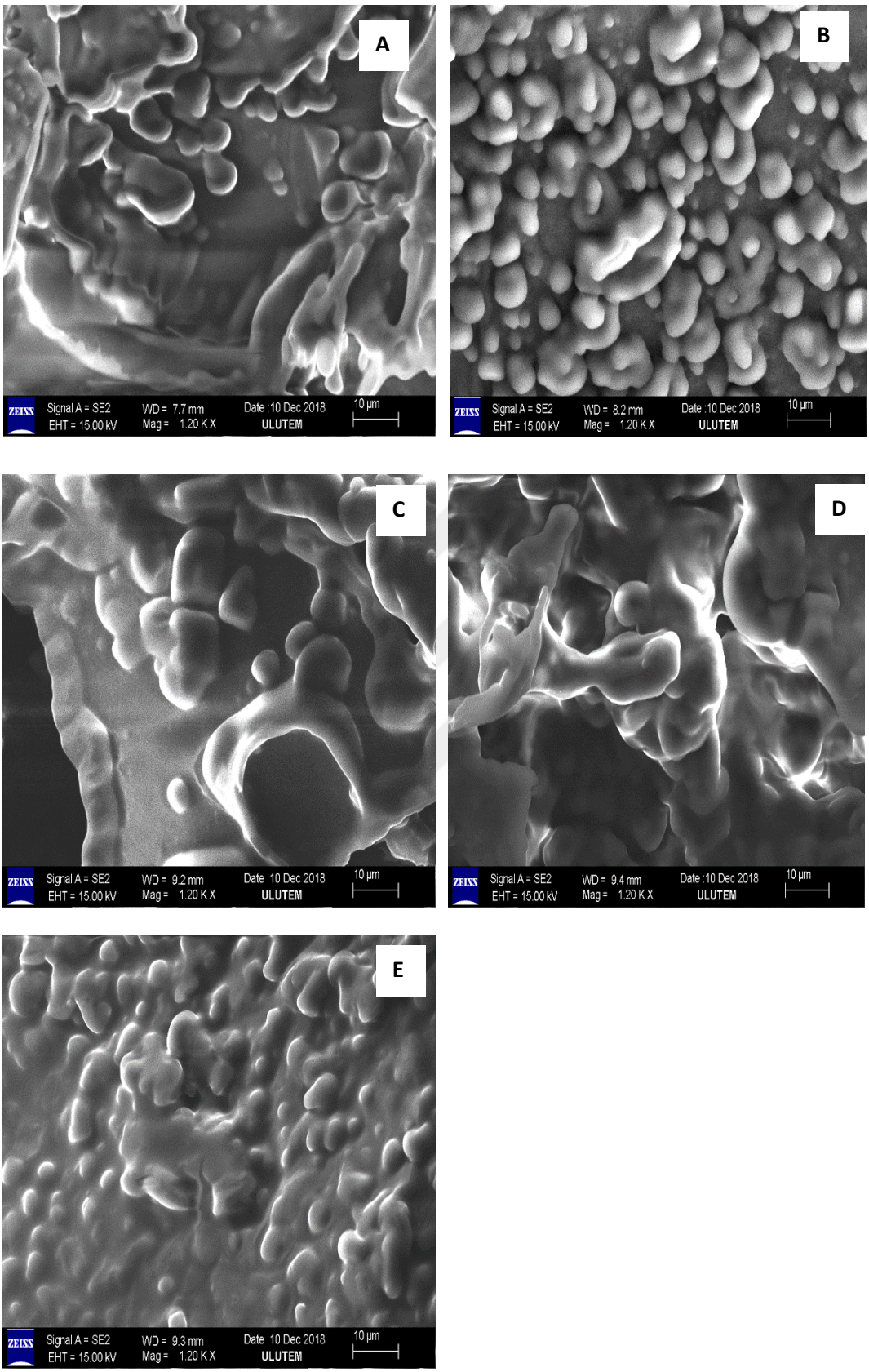

Figure 4. 33 Influence of changing RSO concentration on Microstructure of encapsules prepared with 2 wt% LF-PPI complexes at pH 5.4 A) 2 wt% RSO oil, B) 4 wt% RSO oil, C) 6 wt% RSO oil, D) 8 wt% RSO oil, E) 10 wt% RSO oil (A-E for 1200x images, 10 µm scale)

4. 6 Formation and Characterization of Encapsulated RSO and CHSO oils at Optimum Conditions

4. 6. 1 Moisture Content of Powders

Moisture content is an important attribute of products since is directly related to stability. Dried products are more stable than liquid formulations, on the subject of the physicochemical aspects and microbiological spoilage. The moisture is mainly related to the drying conditions, however the composition of the formulations also plays an important role because drying could promote changes in water binding and dissociation that will affect the properties the dried product (Labuza et al., 1972).

At the latest stages of our study, we produced RSO and CHSO encapsules coated with individual and mixed LF and PPI. Moisture content of samples were presented in Table 4.10. Moisture content of freeze dried powders obtained in this study ranged from 1.30 to 2.07 (Table 4.10). These results were in agreement with previous studies (Kermasha et al., 2018; Quispe-Condori et al., 2011). Moisture content values of krill oil encapsules that they produced were between 1.5-3%. Encapsules prepared with lactoferrin showed relatively higher moisture content. Gharsallaoui et al. (2007) stated that 3-4% moisture content is considered as minimum specification of most dried powders used in food industry. Besides, higher moisture content is responsible for fungal growth and formation of off-flavor in core oil by enhancing lipid oxidation, resulting in overall degradation of the product.

Table 4. 10 Moisture content of Encapsulated RSO and CHSO produced at optimum conditions (2 wt% LF-PPI complex and 6 wt% RSO or CHSO)

Protein (2 wt%)	Oil (6 wt%)	pH	MC (%)
LF-PPI	RSO	5.4	1.77 ± 0.02
LF-PPI	RSO	7	1.74 ± 0.04
LF	RSO	7	1.86 ± 0.01
PPI	RSO	7	1.49 ± 0.01
LF-PPI	CHSO	5.4	1.53 ± 0.02
LF-PPI	CHSO	7	1.82 ± 0.04
LF	CHSO	7	2.07 ± 0.03
PPI	CHSO	7	1.30 ± 0.12

4. 6. 2 Color Properties of Powder

Color data of the encapsules was shown in Table 4.11. L* is the lightness, a* and b* represent the colors where –a* is greenness, +a* is redness, −b* is blueness, and +b* is yellowness. For the L scale, low number (0-50) indicates darkness where as high number (50-100) indicates lightness of the samples. So that, all samples were in the light range which in accordance with images of them (Figure 4.34 and Figure 4.35). Among the samples, a* value of individual LF coated oils was higher that we expected. This might be due to pink color of the lactoferrin powder (Figure 4.33C and Figure 4.44C). b* values of encapsulated RSO were higher than encapsulated CHSO which was expected because of yellow color of RSO (Table 4.3). Moreover, L value of the powder was higher than the bulk oils (Table 4.3) which indicates the acceptability of the powder for food application.

Table 4. 11 Color values of encapsulated RSO and CHSO produced at optimum conditions (2 wt% LF-PPI complex and 6 wt% RSO or CHSO)

Protein	Oil	pH	L*	a*	b*
LF-PPI	RSO	5.4	71.15 ± 0.12	2.56 ± 0.11	25.61±0.28
LF-PPI	RSO	7	72.50 ± 0.00	2.86±0.02	25.45 ± 0.01
LF	RSO	7	79.30 ± 0.01	4.35±0.01	23.00 ± 0.03
PPI	RSO	7	72.90 ± 0.01	1.64±0.02	27.45 ± 0.00
LF-PPI	CHSO	5.4	70.44 ± 0.00	3.73±0.00	18.60 ± 0.02
LF-PPI	CHSO	7	75.24 ± 0.01	3.33±0.01	17.92 ± 0.03
LF	CHSO	7	76.04 ± 0.01	4.87 ± 0.02	16.73 ± 0.04
PPI	CHSO	7	78.19 ± 0.01	1.82 ± 0.01	18.74 ± 0.01

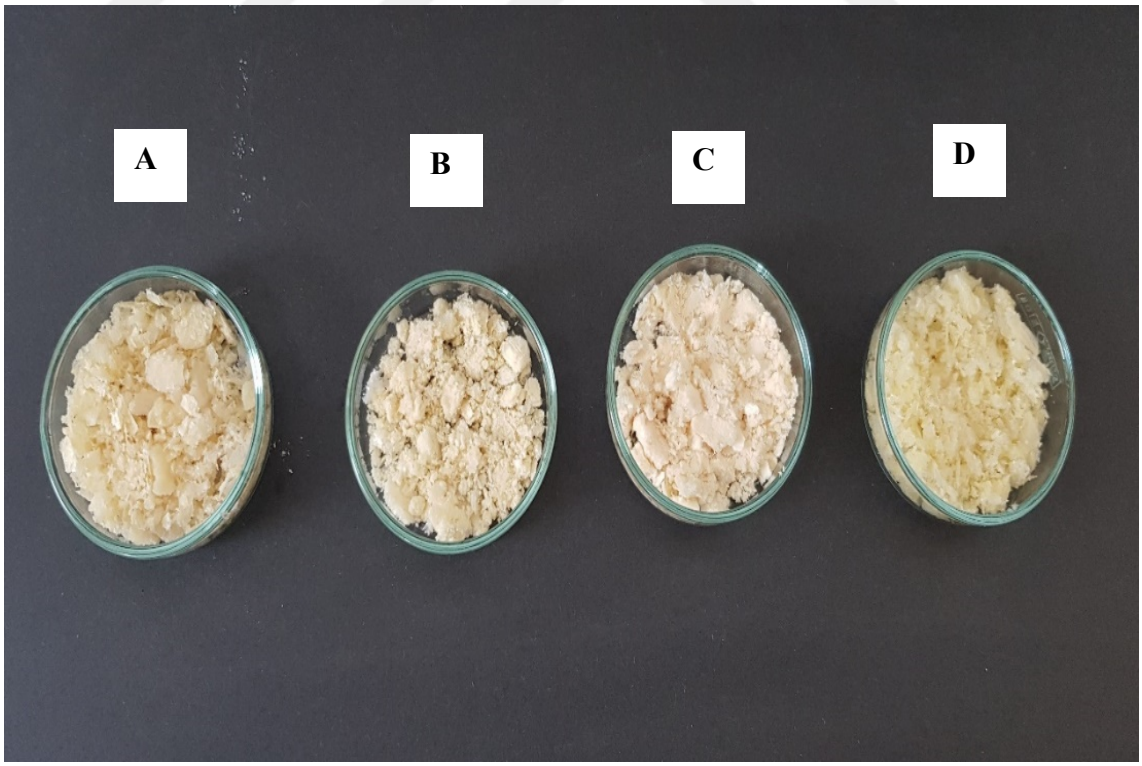

Figure 4. 34 Image of freeze-dried encapsules; A) LF-PPI (2 wt%) coated RSO (6 wt%) at pH 5.4, B) LF-PPI (2 wt%) coated RSO (6 wt%) at pH 7, C) LF (2 wt%) coated RSO (6 wt%) at pH 7, D) PPI (2 wt%) coated RSO (6 wt%) at pH 7

Figure 4. 35 Image of freeze-dried encapsules; A) LF-PPI (2 wt%) coated CHSO (6 wt%) at pH 5.4, B) LF-PPI (2 wt%) coated CHSO (6 wt%) at pH 7, C) LF (2 wt%) coated CHSO (6 wt%) at pH 7, D) PPI (2 wt%) coated CHSO (6 wt%) at pH 7

4. 6. 3 Fourier Transforms Infrared Radiation Analysis

Figure 4.36 and Figure 4.39 shows FTIR spectra of individual freeze dried LF and PPI powder, bulk oils and LF-PPI coated encapsules prepared at pH 5.4 and pH 7 for CHSO and RSO, respectively. The most sensitive regions of FTIR spectra related with the protein structure are amide I among bands 1625–1750 cm^{-1} formed by stretching the C═O (free carboxyl) group, amide II between the bands 1475–1575 cm^{-1} attributed to the stretching of the NH groups, and the amide III between the bands 1225–1425 cm^{-1}. In addition the stretching of the N−H and O−H groups of the free amino acids can also be identified between the bands at 3300 and 3170 cm^{-1} (Santos et al., 2018). Individual LF and PPI show major FTIR spectra at 1635-1641 cm^{-1} (amide I), 1531-1538 (amide II) cm^{-1} and 1391-1398 (amide III) cm^{-1} bands, respectively. Moreover, the stretching of the N−H and O−H groups of the free amino acids can also be identified at 3279-3275 cm^{-1} for individual LF and PPI, respectively.

The bulk oils show sharp peak at 3008-3010 (CH stretching of =C-H bonding), 2922-2924 (aliphatic CH_2 asymmetric stretching vibration), 2854-2854 (aliphatic CH_2 symmetric stretching vibration), 1744-1743 (C=O stretching vibration of the ester

carbonyl functional group of the triglycerides), 1463-1460 (C=H scissors deformation vibration), 1378-1377 (bending vibration of CH_2 groups), 1237 and 1161 (vibration of C-O ester group and CH_2 groups), 1096-1098 (-CH bending and –CH deformation vibration of fatty acids and 722-720 (CH_2 rocking vibration and out of plane vibration of cis substituted olefins) cm^{-1} for CHSO and RSO, respectively (Figure 4.38 for CHSO and Figure 4.41 for RSO).

The all characteristic peaks mentioned above similarly were observed in the FTIR spectra (Figure 4.36A and B for CHSO, Figure 4.39A and B for RSO) of LF-PPI coated encapsules of CHSO and RSO at pH 5.4 and pH 7. This indicates that there was physical interaction rather than chemical interaction between protein complex and oil. Similar behaviour of complexes with krill oil (omega rich) has earlier been reported by Haider et al. (2017). The increasing of the intensity in Amide I, II and III bands implying occurrence of electrostatic interaction between the $-COO^-$ groups of one protein and the $-NH_3^+$ groups of other protein. Also, the shifting of Amide I ($-NH_2$ bending) from 1641 to 1646 indicates that presence of electrostatic interaction between the proteins (Figure 4.37 for CHSO encapsule and Figure 4.40 for RSO encapsule). Similar type of observations were reported by Hosseini et al. (2013). When we compared spectra of individual LF (Figure 4.36D for CHSO encapsule and Figure 4.39D for RSO encapsule) and PPI (Figure 4.36E for CHSO encapsules and Figure 4.39E RSO encapsule) with LF-PPI coated encapsules (Figure 4.36A-B for CHSO encapsule and Figure 4.39A-B for RSO encapsule), the addition of oil resulted in increased intensity of CH_2 streching peak at 2854-2923 cm^{-1} indicating presence of oils in protein matrix (Figure 4.38 for CHSO and Figure 4.41 for RSO). Therefore, we can consider CH_2 stretching as a strong indicator of RSO and CHSO encapsulation in any matrix as Santos et al. (2015) and Haider et al. (2017) stated in their studies. The results showed that CHSO and RSO might be encapsulated into LF-PPI complexes and coacervates

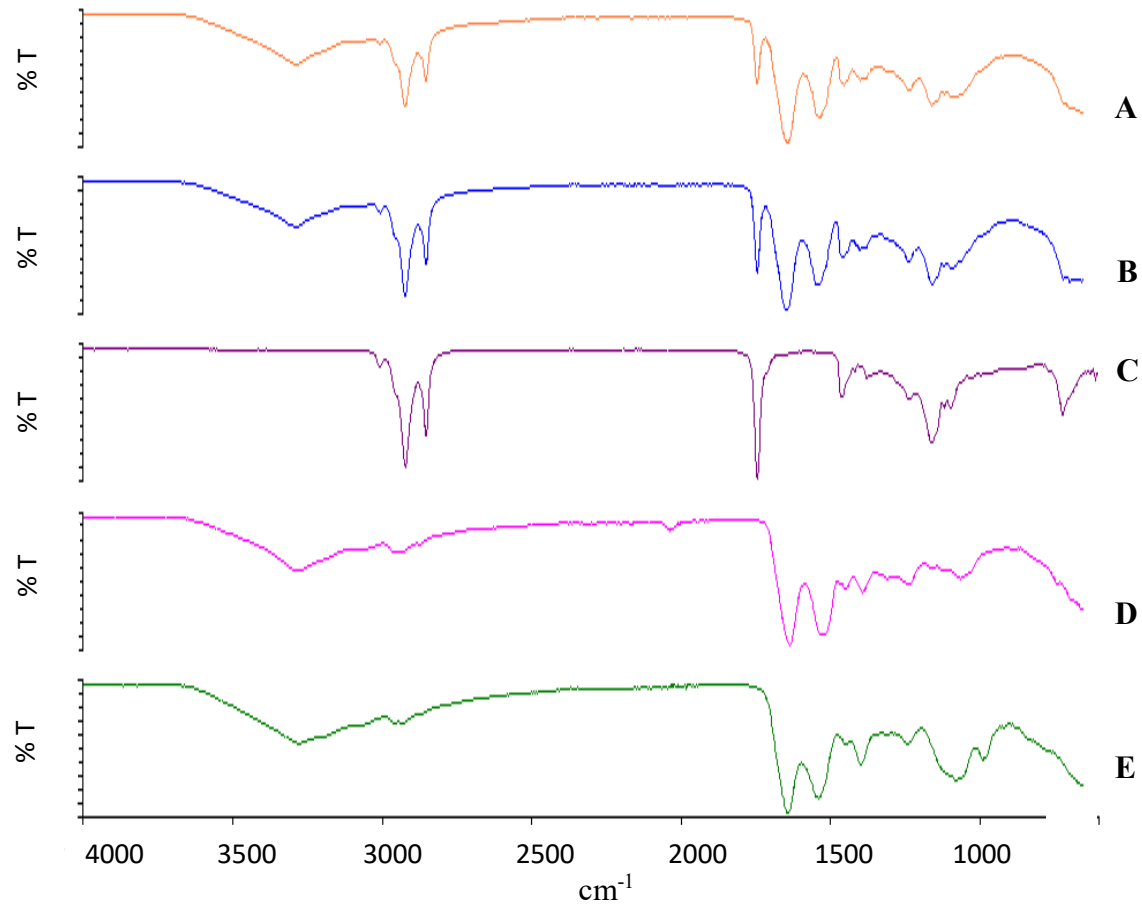

Figure 4. 36 FTIR spectra of A: LF-PPI coated CHSO encapsules at pH 5.4, B: LF-PPI coated CHSO encapsules at pH 7, C: CHSO, D: LF (freeze dried), E: PPI (freeze dried)

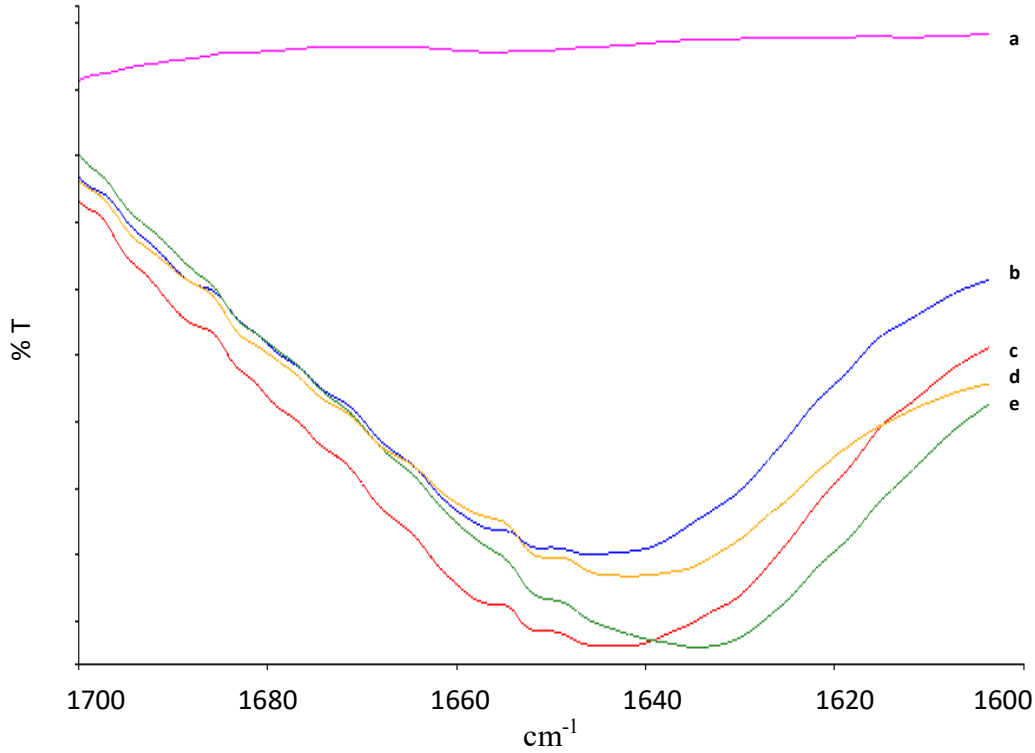

Figure 4. 37 FTIR spectra of a: CHSO, b: LF-PPI coated CHSO encapsules at pH 7, c: LF-PPI coated CHSO encapsules at pH 5.4, d: PPI (freeze dried), e: LF (freeze dried) at Amide I bands (NH_2 bending)

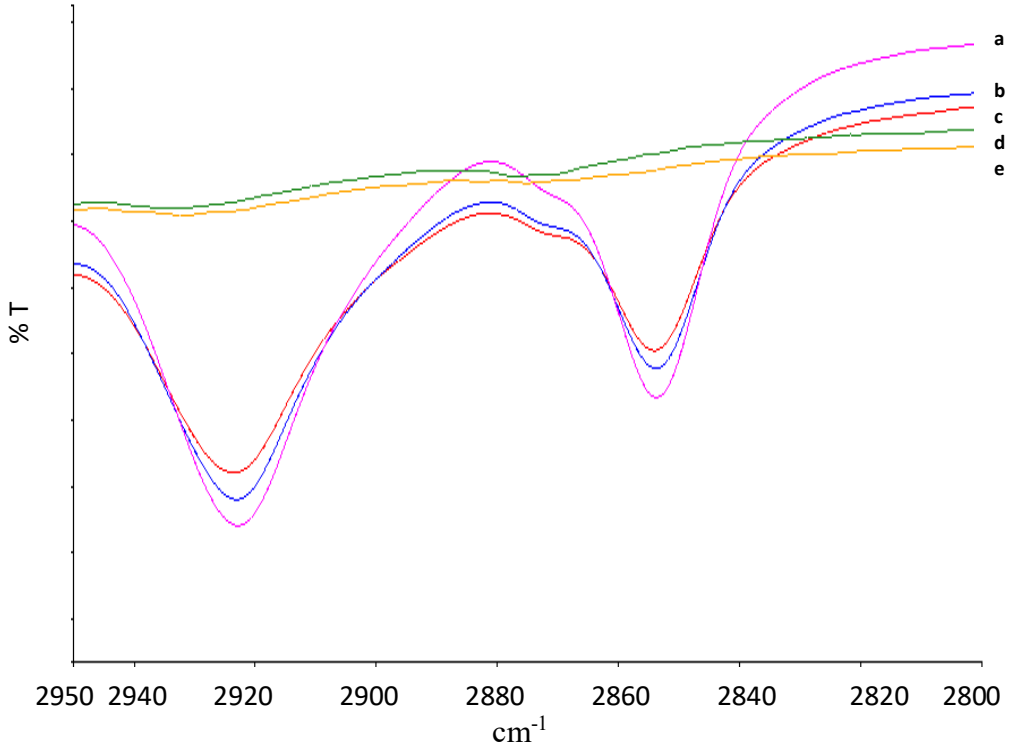

Figure 4. 38 FTIR spectra of a: CHSO, b: LF-PPI coated CHSO encapsules at pH 7, c: LF-PPI coated CHSO encapsules at pH 5.4, d: LF (freeze dried), e: PPI (freeze dried) at CH_2 streching region (2800-2900 cm^{-1})

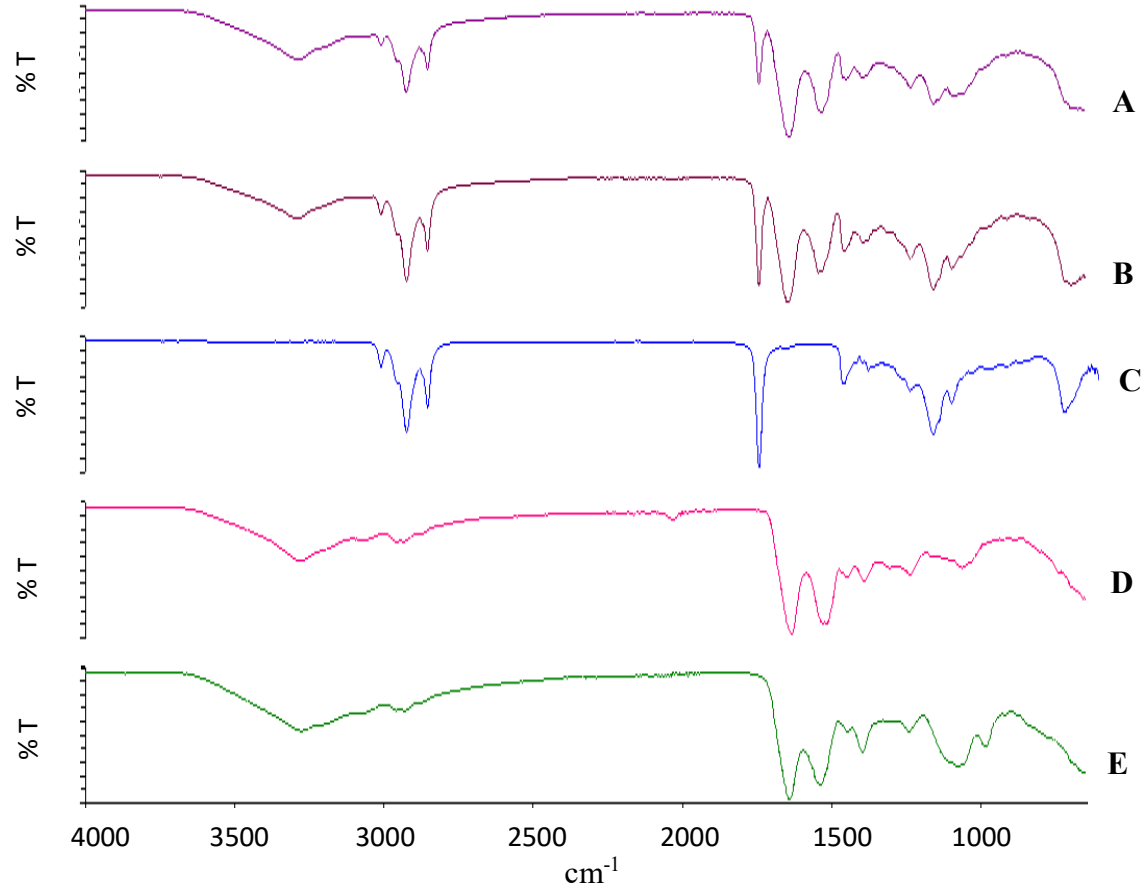

Figure 4. 39 FTIR spectra of A: LF-PPI coated RSO encapsules at pH 5.4, B: LF-PPI coated RSO encapsules at pH 7, C: RSO, D: LF (freeze dried), E: PPI (freeze dried)

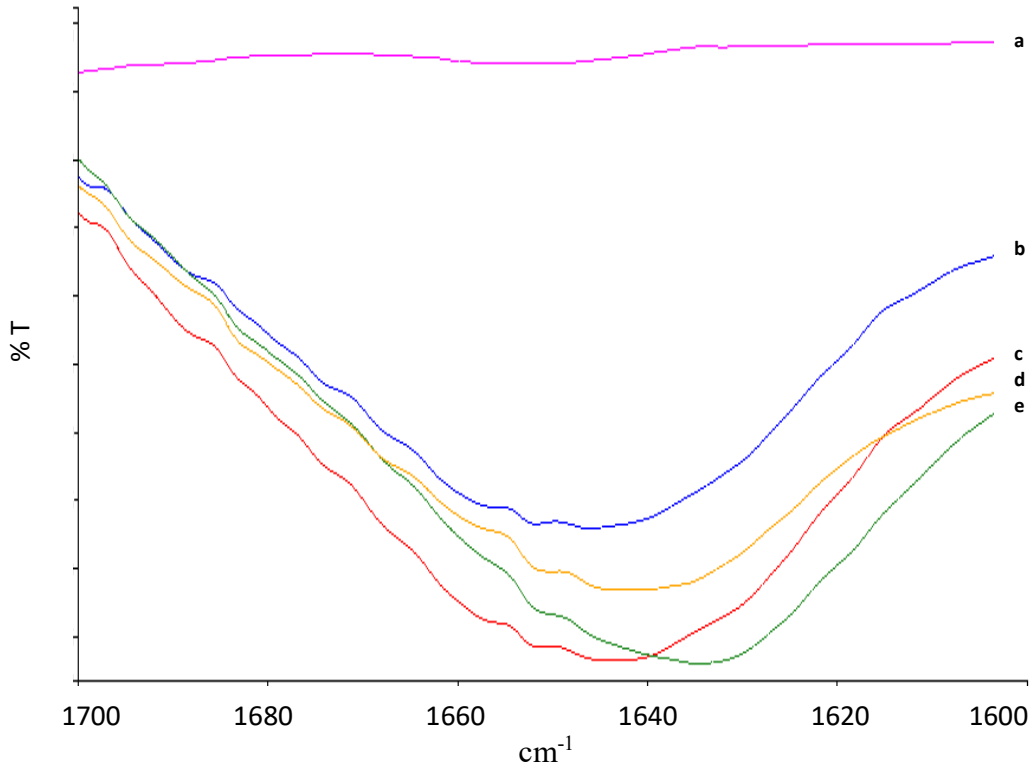

Figure 4. 40FTIR spectra of a: CHSO, b: LF-PPI coated CHSO encapsules at pH 7, c: LF-PPI coated CHSO encapsules at pH 5.4, d: PPI (freeze dried), e: LF (freeze dried) at Amide I bands (NH_2 bending)

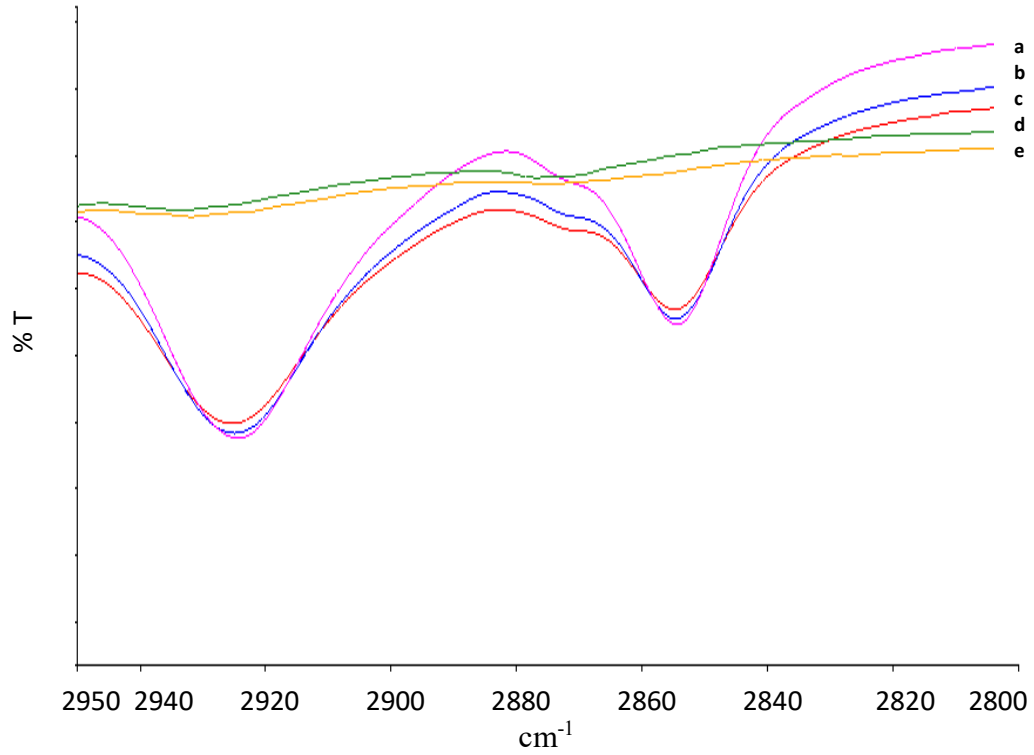

Figure 4. 41 FTIR spectra of a: CHSO, b: LF-PPI coated CHSO encapsules at pH 7, c: LF-PPI coated CHSO encapsules at pH 5.4, d: LF (freeze dried), e: PPI (freeze dried) at CH_2 streching region (2800-2900 cm^{-1})

4. 6. 4 Oxidative Stability of RSO and CHSO oils

Bulk RSO and CHSO and Encapsules prepared with RSO and CHSO were stored at 45°C for 16 days and their peroxide value (PV) were monitored to examine oxidative stability. Encapsules were produced at pH 5.4 (complex coacervation) and pH 7. The PV of encapsulated RSO at pH 7 was increased from 5.83±0.83 to 30.20±0.21 whereas CHSO was increased from 2.27±0.08 to 36.88±0.42 during storage as shown in Figure 4.42 and Figure 4.43, respectively. Besides, the PV of bulk RSO at pH 7 was increased from 3.28±0.00 to 80.20±1.46 whereas CHSO was increased from 1.65±0.00 to 99.58±0.82 during storage as shown in Figure 4.42 and Figure 4.43 as well. It is obvious from the results that encapsulation of RSO and CHSO prevent increasing PV value of the oils. As seen in Figure 4.43 encapsules that formed by complex coacervation were stable than encaspules formed at pH 7. This might be because of coacervate at this pH cause more strength wall around the oils which result in decreasing release of the oils.

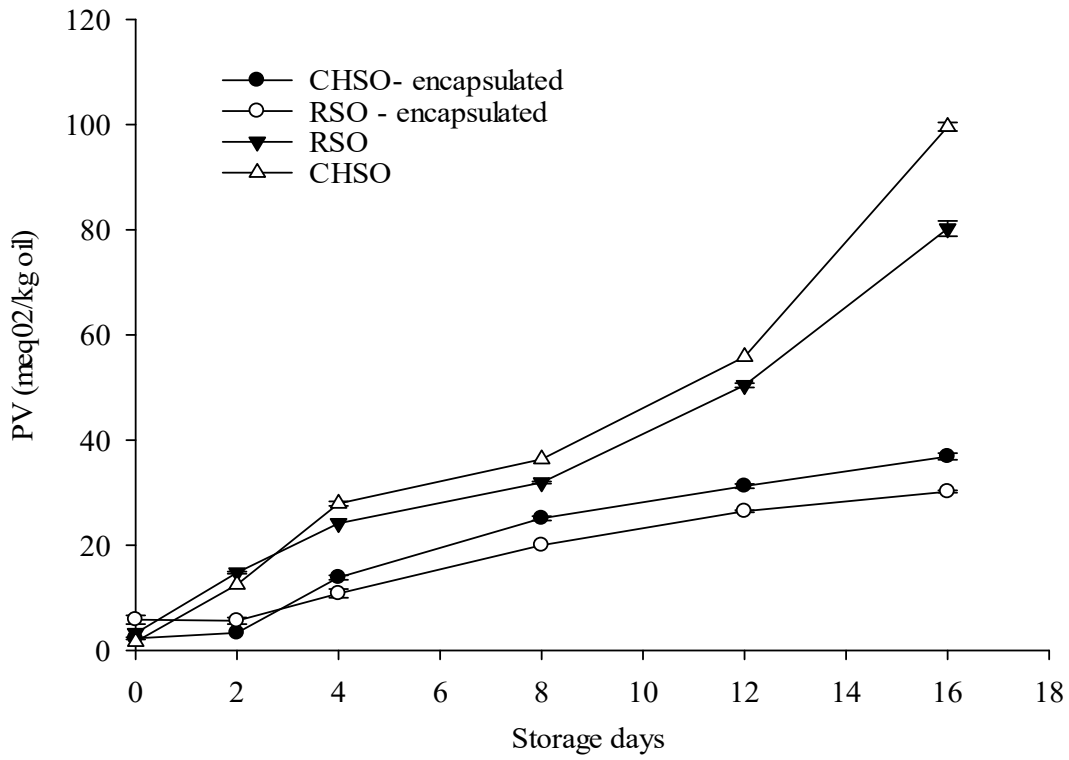

Figure 4. 42 PV of bulk and encapsulated RSO and CHSO oils at pH 7 during storage

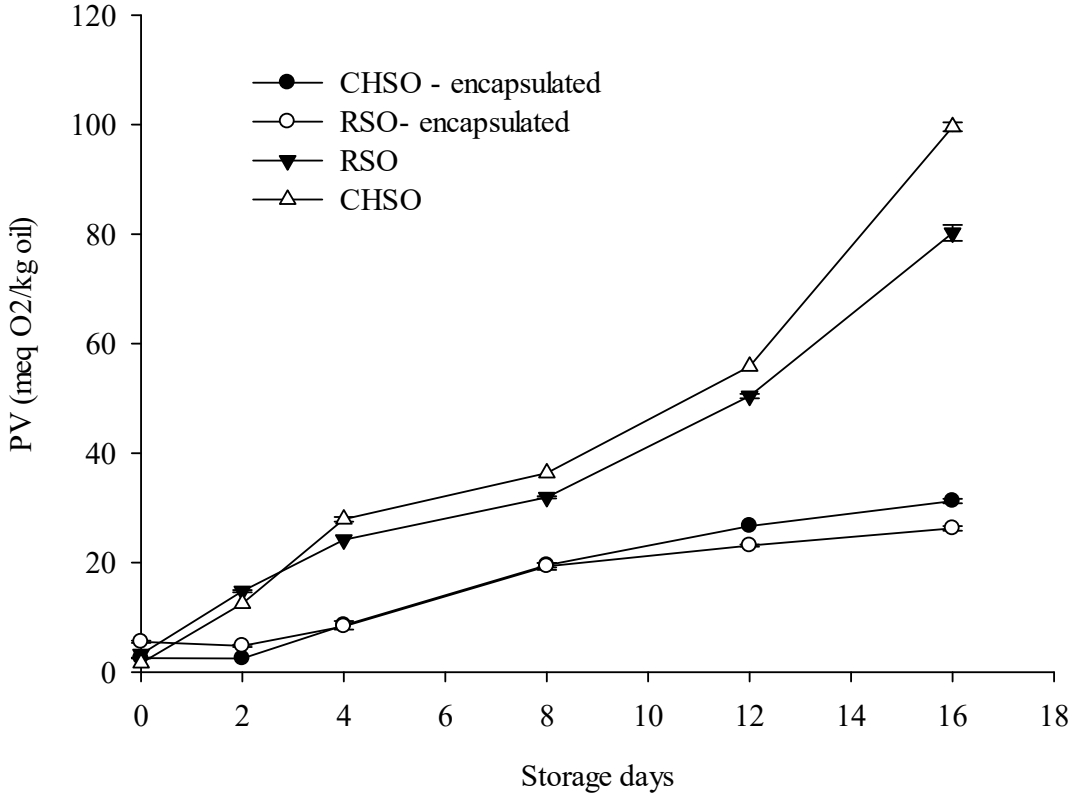

Figure 4. 43 PV of bulk and encapsulated RSO and CHSO oil at pH 5.4 during storage

CONCLUSION

In the first part of study, Mixing cationic lactoferrin (LF) and anionic pea protein isolate (PPI) lead to complex formation and coacervate formation under specific conditions of pH range with maximum level of coacervate formation observed at charge neutrality. The DLS, ζ-potential data and turbidity measurements enabled identification of the optimum pH conditions where coacervation was most favorable (pH 5.4), and where soluble complexes were maximised (pH 7). The SAXS measurements confirmed the formation of heteroprotein complexes with a radius of gyration of ~13 nm at pH 7. The coacervate were observed at pH 5.4 with maximum extensions of about 80 nm. Both, the bimodal size distribution and characteristic length scales deduced from SAXS data are in excellent agreement with the TEM and AFM analysis, later showing a distribution containing strong clusters around 40-50 nm and 60-70 nm, with a predominance of chain-forming LF-PPI nanocomplexes over spherical coacervates.

In the secons part, LF, PPI molecules and LF-PPI complexes were able to coat the surface of the oil droplets. Because of the better phase separation and uniform size distrubition, making preliminary emulsions with LF and then adding PPI which followed by forming complexes and coacervates were chosen as method for further studies.

In the third part, amount of oil that required the saturate 2 wt% of protein was optimized by means of droplet size measurement and rheological analysis which followed by freeze drying of the emulsions. For this purpose, oil concentration was changed from 2 wt% to 10 wt%. We prepared emulsions for both soluble complexes and complex coacervate between LF and PPI (1:1 wt/wt ratio). According to results, 6 wt% oil was chosen for further studies. It was mainly because of the homogeneous size distribution, high encapsulation efficiency and regular encapsule shapes.

In the last part, physicochemical properties of encapsules produced with RSO and CHSO were examined. Moisture content, color properties, functional group observation by FTIR and oxidative stability were evaluated. It was obvious from the results that encapsule formation was achieved by heteroprotein complexes and coacervates and oxidative stability of oils was increased by encapsulation. Additionaly, our complexes and coacervate in nano scale but most our encapsules were in micro scale >0.2µm where as we had <0.2µm in some cases. To eliminate concept confusion, all samples were called as encapsules.

The all results confirmed that lactoferrin and pea protein isolate can form soluble complexes and coacervates. Furthermore, the suitability of emulsion and electrostatic interaction based method for the formation of LF-PPI coated omega rich oils will improve their usage in food industry. But, prior to usage further research is needed on the thermal behaviour and bioavailability of encapsules.

REFERENCES

BS 684 (1987). Methods of analysis fats and fatty oils. *British Standard Institution. London*.

Aberkane, L., Roudaut, G., and Saurel, R. (2014). Encapsulation and Oxidative Stability of PUFA-Rich Oil Microencapsulated by Spray Drying Using Pea Protein and Pectin. *Food and Bioprocess Technology,* **7(5)**, 1505-1517.

Anderson, B. F., Baker, H. M., Dodson, E. J., Norris, G. E., Rumball, S. V., Waters, J. M., and Baker, E. N. (1987). Structure of human lactoferrin at 3.2-A resolution. *Proceedings of the National Academy of Sciences of the United States of America,* **84(7)**, 1769-1773.

Anema, S. G., and de Kruif, C. G. (2011). Interaction of Lactoferrin and Lysozyme with Casein Micelles. *Biomacromolecules,* **12(11)**, 3970-3976.

Anema, S. G., and de Kruif, C. G. (2012). Co-acervates of lactoferrin and caseins. *Soft Matter,* **8(16)**, 4471-4478.

Anema, S. G., and de Kruif, C. G. (2014). Complex coacervates of lactotransferrin and beta-lactoglobulin. *Journal of Colloid and Interface Science,* **430**, 214-220.

Anema, S. G., and de Kruif, C. G. (2016). Phase separation and composition of coacervates of lactoferrin and caseins. *Food Hydrocolloids,* **52**, 670-677.

Antonini, G, Rossi, P, Pitari, G, Marchetti, M, Superti, F, and Valenti, P. (2000). *Role of glycan chains in bovine lactoferrin.* Paper presented at the Lactoferrin: structure, function and applications. Proceedings of the 4th International Conference on Lactoferrin: Structure, Function and Applications, held in Sapporo, Japan, 18-22 May 1999.

Anwar, S Haryani, W., Jenny, and Kunz, B. (2010). Microencapsulation of fish oil by spray granulation and fluid bed film coating. *Journal of food science,* **75(6)**, E359-E371.

AOAC. (1995). Official methods of analysis of Association of Official Analytical Chemists Washington, DC, USA.

Arslan, S., Erbas, M., Tontul, I., and Topuz, A.. (2015). Microencapsulation of probiotic Saccharomyces cerevisiae var. boulardii with different wall materials by spray drying. *LWT - Food Science and Technology,* **63(1)**, 685-690.

Augustin, M. A., and Hemar, Y. (2009). Nano- and micro-structured assemblies for encapsulation of food ingredients. *Chem Soc Rev,* **38(4)**, 902-912.

Aziz, F. R. A., Jai, J., Raslan, R., and Subuki, I. (2016). Microencapsulation of citronella oil by complex coacervation using chitosan-gelatin (b) system: operating design, preparation and characterization. *2016 5th International Conference on Chemical and Process Engineering (Iccpe 2016),* **69**.

Aziz, S., Gill, J., Dutilleul, P., Neufeld, R., and Kermasha, S. (2014). Microencapsulation of krill oil using complex coacervation. *J Microencapsul,* **31(8)**, 774-784.

Bada, J. C., León-Camacho, M., Copovi, P., and Alonso, L. (2013). Characterization of Berry and Currant Seed Oils from Asturias, Spain. *International Journal of Food Properties,* **17(1)**, 77-85.

Bak, I., Lekli, I., Juhasz, B., Varga, E., Varga, B., Gesztelyi, R., Szendrei, L., and Tosaki, A. (2010). Isolation and Analysis of Bioactive Constituents of Sour Cherry (Prunus cerasus) Seed Kernel: An Emerging Functional Food. *Journal of Medicinal Food,* **13(4)**, 905-910.

Bakry, A. M., Abbas, S., Ali, B., Majeed, H., Abouelwafa, M. Y., Mousa, A., and Liang, L. (2016). Microencapsulation of Oils: A Comprehensive Review of Benefits, Techniques, and Applications. *Comprehensive Reviews in Food Science and Food Safety,* **15(1)**, 143-182.

Barac, M., Cabrilo, S., Pesic, M., Stanojevic, S., Zilic, S., Macej, O., and Ristic, N. (2010). Profile and functional properties of seed proteins from six pea (*Pisum sativum*) genotypes. *International Journal of Molecular Sciences,* **11(12)**, 4973-4990.

Barac, M., Pesic, M., Stanojevic, S., Kostic, A., and Cabrilo, S. (2015). Techno-functional properties of pea (Pisum sativum) protein isolates: A review. *Acta Periodica Technologica***(46)**, 1-18.

Barrow, C., and Shahidi, F. (2007). *Marine nutraceuticals and functional foods*: CRC Press.

Bengoechea, C., Jones, O. G., Guerrero, A., and McClements, D. J. (2011). Formation and characterization of lactoferrin/pectin electrostatic complexes: Impact of composition, pH and thermal treatment. *Food Hydrocolloids,* **25(5)**, 1227-1232.

Bergmann, A., Fritz, G., and Glatter, O. (2000). Solving the generalized indirect Fourier transformation (GIFT) by Boltzmann simplex simulated annealing (BSSA). *Journal of Applied Crystallography,* **33(5)**, 1212-1216.

Boye, J., Zare, F., and Pletch, A. (2010). Pulse proteins: Processing, characterization, functional properties and applications in food and feed. *Food Research International,* **43(2)**, 414-431.

Bozan, B., and Temelli, F. (2008). Chemical composition and oxidative stability of flax, safflower and poppy seed and seed oils. *Bioresour Technol,* **99(14)**, 6354-6359.

Can Karaca, A., Nickerson, M. T., and Low, N. H. (2011). Lentil and chickpea protein-stabilized emulsions: optimization of emulsion formulation. *J Agric Food Chem,* **59(24)**, 13203-13211.

Carneiro, H. C. F., Tonon, R. V., Grosso, C. R. F., and Hubinger, M. D. (2013). Encapsulation efficiency and oxidative stability of flaxseed oil microencapsulated by spray drying using different combinations of wall materials. *Journal of Food Engineering,* **115(4)**, 443-451.

Chandrasekara, N., and Shahidi, F. (2011). Oxidative Stability of Cashew Oils from Raw and Roasted Nuts. *Journal of the American Oil Chemists' Society,* **88(8)**, 1197-1202.

Chapeau, A. L., Tavares, Guilherme M., Hamon, Pascaline, Croguennec, Thomas, Poncelet, Denis, and Bouhallab, Saïd. (2016). Spontaneous co-assembly of lactoferrin and β-lactoglobulin as a promising biocarrier for vitamin B9. *Food Hydrocolloids,* **57**, 280-290.

Chawda, P. J., Shi, J., Xue, S., and Quek, S. Y. (2017). Co-encapsulation of bioactives for food applications. *Food Quality & Safety,* **1(4)**, 302-309.

Costantino, H. R., Firouzabadian, L., Hogeland, K., Wu, C., Beganski, C., Carrasquillo, K. G., Córdova, M., Griebenow, K., Zale, S. E., and Tracy, M. A. (2000). Protein spray-freeze drying. Effect of atomization conditions on particle size and stability. *Pharmaceutical research,* **17(11)**, 1374-1382.

Croguennec, T., Tavares, G. M., and Bouhallab, S. (Accepted, In Press). Heteroprotein complex coacervation: A generic process. *Advances in Colloid and Interface Science*.

da Silva, P. T., Fries, L. L. M., de Menezes, C. R., Holkem, A. T., Schwan, C. L., Wigmann, E. F., Bastos, J. D., and da Silva, C. D. (2014). Microencapsulation: concepts, mechanisms, methods and some applications in food technology. *Ciencia Rural,* **44(7)**, 1304-1311.

de Kruif, C. G., Weinbreck, F., and de Vries, R. (2004). Complex coacervation of proteins and anionic polysaccharides. *Current Opinion in Colloid & Interface Science,* **9(5)**, 340-349.

de Vos, P., Faas, M. M., Spasojevic, M., and Sikkema, J. (2010). Encapsulation for preservation of functionality and targeted delivery of bioactive food components. *International Dairy Journal,* **20(4)**, 292-302.

Desai, K. G. H., and Jin Park, H. (2005). Recent Developments in Microencapsulation of Food Ingredients. *Drying Technology,* **23(7)**, 1361-1394.

Dias, M. I., Ferreira, I. C., and Barreiro, M. F. (2015). Microencapsulation of bioactives for food applications. *Food Funct,* **6(4)**, 1035-1052.

Dickinson, E. (2008). Interfacial structure and stability of food emulsions as affected by protein-polysaccharide interactions. *Soft Matter,* **4(5)**, 932-942.

Dimic, E., Vujasinovic, V., Radocaj, O., and Pastor, O. (2012). Characteristics of blackberry and raspberry seeds and oils. *Acta periodica technologica***(43)**, 1-9.

Dordevic, V., Balanc, B., Belscak-Cvitanovic, A., Levic, S., Trifkovic, K., Kalusevic, A., Kostic, I., Komes, D., Bugarski, B., and Nedovic, V. (2015). Trends in Encapsulation Technologies for Delivery of Food Bioactive Compounds. *Food Engineering Reviews,* **7(4)**, 452-490.

Du, X. S., Seeman, D., Dubin, P. L., and Hoagland, D. A. (2015). Nonfreezing Water Structuration in Heteroprotein Coacervates. *Langmuir,* **31(31)**, 8661-8666.

Dyson, R. W. (1987). *Specialty polymers*: Springer.

Eghbal, N., and Choudhary, R. (2018). Complex coacervation: coacervation: Encapsulation and controlled release of active agents in food systems. *Lwt-Food Science and Technology,* **90**, 254-264.

Erçelebi, E., and Ibanoglu, E. (2009). *Characterization of Phase Separation Behavior, Emulsion Stability, Rheology, and Microstructure of Egg White–Polysaccharide Mixtures* (Vol. 74).

Fang, Z. X., and Bhandari, B. (2010). Encapsulation of polyphenols - a review. *Trends in Food Science & Technology,* **21(10)**, 510-523.

Farhoosh, R. (2007). The Effect of Operational Parameters of the Rancimat Method on the Determination of the Oxidative Stability Measures and Shelf-Life Prediction of Soybean Oil. *Journal of the American Oil Chemists' Society,* **84(3)**, 205-209.

Flanagan, S. E., Malanowski, A. J., Kizilay, E., Seeman, D., Dubin, P. L., Donato-Capel, L., Bovetto, L., and Schmitt, C. (2015). Complex Equilibria, Speciation, and Heteroprotein Coacervation of Lactoferrin and beta-Lactoglobulin. *Langmuir,* **31(5)**, 1776-1783.

Frankel, E. N., Satue-Gracia, T., Meyer, A. S., and German, J. B. (2002). Oxidative stability of fish and algae oils containing long-chain polyunsaturated fatty acids in bulk and in oil-in-water emulsions. *J Agric Food Chem,* **50(7)**, 2094-2099.

Frascareli, E. C., Silva, V. M., Tonon, R. V., and Hubinger, M. D. (2012). Effect of process conditions on the microencapsulation of coffee oil by spray drying. *Food and Bioproducts Processing,* **90(3)**, 413-424.

Gharsallaoui, A., Cases, El., Chambin, O., and Saurel, R. (2009). Interfacial and Emulsifying Characteristics of Acid-treated Pea Protein. *Food Biophysics,* **4(4)**, 273-280.

Gharsallaoui, A., Roudaut, G., Chambin, O., Voilley, A., and Saurel, R. (2007). Applications of spray-drying in microencapsulation of food ingredients: An overview. *Food Research International,* **40(9)**, 1107-1121.

Ghosh, S. K. (2006). Functional Coatings and Microencapsulation: A General Perspective *Functional Coatings*.

Gouin, S. (2004). Microencapsulation. *Trends in Food Science & Technology,* **15(7-8)**, 330-347.

Grossmann, J. G., Neu, M., Pantos, E., Schwab, F. J., Evans, R. W., Townes-Andrews, E., Lindley, P. F., Appel, H., Thies, W. G., and Hasnain, S. S. (1992). X-ray solution scattering reveals conformational changes upon iron uptake in lactoferrin, serum and ovo-transferrins. *Journal of Molecular Biology,* **225(3)**, 811-819.

Haider, J., Majeed, H., Williams, P. A, Safdar, W., and Zhong, F. (2017). Formation of chitosan nanoparticles to encapsulate krill oil (Euphausia superba) for application as a dietary supplement. *Food Hydrocolloids,* **63**, 27-34.

Heinzelmann, K., Franke, K., Jensen, B., and Haahr, A. M. (2000). Protection of fish oil from oxidation by microencapsulation using freeze-drying techniques. *European Journal of Lipid Science and Technology,* **102(2)**, 114-121.

Hosseini, S. F., Zandi, M., Rezaei, M., and Farahmandghavi, F. (2013). Two-step method for encapsulation of oregano essential oil in chitosan nanoparticles: preparation, characterization and in vitro release study. *Carbohydr Polym,* **95(1)**, 50-56.

Huang, G. Q., Sun, Y. T., Xiao, J. X., and Yang, J. (2012). Complex coacervation of soybean protein isolate and chitosan. *Food Chemistry,* **135(2)**, 534-539.

Hwang, M. T. P., Ding, X. C., Gao, J., Acharya, A. P., Little, S. R., and Wang, Y. D. (2018). A biocompatible betaine-functionalized polycation for coacervation. *Soft Matter,* **14(3)**, 387-395.

I'Anson, K. J., Miles, M. J., Bacon, J. R., Carr, H. J., Lambert, N., Morris, V. J., and Wright, D. J. (1988). Structure of the 7S globulin (vicilin) from pea (Pisum sativum). *International Journal of Biological Macromolecules,* **10(5)**, 311-317.

IUPAC. (1987). Methods 2301. Preparation of the fatty acid methyl esters. .

Jin, K. M., and Kim, Y. H. (2008). Injectable, thermo-reversible and complex coacervate combination gels for protein drug delivery. *Journal of Controlled Release,* **127(3)**, 249-256.

Jordan, R. G. (2010). Prenatal omega-3 fatty acids: review and recommendations. *The Journal of Midwifery & Women's Health,* **55(6)**, 520-528.

Jyothi, N. V., Prasanna, P. M., Sakarkar, S. N., Prabha, K. S., Ramaiah, P. S., and Srawan, G. Y. (2010). Microencapsulation techniques, factors influencing encapsulation efficiency. *J Microencapsul,* **27(3)**, 187-197.

Kaibara, K., Okazaki, T., Bohidar, H. B., and Dubin, P. L. (2000). pH-induced coacervation in complexes of bovine serum albumin and cationic polyelectrolytes. *Biomacromolecules,* **1(1)**, 100-107.

Kaushik, P., Dowling, K., Barrow, C. J., and Adhikari, B. (2015). Microencapsulation of omega-3 fatty acids: A review of microencapsulation and characterization methods. *Journal of Functional Foods,* **19**, 868-881.

Kermasha, S., Aziz, S., Gill, J., and Neufeld, R. (2018). Microencapsulation of esterified krill oil, using complex coacervation. *J Microencapsul,* **35(1)**, 36-48.

Kizilay, E., Kayitmazer, A. B., and Dubin, P. L. (2011). Complexation and coacervation of polyelectrolytes with oppositely charged colloids. *Advances in Colloid and Interface Science,* **167(1-2)**, 24-37.

Kizilay, E., Seeman, D., Yan, Y. F., Du, X. S., Dubin, P. L., Donato-Capel, L., Bovetto, L., and Schmitt, C. (2014). Structure of bovine beta-lactoglobulin-lactoferrin coacervates. *Soft Matter,* **10(37)**, 7262-7268.

Klaypradit, W., and Huang, Y. W. (2008). Fish oil encapsulation with chitosan using ultrasonic atomizer. *LWT-Food Science and Technology,* **41(6)**, 1133-1139.

Kuang, S. S., Oliveira, J. C., and Crean, A. M. (2010). Microencapsulation as a Tool for Incorporating Bioactive Ingredients into Food. *Critical Reviews in Food Science and Nutrition,* **50(10)**, 951-968.

Kulås, E., and Ackman, R. G. (2001). Different tocopherols and the relationship between two methods for determination of primary oxidation products in fish oil. *Journal of Agricultural and Food Chemistry,* **49(4)**, 1724-1729.

Kurut, A., Persson, B. A., Åkesson, T., Forsman, J., and Lund, M. (2012). Anisotropic interactions in protein mixtures: Self assembly and phase behavior in aqueous solution. *The journal of physical chemistry letters,* **3(6)**, 731-734.

Labuza, TP, McNally, L., Gallagher, D., Hawkes, J, and Hurtado, F. (1972). Stability of intermediate moisture foods. 1. Lipid oxidation. *Journal of Food Science,* **37(1)**, 154-159.

Lam, A. C. Y., Can Karaca, A., Tyler, R. T., and Nickerson, M. T. (2016). Pea protein isolates: Structure, extraction, and functionality. *Food Reviews International,* **34(2)**, 126-147.

Lamprecht, A., Schafer, U. F., and Lehr, C. M. (2000). Characterization of microcapsules by confocal laser scanning microscopy: structure, capsule wall composition and encapsulation rate. *European Journal of Pharmaceutics and Biopharmaceutics,* **49(1)**, 1-9.

Le, H. D., and Le, V. V. (2015). Application of ultrasound to microencapsulation of coconut milk fat by spray drying method. *J Food Sci Technol,* **52(4)**, 2474-2478.

Leong, T. S., Martin, G. J., and Ashokkumar, M. (2017). Ultrasonic encapsulation - A review. *Ultrason Sonochem,* **35(Pt B)**, 605-614.

Lesmes, U., and McClements, D. J. (2009). Structure-function relationships to guide rational design and fabrication of particulate food delivery systems. *Trends in Food Science & Technology,* **20(10)**, 448-457.

Li, X., Wang, X., Xu, D., Cao, Y., Wang, S., Wang, B., Sun, B., Yuan, F., and Gao, Y. (2018). Enhancing physicochemical properties of emulsions by heteroaggregation of oppositely charged lactoferrin coated lutein droplets and whey protein isolate coated DHA droplets. *Food Chem,* **239**, 75-85.

Liberatore, M. W., Wyatt, N. B., Henry, M., Dubin, P. L., and Foun, E. (2009). Shear-Induced Phase Separation in Polyelectrolyte/Mixed Micelle Coacervates. *Langmuir,* **25(23)**, 13376-13383.

Liu, S., Low, N. H., and Nickerson, Michael T. (2010). Entrapment of Flaxseed Oil Within Gelatin-Gum Arabic Capsules. *Journal of the American Oil Chemists' Society,* **87(7)**, 809-815.

Liu, S., Low, N. H., and Nickerson, M. T. (2009). Effect of pH, salt, and biopolymer ratio on the formation of pea protein isolate–gum arabic complexes. *Journal of Agricultural and Food Chemistry,* **57(4)**, 1521-1526.

Mao, Y. and McClements, D. J. (2011). Modulation of bulk physicochemical properties of emulsions by hetero-aggregation of oppositely charged protein-coated lipid droplets. *Food Hydrocolloids,* **25(5)**, 1201-1209.

Mao, Y., and McClements, D. J. (2013). Modification of emulsion properties by heteroaggregation of oppositely charged starch-coated and protein-coated fat droplets. *Food Hydrocolloids,* **33(2)**, 320-326.

Marfil, P. H. M., Paulo, B. B., Alvim, I. D., and Nicoletti, V. R. (2018). Production and characterization of palm oil microcapsules obtained by complex coacervation in gelatin/gum Arabic. *Journal of Food Process Engineering,* **41(4)**.

McClements, D. J. (1997). Ultrasonic characterization of foods and drinks: Principles, methods, and applications. *Critical Reviews in Food Science and Nutrition,* **37(1)**, 1-46.

McClements, D. J., Decker, E. A., Park, Y., and Weiss, J. (2009). Structural Design Principles for Delivery of Bioactive Components in Nutraceuticals and Functional Foods. *Critical Reviews in Food Science and Nutrition,* **49(6)**, 577-606.

McLennan, P. L., and Abeywardena, M. Y. (2005). Membrane basis for fish oil effects on the heart: linking natural hibernators to prevention of human sudden cardiac death. *The Journal of membrane biology,* **206(2)**, 85-102.

Mela, I., Aumaitre, E., Williamson, A. M., and Yakubov, G. E. (2010). Charge reversal by salt-induced aggregation in aqueous lactoferrin solutions. *Colloids and Surfaces B: Biointerfaces,* **78(1)**, 53-60.

Mertens, C., Dehon, L., Bourgeois, A., Verhaeghe-Cartrysse, C., and Blecker, C. (2012). Agronomical factors influencing the legumin/vicilin ratio in pea (Pisum sativum L.) seeds. *Journal of the Science of Food and Agriculture,* **92(8)**, 1591-1596.

Mession, J. L., Sok, N., Assifaoui, A., and Saurel, R. (2013). Thermal Denaturation of Pea Globulins (Pisum sativum L.)—Molecular Interactions Leading to Heat-Induced Protein Aggregation. *Journal of Agricultural and Food Chemistry,* **61(6)**, 1196-1204.

Micić, D. M., Ostojić, S. B., Simonović, M. B., Krstić, G., Pezo, L. L., and Simonović, B. R. (2015). Kinetics of blackberry and raspberry seed oils oxidation by DSC. *Thermochimica Acta,* **601**, 39-44.

Monica, Trif, Ansorge-Schumacher, Marion, Socaciu, Carmen, and Diehl, HA. (2007). Determination of encapsulated Sea buckthorn oil oxidation using FTIR-ATR spectroscopy. *Bulletin USAMV-CN,* **63**, 64.

Moore, S. A., Anderson, B. F., Groom, C. R., Haridas, M., and Baker, E. N. (1997). Three-dimensional structure of diferric bovine lactoferrin at 2.8 A resolution. *J Mol Biol,* **274(2)**, 222-236.

Mumenthaler, M, and Leuenberger, H. (1991). Atmospheric spray-freeze drying: a suitable alternative in freeze-drying technology. *International journal of pharmaceutics,* **72(2)**, 97-110.

Nedovic, V., Kalusevic, A., Manojlovic, V., Levic, S., and Bugarski, B. (2011). An overview of encapsulation technologies for food applications. *11th International Congress on Engineering and Food (Icef11),* **1**, 1806-1815.

Nigen, M., Croguennec, T., Madec, M. N., and Bouhallab, S. (2007a). Apo alpha-lactalbumin and lysozyme are colocalized in their subsequently formed spherical supramolecular assembly. *Febs Journal,* **274(23)**, 6085-6093.

Nigen, M., Croguennec, T., Renard, D., and Bouhallab, S. (2007b). Temperature affects the supramolecular structures resulting from alpha-lactalbumin-lysozyme interaction. *Biochemistry,* **46(5)**, 1248-1255.

Nigen, M., Gaillard, C., Croguennec, T., Madec, M. N., and Bouhallab, S. (2010). Dynamic and supramolecular organisation of alpha-lactalbumin/lysozyme microspheres: A microscopic study. *Biophysical Chemistry,* **146(1)**, 30-35.

Nigen, M., Le, Tilly, V., Croguennec, T., Drouin-Kucma, D., and Bouhallab, S. (2009). Molecular interaction between apo or holo α-lactalbumin and lysozyme: Formation of heterodimers as assessed by fluorescence measurements. *Biochimica et Biophysica Acta (BBA)-Proteins and Proteomics,* **1794(4)**, 709-715.

Oetjen, G.W., and Haseley, P. (2004). *Freeze-drying*: John Wiley & Sons.

Onwulata, C. I. (2012). Encapsulation of New Active Ingredients. *Annual Review of Food Science and Technology, Vol 3,* **3**, 183-202.

Oomah, B. D., Ladet, S., Godfrey, D. V., Liang, J., and Girard, B. (2000). Characteristics of raspberry (Rubus idaeus L.) seed oil. *Food chemistry,* **69(2)**, 187-193.

Orsavova, J., Misurcova, L., Ambrozova, J., Vicha, R., and Mlcek, J. (2015). Fatty Acids Composition of Vegetable Oils and Its Contribution to Dietary Energy Intake and Dependence of Cardiovascular Mortality on Dietary Intake of Fatty Acids. *International Journal of Molecular Sciences,* **16(6)**, 12871-12890.

Parry, J., Su, L., Luther, M., Zhou, K., Yurawecz, M. P., Whittaker, P., and Yu, L. (2005). Fatty acid composition and antioxidant properties of cold-pressed marionberry, boysenberry, red raspberry, and blueberry seed oils. *J Agric Food Chem,* **53(3)**, 566-573.

Pastre, D., Pietrement, O., Fusil, S., Landousy, F., Jeusset, J., David, M. O., Hamon, L., Le Cam, E., and Zozime, A. (2003). Adsorption of DNA to mica mediated by divalent counterions: a theoretical and experimental study. *Biophys J,* **85(4)**, 2507-2518.

Patil-Sen, Y., Sadeghpour, A., Rappolt, M., and Kulkarni, C. V. (2016). Facile preparation of internally self-assembled lipid particles stabilized by carbon nanotubes. **(108)**, e53489.

Peixoto, P. D., Tavares, G. M., Croguennec, T., Nicolas, A., Hamon, P., Roiland, C., and Bouhallab, S. (2016). Structure and Dynamics of Heteroprotein Coacervates. *Langmuir,* **32(31)**, 7821-7828.

Piacentini, E., Giorno, L., Dragosavac, M. M., Vladisavljevic, G. T., and Holdich, R. G. (2013). Microencapsulation of oil droplets using cold water fish gelatine/gum arabic complex coacervation by membrane emulsification. *Food Research International,* **53(1)**, 362-372.

Piazza, L., and Roversi, T. (2011). Preliminary study on microbeads production by co-extrusion technology. *11th International Congress on Engineering and Food (Icef11),* **1**, 1374-1380.

Plietz, P., Zirwer, D., Schlesier, B., Gast, K., and Damaschun, G. (1984). Shape, symmetry, hydration and secondary structure of the legumin from Vicia faba in solution. *Biochimica et Biophysica Acta (BBA) - Protein Structure and Molecular Enzymology,* **784(2)**, 140-146.

Priftis, D., Leon, L., Song, Z. Y., Perry, S. L., Margossian, K. O., Tropnikova, A., Cheng, J. J., and Tirrell, M. (2015). Self-Assembly of alpha-Helical Polypeptides Driven by Complex Coacervation. *Angewandte Chemie-International Edition,* **54(38)**, 11128-11132.

Qazvini, N. T., Bolisetty, S., Adamcik, J., and Mezzenga, R. (2012). Self-healing fish gelatin/sodium montmorillonite biohybrid coacervates: Structural and rheological characterization. *Biomacromolecules,* **13(7)**, 2136-2147.

Quinn, MK, Gnan, N, James, S, Ninarello, A, Sciortino, F, Zaccarelli, E, and McManus, Jennifer J. (2015). How fluorescent labelling alters the solution behaviour of proteins. *Physical Chemistry Chemical Physics,* **17(46)**, 31177-31187.

Quispe-Condori, S., Saldaña, M. D. A., and Temelli, F. (2011). Microencapsulation of flax oil with zein using spray and freeze drying. *LWT - Food Science and Technology,* **44(9)**, 1880-1887.

Rustan, A. C., and Drevon, C. A. (2001). Fatty Acids: Structures and Properties *eLS*.

Rutz, J. K., Borges, C. D., Zambiazi, R. C., Crizel-Cardozo, M. M., Kuck, L. S., and Norena, C. P. (2017). Microencapsulation of palm oil by complex coacervation for application in food systems. *Food Chem,* **220**, 59-66.

Salvatore, D., Croguennec, T., Bouhallab, S., Forge, V., and Nicolai, T. (2011). Kinetics and structure during self-assembly of oppositely charged proteins in aqueous solution. *Biomacromolecules,* **12(5)**, 1920-1926.

Santos, M. B., da Costa, A. R., and Garcia-Rojas, E. E. (2018). Heteroprotein complex coacervates of ovalbumin and lysozyme: Formation and thermodynamic characterization. *International Journal of Biological Macromolecules,* **106**, 1323-1329.

Santos, M. G., Bozza, F. T., Thomazini, M., and Favaro-Trindade, C. S. (2015). Microencapsulation of xylitol by double emulsion followed by complex coacervation. *Food Chem,* **171**, 32-39.

Sarkar, A., Goh, K. K. T., and Singh, H. (2009). Colloidal stability and interactions of milk-protein-stabilized emulsions in an artificial saliva. *Food Hydrocolloids,* **23(5)**, 1270-1278.

Sarkar, A., Kamaruddin, H., Bentley, A., and Wang, S. (2016). Emulsion stabilization by tomato seed protein isolate: Influence of pH, ionic strength and thermal treatment. *Food Hydrocolloids,* **57**, 160-168.

Schmitt, C., and Turgeon, S. L. (2011). Protein/polysaccharide complexes and coacervates in food systems. *Advances in Colloid and Interface Science,* **167(1-2)**, 63-70.

Schmitt, C., Sanchez, C., Desobry-Banon, S., and Hardy, J. (1998). Structure and Technofunctional Properties of Protein-Polysaccharide Complexes: A Review. *Critical Reviews in Food Science and Nutrition,* **38(8)**, 689-753.

Semenova, M. G., and Dickinson, E. (2010). *Biopolymers in food colloids: Thermodynamics and molecular interactions*: CRC Press.

Shi, L., Beamer, S. K., Yang, H., and Jaczynski, J. (2018). Micro-emulsification/encapsulation of krill oil by complex coacervation with krill protein isolated using isoelectric solubilization/precipitation. *Food Chem,* **244**, 284-291.

Simopoulos, A. P. (2008). The Importance of the Omega-6/Omega-3 Fatty Acid Ratio in Cardiovascular Disease and Other Chronic Diseases. *Experimental Biology and Medicine,* **233(6)**, 674-688.

Singh, H., and Sarkar, A. (2011). Behaviour of protein-stabilised emulsions under various physiological conditions. *Advances in Colloid and Interface Science,* **165(1)**, 47-57.

Šućurović, A., Vukelić, N., Ignjatović, L., Brčeski, I., and Jovanović, D. (2009). Physical-chemical characteristics and oxidative stability of oil obtained from lyophilized raspberry seed. *European Journal of Lipid Science and Technology,* **111(11)**, 1133-1141.

Svergun, D. I, and Koch, M. HJ. (2003). Small-angle scattering studies of biological macromolecules in solution. *Reports on Progress in Physics,* **66(10)**, 1735.

Tavares, G. M., Croguennec, T., Carvalho, A. F., and Bouhallab, S. (2014). Milk proteins as encapsulation devices and delivery vehicles: Applications and trends. *Trends in Food Science & Technology,* **37(1)**, 5-20.

Tavares, G. M., Croguennec, T., Hamon, P., Carvalho, A. F., and Bouhallab, S. (2015). Selective coacervation between lactoferrin and the two isoforms of β-lactoglobulin. *Food Hydrocolloids,* **48**, 238-247.

Timilsena, Y. P., Adhikari, R., Barrow, C. J., and Adhikari, B. (2016a). Microencapsulation of chia seed oil using chia seed protein isolate-chia seed gum complex coacervates. *International Journal of Biological Macromolecules,* **91**, 347-357.

Timilsena, Y. P., Wang, B., Adhikari, R., and Adhikari, B. (2016b). Preparation and characterization of chia seed protein isolate-chia seed gum complex coacervates. *Food Hydrocolloids,* **52**, 554-563.

Timilsena, Y. P., Wang, B., Adhikari, R., and Adhikari, B. (2017). Advances in microencapsulation of polyunsaturated fatty acids (PUFAs)-rich plant oils using complex coacervation: A review. *Food Hydrocolloids,* **69**, 369-381.

Toh, Y. C., Ho, S. T., Zhou, Y., Hutmacher, D. W., and Yu, H. (2005). Application of a polyelectrolyte improve seeding efficiency of bone complex coacervation method to marrow stromal cells in a 3D culture system. *Biomaterials,* **26(19)**, 4149-4160.

Tokle, T., and McClements, D. J. (2011). Physicochemical properties of lactoferrin stabilized oil-in-water emulsions: Effects of pH, salt and heating. *Food Hydrocolloids,* **25(5)**, 976-982.

Turgeon, S. L., Beaulieu, M., Schmitt, C., and Sanchez, C. (2003). Protein-polysaccharide interactions: phase-ordering kinetics, thermodynamic and structural aspects. *Current Opinion in Colloid & Interface Science,* **8(4-5)**, 401-414.

Turgeon, S. L., Schmitt, C., and Sanchez, C. (2007). Protein–polysaccharide complexes and coacervates. *Current Opinion in Colloid & Interface Science,* **12(4-5)**, 166-178.

Uluata, S., and Ozdemir, N. (2012). Antioxidant Activities and Oxidative Stabilities of Some Unconventional Oilseeds. *Journal of the American Oil Chemists' Society,* **89(4)**, 551-559.

Van Hoed, V., Barbouche, I., De Clercq, N., Dewettinck, K., Slah, M., Leber, E., and Verhé, R. (2011). Influence of filtering of cold pressed berry seed oils on their antioxidant profile and quality characteristics. *Food Chemistry,* **127(4)**, 1848-1855.

Vongsvivut, J., Heraud, P., Zhang, W., Kralovec, J. A., McNaughton, D., and Barrow, C. J. (2012). Quantitative determination of fatty acid compositions in micro-encapsulated fish-oil supplements using Fourier transform infrared (FTIR) spectroscopy. *Food chemistry,* **135(2)**, 603-609.

Wang, X.-Yu, Yang, D., Gan, L. J., Zhang, H., Shin, J. A., Lee, Y. H., Jang, Y. S., and Lee, Ki-T. (2015). Effect of positional distribution of linoleic acid on oxidative stability of triacylglycerol molecules determined by 1H NMR. *Journal of the American Oil Chemists' Society,* **92(2)**, 157-165.

Wang, Y. L., Kimura, K., Huang, Q. R., Dubin, P. L., and Jaeger, W. (1999). Effects of salt on polyelectrolyte-micelle coacervation. *Macromolecules,* **32(21)**, 7128-7134.

Wang, Y., Gao, J. Y., and Dubin, P. L. (1996). Protein separation via polyelectrolyte coacervation: Selectivity and efficiency. *Biotechnology Progress,* **12(3)**, 356-362.

Weinbreck, F., Minor, M., and de Kruif, C. G. (2004). Microencapsulation of oils using whey protein/gum Arabic coacervates. *J Microencapsul,* **21(6)**, 667-679.

Weitz, D., Weintraub, H., Fisher, E., and Schwartzbard, A. Z. (2010). Fish oil for the treatment of cardiovascular disease. *Cardiology in review,* **18(5)**, 258.

Welland, M. E., Miles, M. J., Lambert, N., Morris, V. J., Coombs, J. H., and Pethica, J. B. (1989). Structure of the globular protein vicilin revealed by scanning tunnelling microscopy. *International Journal of Biological Macromolecules,* **11(1)**, 29-32.

Wilkowska, A., Ambroziak, W., Czyżowska, A., and Adamiec, J. (2016). Effect of Microencapsulation by Spray-Drying and Freeze-Drying Technique on the Antioxidant Properties of Blueberry (Vaccinium myrtillus) Juice Polyphenolic Compounds. **66(1)**, 11.

Wilson, E. V., and Horan, T. (2007). Research in e-Health: Guest Editors' Introduction to the Special Issue. *e-Service Journal,* **5(2)**, 1-4.

Wu, B. C., Degner, B., and McClements, D. J. (2014). Soft matter strategies for controlling food texture: formation of hydrogel particles by biopolymer complex coacervation. *J Phys Condens Matter,* **26(46)**, 464104.

Wu, K. G., and Xiao, Q. (2005). Microencapsulation of fish oil by simple coacervation of hydroxypropyl methylcellulose. *Chinese Journal of Chemistry,* **23(11)**, 1569-1572.

Yan, Y. F., Kizilay, E., Seeman, D., Flanagan, S., Dubin, P. L., Bovetto, L., Donato, L., and Schmitt, C. (2013). Heteroprotein Complex Coacervation: Bovine beta-Lactoglobulin and Lactoferrin. *Langmuir,* **29(50)**, 15614-15623.

Yeboah, E. M. O., Kobue-Lekalake, R. I., Jackson, J. C., Muriithi, E. N., Matenanga, O., and Yeboah, S. O. (2017). Application of high resolution NMR, FTIR, and GC–MS to a comparative study of some indigenous seed oils from Botswana. *Innovative Food Science & Emerging Technologies,* **44**, 181-190.

Yılmaz, C., and Gökmen, V. (2013). Compositional characteristics of sour cherry kernel and its oil as influenced by different extraction and roasting conditions. *Industrial Crops and Products,* **49**, 130-135.

Yılmaz, F. M., Görgüç, A., Karaaslan, M., Vardin, H., Ersus B. S., Uygun, Ö., and Bircan, C. (2018). Sour Cherry By-products: Compositions, Functional Properties and Recovery Potentials–A Review. *Critical reviews in food science and nutrition*, 1-15.

Zhang, W., Yan, C., May, J., and Barrow, C. (2009). Whey protein and gum Arabic encapsulated Omega-3 lipids. The effect of material properties on coacervation. *Agro food industry hi-tech,* **20(4)**, 20-23.

Zhao, J. J., Wei, T., Wei, Z. H., Yuan, F., and Gao, Y. X. (2015). Influence of soybean soluble polysaccharides and beet pectin on the physicochemical properties of lactoferrin-coated orange oil emulsion. *Food Hydrocolloids,* **44**, 443-452.

Zhao, J., Wei, T., Wei, Z., Yuan, F., and Gao, Y. (2015). Influence of soybean soluble polysaccharides and beet pectin on the physicochemical properties of lactoferrin-coated orange oil emulsion. *Food Hydrocolloids,* **44**, 443-452.

Zuidam, N. J., and Shimoni, E. (2010). Overview of Microencapsulates for Use in Food Products or Processes and Methods to Make Them. In N. J. Zuidam andViktor Nedovic (Eds.), *Encapsulation Technologies for Active Food Ingredients and Food Processing* (pp. 3-29). New York, NY: Springer New York.

APPENDIX

Table A. 1 Sauter mean diameter (d_{32}) and volume mean diameter (d_{43}) of emulsions prepared with different RSO concentration at pH 5.4

Protein concentration (wt%)	Oil concentration (wt%)	pH	d_{32}	d_{43}
2	2	5.4	0.77 ± 0.02^{a}	3.14 ± 0.13^{a}
2	4	5.4	1.29 ± 0.00^{b}	1.72 ± 0.01^{b}
2	6	5.4	1.45 ± 0.00^{c}	1.70 ± 0.00^{b}
2	8	5.4	1.72 ± 0.11^{d}	2.01 ± 0.08^{c}
2	10	5.4	1.73 ± 0.08^{d}	2.75 ± 0.02^{d}

Means followed by the same small letter within same column are not significantly different at 0.05 significance level according to Duncan's multiple range test

Table A. 2 Sauter mean diameter (d_{32}) and volume mean diameter (d_{43}) of emulsions prepared with different RSO concentration at pH 7

Protein concentration (wt%)	Oil concentration (wt%)	pH	d_{32}	d_{43}
2	2	7	1.16 ± 0.00^{a}	1.38 ± 0.00^{a}
2	4	7	1.12 ± 0.00^{b}	1.33 ± 0.00^{b}
2	6	7	1.51 ± 0.00^{c}	1.76 ± 0.00^{c}
2	8	7	1.41 ± 0.01^{d}	1.66 ± 0.01^{d}
2	10	7	1.17 ± 0.00^{a}	1.56 ± 0.00^{e}

Means followed by the same small letter within same column are not significantly different at 0.05 significance level according to Duncan's multiple range test

Table A. 3 MC, EY, LC, LE and EE (%) of encapsules prepared with different RSO concentration at pH 7

Protein concentration (wt%)	Oil concentration (wt%)	pH	MC (%)	EY (%)	LC (%)	LE (%)	EE (%)
2	2	7	2.72 ± 0.01[a]	94.83 ± 0.25[a]	81.10 ± 0.10[a]	39.80 ± 0.10[a]	49.08 ± 0.18[a]
2	4	7	1.85 ± 0.01[b]	97.76 ± 0.39[a]	81.80 ± 0.00[b]	37.10 ± 0.10[b]	45.35 ± 0.12[b]
2	6	7	1.52 ± 0.01[c]	98.36 ± 0.44[a]	82.05 ± 0.05[bc]	35.40 ± 0.00[c]	43.14 ± 0.03[c]
2	8	7	1.64 ± 0.02[d]	97.78 ± 0.22[a]	82.20 ± 0.10[c]	31.70 ± 0.60[d]	38.56 ± 0.68[d]
2	10	7	0.86 ± 0.02[e]	92.76 ± 1.08[a]	82.55 ± 0.05[d]	28.85 ± 0.05[e]	34.95 ± 0.08[e]

Means followed by the same small letter within same column are not significantly different at 0.05 significance level according to Duncan's multiple range test

Table A. 4 MC, EY, LC, LE and EE (%) of encapsules prepared with different RSO concentration at pH 5.4

Protein concentration (wt%)	Oil concentration (wt%)	pH	MC (%)	EY (%)	LC (%)	LE (%)	EE (%)
2	2	5.4	3.05 ± 0.05[a]	95.75 ± 0.56[a]	80.75 ± 0.05[a]	46.65 ± 0.15[a]	57.77 ± 0.15[a]
2	4	5.4	2.51 ± 0.01[b]	95.08 ± 0.05[a]	81.20 ± 0.00[b]	41.90 ± 0.30[b]	51.60 ± 0.37[b]
2	6	5.4	2.81 ± 0.01[c]	97.42 ± 0.31[b]	81.45 ± 0.05[c]	39.98 ± 0.29[c]	48.97 ± 0.33[c]
2	8	5.4	1.61 ± 0.01[d]	96.50 ± 0.14[ab]	82.05 ± 0.05[d]	36.20 ± 0.10[d]	44.12 ± 0.15[d]
2	10	5.4	1.20 ± 0.00[e]	96.08 ± 0.57[ab]	82.35 ± 0.05[e]	34.05 ± 0.35[e]	41.35 ± 0.40[e]

Means followed by the same small letter within same column are not significantly different at 0.05 significance level according to Duncan's multiple range test

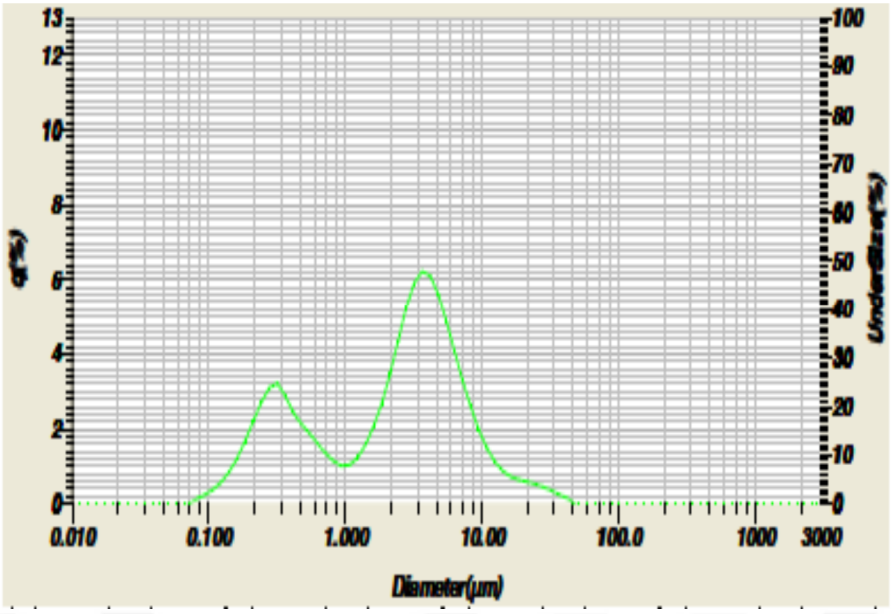

Figure A. 1 Droplet size volume distribution of LF-PPI coated emulsion with 2 wt% oil at pH 5.4

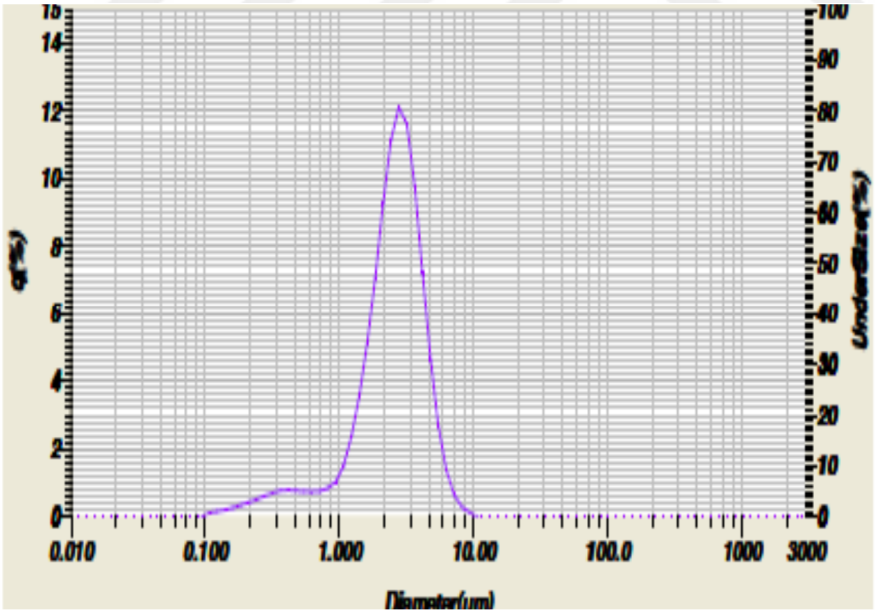

Figure A. 2 Droplet size volume distribution of LF-PPI coated emulsion with 10 wt% oil at pH 5.

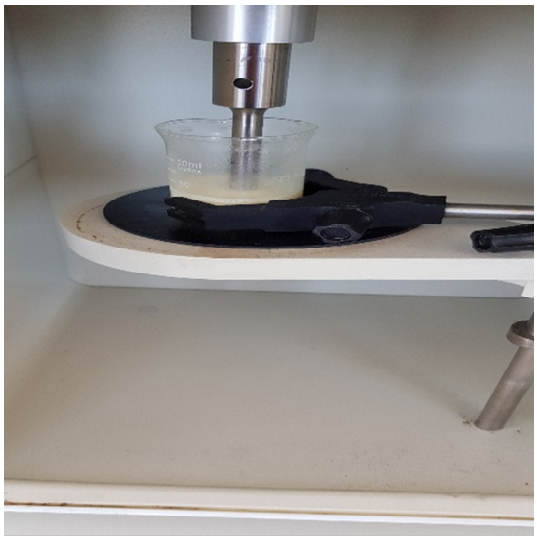

Figure A. 3 Image of Ultrasound application

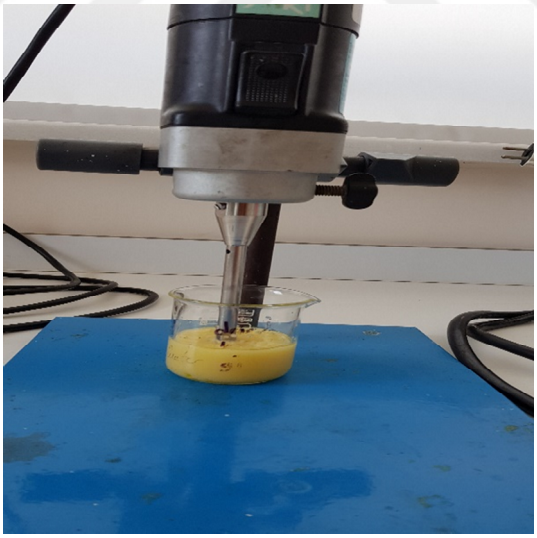

Figure A. 4 Image of high speed homogenizer application

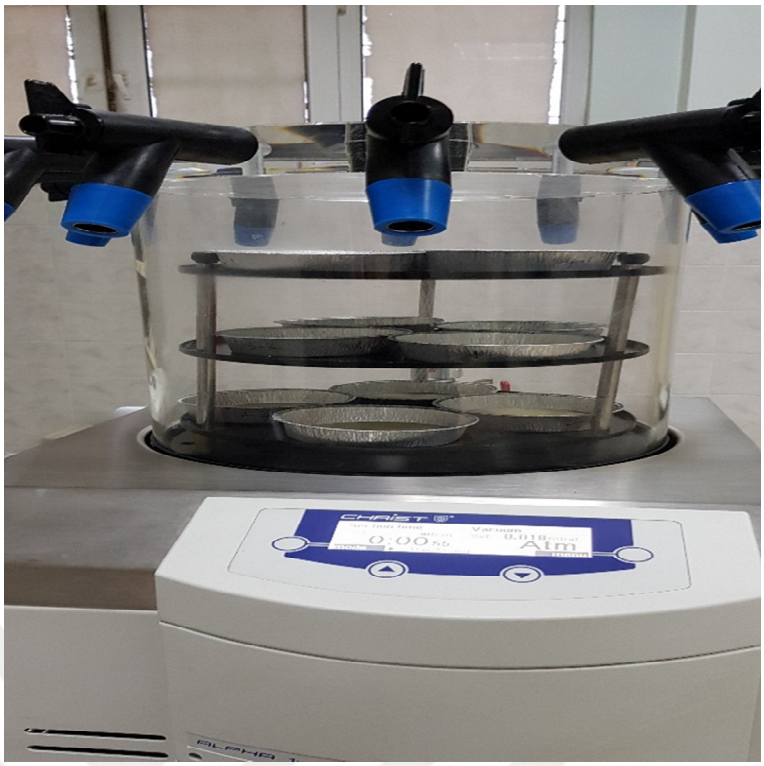

Figure A. 5 Image of Freeze drying of samples

A **B**

Figure A. 6 Emulsion Sample A) Before Freeze Drying B) After Freeze Drying

Table A. 5 ANOVA result of Influence of changing RSO concentration on Volume mean diameter (d_{43}) value of emulsions prepared with 2 wt% LF-PPI complexes at pH 7

ANOVA

d43

	Sum of Squares	df	Mean Square	F	Sig.
Between Groups	.401	4	.100	3005.300	.000
Within Groups	.000	10	.000		
Total	.401	14			

Table A. 6 Multiple range test result for Volume mean diameter (d_{43}) value of emulsions prepared with 2 wt% LF-PPI complexes and RSO (different concentration) at pH 7

d43

Duncan[a]

		Subset for alpha = 0.05				
oilconc	N	1	2	3	4	5
4%	3	1.3300				
2%	3		1.3800			
10%	3			1.5567		
8%	3				1.6633	
6%	3					1.7600
Sig.		1.000	1.000	1.000	1.000	1.000

Means for groups in homogeneous subsets are displayed.

a. Uses Harmonic Mean Sample Size = 3.000.

Table A. 7 ANOVA result of Influence of changing RSO concentration on Sauter mean diameter (d_{32}) value of emulsions prepared with 2 wt% LF-PPI complexes at pH 7

ANOVA

d32

	Sum of Squares	df	Mean Square	F	Sig.
Between Groups	.371	4	.093	1737.688	.000
Within Groups	.001	10	.000		
Total	.371	14			

Table A. 8 Multiple range test result for Sauter mean diameter (d_{32}) value of emulsions prepared with 2 wt% LF-PPI complexes and RSO (different concentration) at pH 7

d32

Duncan[a]

oilconc	N	Subset for alpha = 0.05			
		1	2	3	4
4%	3	1.1167			
2%	3		1.1567		
10%	3		1.1667		
8%	3			1.4133	
6%	3				1.5067
Sig.		1.000	.124	1.000	1.000

Means for groups in homogeneous subsets are displayed.

a. Uses Harmonic Mean Sample Size = 3.000.

Table A. 9 ANOVA result of Influence of changing RSO concentration on Volume mean diameter (d_{43}) value of emulsions prepared with 2 wt% LF-PPI complexes at pH 5.4

ANOVA

d43

	Sum of Squares	df	Mean Square	F	Sig.
Between Groups	5.060	4	1.265	171.258	.000
Within Groups	.074	10	.007		
Total	5.134	14			

Table A. 10 Multiple range test result for Volume mean diameter (d43) value of emulsions prepared with 2 wt% LF-PPI complexes and RSO (different concentration) at pH 5.4

d43

Duncan[a]

Oilcon	N	Subset for alpha = 0.05			
		1	2	3	4
6%	3	1.7000			
4%	3	1.7167			
8%	3		2.0133		
10%	3			2.7467	
2%	3				3.1433
Sig.		.817	1.000	1.000	1.000

Means for groups in homogeneous subsets are displayed.

a. Uses Harmonic Mean Sample Size = 3.000.

Table A. 11 ANOVA result of Influence of changing RSO concentration on Sauter mean diameter (d_{32}) value of emulsions prepared with 2 wt% LF-PPI complexes at pH 5.4

ANOVA

d32

	Sum of Squares	df	Mean Square	F	Sig.
Between Groups	1.865	4	.466	77.367	.000
Within Groups	.060	10	.006		
Total	1.925	14			

Table A. 12 Multiple range test result for Sauter mean diameter (d_{32}) value of emulsions prepared with 2 wt% LF-PPI complexes and RSO (different concentration) at pH 5.4

d32

Duncan[a]

		Subset for alpha = 0.05			
Oilcon	N	1	2	3	4
2%	3	.7733			
4%	3		1.2867		
6%	3			1.4533	
8%	3				1.7200
10%	3				1.7333
Sig.		1.000	1.000	1.000	.838

Means for groups in homogeneous subsets are displayed.

a. Uses Harmonic Mean Sample Size = 3.000.

Table A. 13 ANOVA result of Influence of changing RSO concentration on Encapsulation Yield value of emulsions prepared with 2 wt% LF-PPI complexes at pH 5.4

ANOVA

EY

	Sum of Squares	df	Mean Square	F	Sig.
Between Groups	6.093	4	1.523	5.095	.052
Within Groups	1.495	5	.299		
Total	7.588	9			

Table A. 14 Multiple range test result for Encapsulation Yield value of emulsions prepared with 2 wt% LF-PPI complexes and RSO (different concentration) at pH 5.4

EY

Duncan[a]

oilcon	N	Subset for alpha = 0.05	
		1	2
4%	2	95.0850	
2%	2	95.7500	
10%	2	96.0750	96.0750
8%	2	96.5000	96.5000
6%	2		97.4250
Sig.		.056	.062

Means for groups in homogeneous subsets are displayed.

a. Uses Harmonic Mean Sample Size = 2.000.

Table A. 15 ANOVA result of Influence of changing RSO concentration on Moisture Content value of emulsions prepared with 2 wt% LF-PPI complexes at pH 5.4

ANOVA

MC

	Sum of Squares	df	Mean Square	F	Sig.
Between Groups	5.060	4	1.265	944.078	.000
Within Groups	.007	5	.001		
Total	5.067	9			

Table A. 16 Multiple range test result for Moisture Content value of emulsions prepared with 2 wt% LF-PPI complexes and RSO (different concentration) at pH 5.4

MC

Duncan[a]

oilcon	N	Subset for alpha = 0.05				
		1	2	3	4	5
10%	2	1.2050				
8%	2		1.6100			
4%	2			2.5100		
6%	2				2.8100	
2%	2					3.0550
Sig.		1.000	1.000	1.000	1.000	1.000

Means for groups in homogeneous subsets are displayed.

a. Uses Harmonic Mean Sample Size = 2.000.

Table A. 17 ANOVA result of Influence of changing RSO concentration on Encapsulation Efficiency value of emulsions prepared with 2 wt% LF-PPI complexes at pH 5.4

ANOVA

EE

	Sum of Squares	df	Mean Square	F	Sig.
Between Groups	331.607	4	82.902	467.263	.000
Within Groups	.887	5	.177		
Total	332.495	9			

Table A. 18 Multiple range test result for Encapsulation Efficiency value of emulsions prepared with 2 wt% LF-PPI complexes and RSO (different concentration) at pH 5.4

EE

Duncan[a]

		Subset for alpha = 0.05				
oilcon	N	1	2	3	4	5
10%	2	41.3450				
8%	2		44.1200			
6%	2			48.9750		
4%	2				51.6000	
2%	2					57.7700
Sig.		1.000	1.000	1.000	1.000	1.000

Means for groups in homogeneous subsets are displayed.

a. Uses Harmonic Mean Sample Size = 2.000.

Table A. 19 ANOVA result of Influence of changing RSO concentration on Loading Efficency value of emulsions prepared with 2 wt% LF-PPI complexes at pH 5.4

ANOVA

LOE

	Sum of Squares	df	Mean Square	F	Sig.
Between Groups	194.688	4	48.672	369.735	.000
Within Groups	.658	5	.132		
Total	195.346	9			

Table A. 20 Multiple range test result for Loading Efficiency value of emulsions prepared with 2 wt% LF-PPI complexes and RSO (different concentration) at pH 5.4

LOE

Duncan[a]

oilcon	N	Subset for alpha = 0.05				
		1	2	3	4	5
10%	2	34.0500				
8%	2		36.2000			
6%	2			39.8900		
4%	2				41.9000	
2%	2					46.6500
Sig.		1.000	1.000	1.000	1.000	1.000

Means for groups in homogeneous subsets are displayed.

a. Uses Harmonic Mean Sample Size = 2.000.

Table A. 21 ANOVA result of Influence of changing RSO concentration on Loading Capacity value of emulsions prepared with 2 wt% LF-PPI complexes at pH 5.4

ANOVA

LC

	Sum of Squares	df	Mean Square	F	Sig.
Between Groups	3.324	4	.831	207.750	.000
Within Groups	.020	5	.004		
Total	3.344	9			

Table A. 22 Multiple range test result for Loading Capacity value of emulsions prepared with 2 wt% LF-PPI complexes and RSO (different concentration) at pH 5.4

LC

Duncan[a]

oilcon	N	Subset for alpha = 0.05				
		1	2	3	4	5
2%	2	80.7500				
4%	2		81.2000			
6%	2			81.4500		
8%	2				82.0500	
10%	2					82.3500
Sig.		1.000	1.000	1.000	1.000	1.000

Means for groups in homogeneous subsets are displayed.

a. Uses Harmonic Mean Sample Size = 2.000.

Table A. 23 ANOVA result of Influence of changing RSO concentration on Encapsulation Yield value of emulsions prepared with 2 wt% LF-PPI complexes at pH 7

ANOVA

EY

	Sum of Squares	df	Mean Square	F	Sig.
Between Groups	45.631	4	11.408	1.684	.288
Within Groups	33.869	5	6.774		
Total	79.500	9			

Table A. 24 Multiple range test result for Encapsulation Yield value of emulsions prepared with 2 wt% LF-PPI complexes and RSO (different concentration) at pH 7

EY

Duncan[a]

		Subset for alpha = 0.05
oilcon	N	1
10%	2	92.7600
2%	2	94.8350
4%	2	97.6150
8%	2	97.7800
6%	2	98.3550
Sig.		.094

Means for groups in homogeneous subsets are displayed.

a. Uses Harmonic Mean Sample Size = 2.000.

Table A. 25 ANOVA result of Influence of changing RSO concentration on Moisture Content value of emulsions prepared with 2 wt% LF-PPI complexes at pH 7

ANOVA

MC

	Sum of Squares	df	Mean Square	F	Sig.
Between Groups	3.597	4	.899	1635.209	.000
Within Groups	.003	5	.001		
Total	3.600	9			

Table A. 26 Multiple range test result for Moisture Content value of emulsions prepared with 2 wt% LF-PPI complexes and RSO (different concentration) at pH 7

MC

Duncan[a]

oilcon	N	Subset for alpha = 0.05				
		1	2	3	4	5
10%	2	.8650				
6%	2		1.5200			
8%	2			1.6450		
4%	2				1.8300	
2%	2					2.7250
Sig.		1.000	1.000	1.000	1.000	1.000

Means for groups in homogeneous subsets are displayed.

a. Uses Harmonic Mean Sample Size = 2.000.

Table A. 27 ANOVA result of Influence of changing RSO concentration on Encapsulation Efficiency value of emulsions prepared with 2 wt% LF-PPI complexes at pH 7

ANOVA

EE

	Sum of Squares	df	Mean Square	F	Sig.
Between Groups	247.097	4	61.774	298.874	.000
Within Groups	1.033	5	.207		
Total	248.131	9			

Table A. 28 Multiple range test result for Encapsulation Efficiency value of emulsions prepared with 2 wt% LF-PPI complexes and RSO (different concentration) at pH 7

EE

Duncan[a]

oilcon	N	Subset for alpha = 0.05				
		1	2	3	4	5
10%	2	34.9450				
8%	2		38.5650			
6%	2			43.1450		
4%	2				45.3550	
2%	2					49.0450
Sig.		1.000	1.000	1.000	1.000	1.000

Means for groups in homogeneous subsets are displayed.

a. Uses Harmonic Mean Sample Size = 2.000.

Table A 29 ANOVA result of Influence of changing RSO concentration on Loading Efficiency value of emulsions prepared with 2 wt% LF-PPI complexes at pH 7

ANOVA

LOE

	Sum of Squares	df	Mean Square	F	Sig.
Between Groups	147.006	4	36.751	875.036	.000
Within Groups	.210	5	.042		
Total	147.216	9			

Table A. 30 Multiple range test result for Loading Efficiency value of emulsions prepared with 2 wt% LF-PPI complexes and RSO (different concentration) at pH 7

LOE

Duncan[a]

		Subset for alpha = 0.05				
oilcon	N	1	2	3	4	5
10%	2	28.8500				
8%	2		32.0000			
6%	2			35.4000		
4%	2				37.0500	
2%	2					39.8000
Sig.		1.000	1.000	1.000	1.000	1.000

Means for groups in homogeneous subsets are displayed.

a. Uses Harmonic Mean Sample Size = 2.000.

Table A. 31 ANOVA result of Influence of changing RSO concentration on Loading Capacity value of emulsions prepared with 2 wt% LF-PPI complexes at pH 7

ANOVA

LC

	Sum of Squares	df	Mean Square	F	Sig.
Between Groups	2.354	4	.589	58.850	.000
Within Groups	.050	5	.010		
Total	2.404	9			

Table A. 32 Multiple range test result for Loading Capacity value of emulsions prepared with 2 wt% LF-PPI complexes and RSO (different concentration) at pH 7

LC

Duncan[a]

oilcon	N	Subset for alpha = 0.05			
		1	2	3	4
2%	2	81.1000			
4%	2		81.8000		
6%	2		82.0500	82.0500	
8%	2			82.2000	
10%	2				82.5500
Sig.		1.000	.054	.194	1.000

Means for groups in homogeneous subsets are displayed.

a. Uses Harmonic Mean Sample Size = 2.000.

CURRICULUM VITAE

PERSONAL INFORMATION

E-Mail: adal@gantep.edu.tr

Address: Gaziantep Üniversitesi, Gıda Mühendisliği Bölümü 27310 Şehitkamil/GAZİANTEP

EDUCATION

Doctor of Philosophy, in Food Science, University of Gaziantep, Gaziantep, Turkey, 2012-2019.

Supervisor: Prof. Dr. Esra İBANOĞLU, University of Gaziantep, Dept. of Food Engineering

Thesis title:
Encapsulation of oils from sour cherry kernel and berry seeds by protein-polysaccharide complexes

Master of Science, in Food Science, University of Gaziantep, Gaziantep, Turkey, 2009-2011.

Supervisor: Prof. Dr. Sami EREN, University of Gaziantep, Dept. of Food Engineering

Thesis title:
The Effect of Oregano and Rosemary Essential Oils on Shelf Life of Pistachio Nut Puree

Bachelor of Science in Food Engineering,

University of Helsinki, Food Technology, Finland, 2009 (II. Semester)

University of Gaziantep, Gaziantep, Turkey, 2004-2009 (I. Semester)

JOB/RESEARCH EXPERIENCE

Research Assistant (February 11, 2013-): Department of Food Engineering, University of Gaziantep, Gaziantep, Turkey.

Visiting Researcher (September 1, 2015 - February 28, 2016) School of Food Science and Nutrition, University of Leeds, United Kingdom

Food Engineer (June 30, 2009-2011): ASIM SAMLI Agricultural Products Export, Import and Trading SA, Gaziantep, Turkey.

Project Engineer (November 01, 2009-2011): The scientific and technological research of council of Turkey (TÜBİTAK), Ankara, Turkey, (The project title: The detection of effects of plant antioxidants on prolonging shelf life of pistachio puree and developing quality parameters of final product).

Technical Assistant (February, 2009): Department of Food Technology, University of Helsinki, Helsinki, Finland, (The project title: Effects of process variables and addition of polydextrose and whey protein isolate on the properties of barley extrudates).

Undergraduate study (February, 2009): Department of Applied Biochemistry in Food and Environmental Science, University of Helsinki, Helsinki, Finland. *Escherichia coli* cloning in Gene technology laboratory.

Undergraduate project design (September, 2008): Department of Food Engineering, University of Gaziantep, Gaziantep, Turkey. Pomegranate juice production, factory plan, feasibility calculation, process design

INTERSHIP EXPERIENCE

June-August 2008: Intern at Yaşar Dondurma ve Gıda Maddeleri A.Ş. (Ice-cream Factory), Kahramanmaraş, Turkey.

June -August 2007: Intern at Beslen Macaroni, Gaziantep, Turkey.

LANGUAGE

English: Advanced

German: Beginner

Finnish: Beginner

PUBLICATIONS

Adal, E., Sadeghpour, A., Connell, S., Rappolt, M., Ibanoglu, E., & Sarkar, A. (2017). Heteroprotein Complex Formation of Bovine Lactoferrin and Pea Protein Isolate: A Multiscale Structural Analysis. Biomacromolecules, 18(2), 625-635.

Adal, E., İbanoğlu, Ş., İbanoğlu, E. (2017). Microencapsulation of seed oil by heteroprotein complex coacervation. International Congress on Medicinal and Aromatic Plants, 10-12 May, Konya, Turkey.

Adal, E., İbanoğlu, Ş., İbanoğlu, E. (2017). Antioxidant activity, Phenolic Content, Fatty acid composition and Oxidative stability of berry seed oils. International Congress on Medicinal and Aromatic Plants, 10-12 May, Konya, Turkey.

Adal, E., İbanoğlu, Ş., İbanoğlu, E. (2017). Encapsulation of berry seed oils by complex coacervation with proteins. International Conference on Agriculture, Forest, Food Sceinces and Technology, 15-17 May, Cappadocia, Turkey.

Adal, E., İbanoğlu, E. (2017). Fatty acid compositions and oxidative stability of berry and cherry seed oils by DSC and Rancimat methods. 15th Euro Fed Lipid Congress: Oils, Fats, and Lipids: New Technologies and Applications for a Healthier Life, 27-30 August, Uppsala, Sweden.

Adal, E., İbanoğlu, Ş., İbanoğlu, E. (2017). Uses of microencapsulated Omega3 fatty acid rich oils in food systems. 15th Euro Fed Lipid Congress: Oils, Fats, and Lipids: New Technologies and Applications for a Healthier Life, 27-30 August, Uppsala, Sweden.

Adal, E., İbanoğlu, Ş., İbanoğlu, E. (2018). Encapsulation of omega fatty acids by complex coacervation. II. International Congress on Multidisciplinary Studies, 4-5 May, Adana, Turkey

Adal, E., İbanoğlu, Ş., İbanoğlu, E. (2018). Use of Lactoferrin as wall material in encapsulation. II. International Congress on Multidisciplinary Studies, 4-5 May, Adana, Turkey

İbanoğlu, E., Adal, E., İbanoğlu, Ş. (2018). Antioxidant activity and Oxidative stability of berry seed oils. 5th International Conference on Food Security and Nutrition, 9-11 April, Copenhagen, Denmark

Adal, E., and Eren, S. (2010). The effects of natural antioxidants on prolonging shelf life of pistachio puree. 1st International Congress on Food Technology, 03-06 November 2010, Antalya, Turkey.

Adal, E., and Eren, S. (2011). Effect of adding essential oil from *Origanum onites* on oxidative stability of pistachio paste. 9th Euro Fed Lipid Congress, 18-21 September 2011, Rotterdam, Holland.

Adal, E., and Eren, S. (2012). Antep Fıstığı Yağının Yağ Asidi Kompozisyonunun ve Oksidatif Stabilitesinin Belirlenmesi, 1. Bitkisel Yağ Kongresi, 12-14 Nisan 2012, Adana, Türkiye.

Adal, E., and Eren, S. (2012). Shelf life prediction method of pistachio puree by Rancimat method. IFT Annual meeting and Food Expo., 25-28 June 2012, Las Vegas, USA.

Adal, E., and Eren, S. (2012). The effect of Oregano essential oil on shelf-life of pistachio nut puree. 10th Euro Fed Lipid Congress, 25-28 September 2012, Krakow, Poland.

SPECIAL SKILLS

Tools: HPLC, GC, Rancimat (Metrohm 743), Twin screw extruder (Thermo), Texture analyser (Instron), DSC, Spectrophotometer, Polarimeter, Refractometer.

Certificates: ISO 22000:2005, HACCP, ISO 14001, OHSAS 18001, SEDEX

Computer: Microsoft Office; excel, word, powerpoint, access, internet, publisher, Visio, MATLAB, SPSS, Chemwindow, Design Expert and Sigma Plot programmes

MEMBERSHIP

IFT (Institute of Food Technologists, Chicago, USA)

Euro fed lipid (European Federation for the Science and Technology of Lipids)

Yabited (Turkish lipid Group)